Summer 2024

Batch Culture Models of the Murine Gut Microbiome & The Impact of Simple Dormancy on Dormancy-Capable Microorganisms Models

Ana C. Mendez
University of Texas at Arlington

BATCH CULTURE MODELS OF THE MURINE GUT MICROBIOME & THE IMPACT OF SIMPLE DORMANCY ON DORMANCY-CAPABLE MICROORGANISMS MODELS

by

ANA CLARISA MENDEZ

Presented to the Faculty of the Graduate School of
The University of Texas at Arlington in Partial Fulfillment
of the Requirements
for the Degree of

DOCTOR OF PHILOSOPHY

THE UNIVERSITY OF TEXAS AT ARLINGTON

August 2024

ACKNOWLEDGEMENTS

Foremost, I am grateful to my advisor, Dr. Hristo V Kojouharov, for the countless hours, conversations, and meetings that have shaped my dissertation and my identity as a mathematician. Also, I would like to thank Dr. Jianzhong Su, Dr. Gaik Ambartsoumian, and Dr. Souvik Roy for dedicating their time to serving on my various committees throughout the years. A special thank you to Dr. Kojouharov, Dr. Roy, and Dr. Ali, whose letters and kind words allowed me to take the first step into my career as a mathematician and educator.

To my support system: words cannot describe my love and admiration, but I can still try. Isaac, my son, you are my strength and drive. I hope my labors will provide you with a nurturing home and secure future. To Ivan, my future husband and best friend: Your efforts are always at the forefront of my mind, and I will forever try to be just as giving and loving as you are. To my family, Ricardo, Blanca, Rogelio, and Ellie: your endless care has allowed me to get this far, and I hope to one day return the fruits of your labor twofold. Last but not least, to my childhood friends turned into life-long friends, Mera and Yalitzia: thank you for never once doubting I would walk away with a PhD.

July 19, 2024

ABSTRACT

BATCH CULTURE MODELS OF THE MURINE GUT MICROBIOME & THE IMPACT OF SIMPLE DORMANCY ON DORMANCY-CAPABLE MICROORGANISMS MODELS

Ana Clarisa Mendez, Ph.D.

The University of Texas at Arlington, 2024

Supervising Professor: Hristo V. Kojouharov

The proposed mathematical biology research utilizes mathematical models to gain insight into biological systems. These systems of ordinary differential equations model diverse topics, ranging from gut microbiomes to harmful algal blooms. A complete stability analysis, supporting phase plane portraits, bifurcation diagrams, and numerical simulations will accompany the models presented.

In Chapter 2, the murine gut microbiome is modeled to match laboratory experiments in the literature [27]. In these experiments, mice eat plasmid-carrying "donor" bacteria and naturally carry plasmid-free "resident" bacteria in their gut. The models aim to capture the behavior of plasmids, donor bacteria, and resident bacteria.

Chapter 3 explores dormancy and its impact on the population dynamics of microorganisms across different environments. Dormancy is a state of reduced metabolic activity that enables dormancy-capable organisms to survive unfavorable or harsh conditions. Each of the three dormancy models presented concerns a select

combination of these topics: the murine gut microbiome, golden algae, nutrient recycling, batch cultures, and chemostats.

Lastly, Chapter 4 provides a biological interpretation of the theoretical results and situates each model in context with others found here and in recent mathematical and scientific literature.

TABLE OF CONTENTS

CHAPTER 1

Introduction

The proposed mathematical biology research employs mathematical models to enhance the understanding of biological systems. These systems of ordinary differential equations model various topics, ranging from gut microbiomes to harmful algal blooms. The following brief introduction to these topics will offer biological context to the models presented in this dissertation.

Chapter 2 models the murine gut microbiome to match laboratory experiments in the scientific literature, which we previously simulated [27]. Murine refers to mice, and the murine gut microbiome pertains to the microorganisms residing in the digestive tract of mice. Of particular interest is *Escherichia coli*, a bacteria and "model organism" that is often genetically engineered to contain plasmids [25]. Plasmids are small, circular, double-stranded DNA molecules that exist outside the chromosomal DNA of a cell; plasmids can be expelled, taken up from the environment, or transferred between bacterial cells [52]. During the experiments, mice consumed *E. coli* that contained a genetically engineered plasmid with both a reporter gene and an antibiotic resistance gene. Then, bacteria collected from the murine fecal pellets are quantified via plate assay to examine the persistence of the plasmid in the murine gut.

We create mathematical models of paired ordinary differential equations to represent the population dynamics of plasmid-carrying and plasmid-free bacteria in the murine gut microbiome. The fundamental dynamics of the batch culture models are plasmid loss, plasmid uptake, and plasmid transfer between cells. These models

will help us understand competition and co-existence between these bacteria and predict the prevalence of plasmid-carrying bacteria within batch cultures. Analyzing and comprehending these bacterial dynamics is a considerable step toward predicting and controlling bacterial growth processes; this control is vital for research, commercial applications, and gut microbiome health and stability.

Chapter 3 explores dormancy and its impact on the population dynamics of different microorganisms. Dormancy is a state of reduced metabolic activity that enables dormancy-capable organisms to survive unfavorable or harsh conditions. Microorganisms exhibit dormancy through different mechanisms: endospores, cysts, akinetes, latency, quiescence, etc. [58]. Below are examples of such microorganisms:

- Bacteria such as *Bacillus subtilis* and *Clostridium botulinum* have the ability to form endospores [40].
- Archaea such as *Halobacterium salinarum* can enter a state of quiescence [30].
- Fungi such as *Aspergillus niger* and *Penicillium chrysogenum* can produce spores [41].
- Protozoa such as *Entamoeba histolytica* can enter a cyst formation [4].
- Algae such as *Prymnesium parvum* can form non-motile dormant cells [20].
- Viruses such as the herpes simplex virus can enter latency periods in host cells [12].

Out of the above group, there are plenty of noteworthy microorganisms. For example, the herpes simplex virus continues to infect roughly 67% of all humans [29]. *Bacillus subtilis* has been found to reside in human gastrointestinal tracts [23], while *Penicillium chrysogenum* is used to make antibiotics [57]. *Prymnesium parvum* can cause harmful algal blooms, decimating local aquatic ecosystems in the process [31]. These microbes have captured the attention of the medical community, governments, and environmental protection agencies and organizations. Using math-

ematical modeling, researchers aim to improve understanding of such species and other dormancy-capable microorganisms.

The dormancy models in this chapter are batch culture and chemostat models, all of which incorporate dormancy as first-order conversion. The first of the three models builds from Chapter 2 and incorporates dormancy in the murine gut microbiome. We have published the second and third models in the scientific literature, incorporating nutrient recycling at different efficiencies [34, 2]. The second model concerns *Prymnesium parvum*, also known as golden algae, in a batch culture setting with complete nutrient conservation [34]. The third model generalizes the Golden Algae model, particularly nutrient recycling, to fit a chemostat setting [2].

CHAPTER 2

Batch Culture Models of Plasmids in the Gut Microbiome

This chapter individually and jointly analyzes the fundamental dynamics of plasmids and bacteria in the gut microbiome. The fundamental dynamics under consideration are plasmid loss, transformation, and conjugation.

2.1 Plasmid Loss Model

In this section, plasmid loss will be the focus and the only plasmid behavior incorporated into the batch culture model presented below. Plasmid loss can occur in several ways: during cell division, cell lysis, or through secretion systems [42, 48]. Furthermore, plasmid-carrying cells often face a metabolic burden due to plasmid replication and production levels [14]. This burden intensifies as the number of plasmid copies produced increases, reducing bacterial replication rates. Bacteria with higher metabolic burdens naturally replicate more slowly and are therefore outperformed by faster-replicating bacteria with fewer metabolic burdens.

2.1.1 Formulation of Plasmid Loss Model

We consider a straightforward batch culture model of bacterial competition between plasmid-carrying donor bacteria, B_P, and plasmid-free resident bacteria, B_A,

in the presence of constant plasmids in a homogeneous environment. Such a model consists of the following system of two ordinary differential equations:

$$\begin{aligned} \frac{dB_P}{dt} &= \underbrace{\alpha_1 B_P \left(1 - \frac{\gamma B_P + B_A}{K}\right)}_{\substack{\text{replication of} \\ \text{plasmid-carrying bacteria}}} - \underbrace{\eta_1 B_P}_{\substack{\text{plasmid} \\ \text{loss}}} \\ \frac{dB_A}{dt} &= \underbrace{\alpha_2 B_A \left(1 - \frac{\gamma B_P + B_A}{K}\right)}_{\substack{\text{replication of} \\ \text{plasmid-free bacteria}}} + \underbrace{\eta_1 B_P}_{\substack{\text{plasmid} \\ \text{loss}}} . \end{aligned} \tag{2.1.1}$$

We assume that bacteria follow a logistical growth with carrying capacity K [24]. Furthermore, experimental evidence suggests that carrying a plasmid imposes a metabolic burden on the bacteria, leading to either a slower growth rate or lower carrying capacity for plasmid-carrying bacteria. In this model, we assume that plasmid-carrying bacteria have a lower maximal growth rate, α_1, than plasmid-free bacteria, α_2, while the relative capacity of B_P is denoted by γ. Thus, $\alpha_1 < \alpha_2$, with $\gamma > 1$. The rate of bacterial death is negligible as we are modeling bacterial experimental growth during the exponential phase in a batch culture. Moreover, we assume plasmids are constant and homogeneous across the environment. Bacteria B_P eliminates its plasmid and becomes B_A at a constant rate η_1. Table 2.1 lists the model parameters with their descriptions and units.

Variable/Parameter	Description	Units
B_P	Donor/plasmid-carrying bacteria	$cells/\mu L$
B_A	Resident/plasmid-free bacteria	$cells/\mu L$
α_1	Replication rate of donor bacteria	$1/hour$
α_2	Replication rate of resident bacteria	$1/hour$
K	Carrying capacity of the environment	$cells/\mu L$
γ	Relative capacity coefficient of B_P	–
η_1	Rate of conversion from donor to resident bacteria	$1/hour$

Table 2.1: Model (2.1.1) parameters with their descriptions and units.

2.1.2 Analysis of Plasmid Loss Model ($\eta_1 \neq 0, \eta_2 = 0, \beta = 0$)

In this subsection, System (2.1.1) is found to have three equilibria. We deduce the criteria for the existence and stability of all equilibria. The stability conditions are then summarized in Table 2.2 and corroborated in Figure 2.1.

By setting the right-hand sides of System (2.1.1) equal to zero, the following three equilibria are found:

$$E^0 = (0,0) = (B_P^0, B_A^0),$$
$$E^1 = (0,K) = (B_P^1, B_A^1),$$
$$E^2 = \left(\frac{\alpha_2 K(\eta_1 - \alpha_1)}{\alpha_1(\alpha_1 - \alpha_2\gamma)}, -\frac{K(\eta_1 - \alpha_1)}{(\alpha_1 - \alpha_2\gamma)}\right) = (B_P^2, B_A^2).$$

Before considering the stability of the equilibria, one must know when and if each equilibrium is biologically feasible. Recall that the values for B_P and B_A that appear in E^i, where $i = 0, 1, 2$, represent population sizes. Hence, these values must all be non-negative.

E^0: Clearly, $B_P^0 = B_A^0 = 0$ are non-negative. Therefore, E^0 is always biologically feasible and always exists.

E^1: Clearly, $B_P^1 = 0$ and $B_A^1 = K$ are non-negative. Therefore, E^1 is always biologically feasible and always exists.

E^2: Lastly, note $B_A^2 = -\frac{\alpha_1}{\alpha_2} B_P^2$. This means B_P^2 and B_A^2 are non-negative if and only if they are equal to zero, i.e. when $E^0 = E^2$. Thus, if $E^0 \neq E^2$, E^2 is never biologically feasible. For our purposes, this means E^2 never exists.

Moving forward, only E^0 and E^1 are eligible for analysis.

Next, we establish the stability conditions for the equilibria E^0 and E^1. The following theorem regards the local stability of the trivial equilibrium E^0.

Theorem 2.1.1. *The trivial equilibrium E^0 is always unstable.*

Proof. The Jacobian evaluated at E^0 is

$$J\left(E^0\right) = \begin{bmatrix} \alpha_1 - \eta_1 & 0 \\ \eta_1 & \alpha_2 \end{bmatrix}.$$

Thus,

$$det\left(J\left(E^0\right)\right) = \alpha_2(\alpha_1 - \eta_1)$$

and

$$tr\left(J\left(E^0\right)\right) = (\alpha_1 - \eta_1) + \alpha_2.$$

By the Routh-Hurwitz stability criterion [39], E^0 is stable when $det\left(J\left(E^0\right)\right) > 0$ and $tr\left(J\left(E^0\right)\right) < 0$. The above conditions are never satisfied simultaneously:

$$\text{Suppose } det\left(J\left(E^0\right)\right) = \alpha_2(\alpha_1 - \eta_1) > 0 \text{ and } tr\left(J\left(E^0\right)\right) = (\alpha_1 - \eta_1) + \alpha_2 < 0.$$
$$\text{Thus, } \alpha_1 - \eta_1 > 0 \text{ and } tr\left(J\left(E^0\right)\right) = (\alpha_1 - \eta_1) + \alpha_2 > 0.$$

A contradiction has been reached. In conclusion, the Routh-Hurwitz stability criterion is never satisfied, and E^0 is always unstable. □

Next, we prove that the boundary equilibrium E^1 is always locally asymptotically stable.

Theorem 2.1.2. *The boundary equilibrium E^1 is always locally asymptotically stable.*

Proof. The Jacobian evaluated at E^1 is

$$J\left(E^1\right) = \begin{bmatrix} -\eta_1 & 0 \\ -\alpha_2\gamma + \eta_1 & -\alpha_2 \end{bmatrix}.$$

By the Routh-Hurwitz stability criterion [39], E^1 is stable when $det\left(J\left(E^1\right)\right) > 0$ and $tr\left(J\left(E^1\right)\right) < 0$. Clearly,

$$det\left(J\left(E^1\right)\right) = \eta_1\alpha_2 > 0$$

and

$$tr\left(J\left(E^1\right)\right) = -(\eta_1 + \alpha_2) < 0.$$

Thus, E^1 is always locally asymptotically stable. □

Furthermore, the above stability analysis is summarized in Table 2.2 and supported by the phase portraits in Figure 2.1.

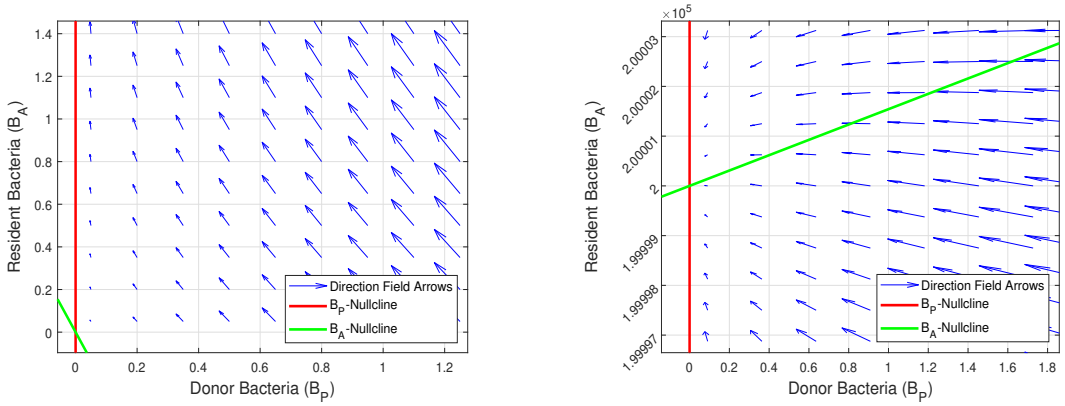

(a) $E^0 = (0, 0)$ unstable (b) $E^1 = (0, K)$ stable

Figure 2.1: Phase portraits of System (2.1.1). The parameter values in (a) and (b) are $\alpha_1 = 3, \alpha_2 = 3.7848, K = 200,000, \gamma = 1.1$, and $\eta_1 = 10$. E^0 is unstable, as shown by the direction field arrows moving away from $E^0 = (0, 0)$. E^1 is locally asymptotically stable, as shown by the direction field arrows moving toward $E^1 = (0, K)$.

Existence and Stability
E^0 exists and unstable
E^1 exists and stable
E^2 does not exist

Table 2.2: Existence and stability of the equilibria of System (2.1.1).

2.1.3 Numerical Simulations and Discussion

In this subsection, we discuss simulations of System (2.1.1), which were created using the Matlab® `ode45` solver. In this model, the only plasmid dynamic is plasmid loss. Hence, conversion only happens in one direction: donor bacteria, B_P, can lose their plasmids and become resident bacteria, B_A. This creates an uneven influx of plasmid-free resident bacteria. It follows that the system will approach a steady state where only the plasmid-free resident bacteria, B_A, persists as inferred by the lone stability of

$$E^1 = (0, K) = \left(B_P^1, B_A^1\right)$$

of System (2.1.1).

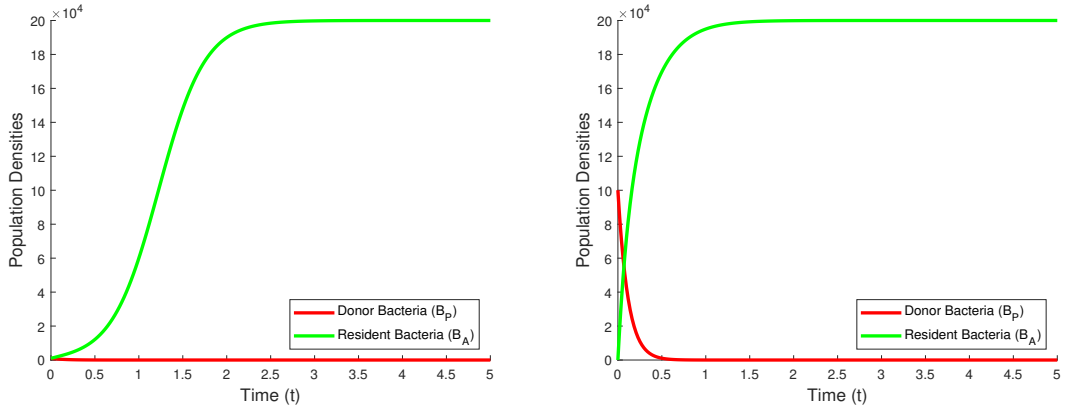

(a) $B_P(0) = 1000, B_A(0) = 1000$ (b) $B_P(0) = 100000, B_A(0) = 10$

Figure 2.2: Numerical simulation of System (2.1.1). In (a) and (b), E^0 is unstable and E^1 is locally asymptotically stable with parameter values $\alpha_1 = 3, \alpha_2 = 3.7848, K = 200,000, \gamma = 1.1$, and $\eta_1 = 10$.

Note the overall outcome of both simulations in Figure 2.2: $B_P = 0$ and $B_A = K$. In (a), the initial population sizes are identical and $\frac{1}{200}$ of the carrying capacity, K. However, in (b), $B_P(0)$ is 100 times bigger, and $B_A(0)$ is 100 times smaller in comparison to (a). Still, the outcomes are identical; this will be the case

for any initial condition with at least one positive value. Furthermore, all numerical simulations of System (2.1.1) can be categorized into two outcomes:

1. If $B_P(0) = B_A(0) = 0$, then the system will remain at $E^0 = (0, 0) = \left(B_P^0, B_A^0\right)$.
2. Otherwise, the system will trend towards and stabilize at $E^1 = (0, K) = \left(B_P^1, B_A^1\right)$.

2.2 Plasmid Acquisition Model

This section focuses on plasmid acquisition. The batch culture model presented below incorporates two manners in which this behavior can occur. One process involves the uptake of free plasmids from the environment through natural transformation. This is a chance event of plasmid movement into the bacteria dependent upon the characteristics of a given bacterial species and cell. The second mechanism accounted for in this model is the transfer of plasmids through conjugation. In this process, a bacteria with a transferable plasmid makes direct contact with a recipient bacteria using its pilus to form a mating pair. After conjugation, both bacteria in the mating pair will possess a plasmid [52].

2.2.1 Formulation of Plasmid Acquisition Model

We build off the previous model and incorporate plasmid acquisition instead of loss. This means plasmid-free resident bacteria, B_A, take in the plasmid via natural transformation and become plasmid-carrying donor bacteria, B_P, at a rate η_2. In

addition, plasmid transfer occurs from B_P to B_A via conjugation at a rate β. Below is the system of ordinary differential equations described above:

$$\begin{aligned}
\frac{dB_P}{dt} &= \underbrace{\alpha_1 B_P\left(1-\frac{\gamma B_P + B_A}{K}\right)}_{\substack{\text{replication of}\\ \text{plasmid-carrying bacteria}}} + \underbrace{\eta_2 B_A}_{\text{transformation}} + \underbrace{\beta B_P B_A}_{\text{conjugation}}, \\
\frac{dB_A}{dt} &= \underbrace{\alpha_2 B_A\left(1-\frac{\gamma B_P + B_A}{K}\right)}_{\substack{\text{replication of}\\ \text{plasmid-free bacteria}}} - \underbrace{\eta_2 B_A}_{\text{transformation}} - \underbrace{\beta B_P B_A}_{\text{conjugation}},
\end{aligned} \tag{2.2.1}$$

Table 2.3 lists the model parameters with their descriptions and units.

Variable/Parameter	Description	Units
B_P	Donor/plasmid-carrying bacteria	$cells/\mu L$
B_A	Resident/plasmid-free bacteria	$cells/\mu L$
α_1	Replication rate of donor bacteria	$1/hour$
α_2	Replication rate of resident bacteria	$1/hour$
K	Carrying capacity of the environment	$cells/\mu L$
γ	Relative capacity coefficient of B_P	–
η_2	Rate of conversion from resident to donor bacteria	$1/hour$
β	Rate of bacterial conjugation	$\mu L/cells/hour$

Table 2.3: Model (2.2.1) parameters with their descriptions and units.

2.2.2 Analysis of Transformation Model ($\eta_1 = 0, \eta_2 \neq 0, \beta = 0$)

In this subsection, we assume $\beta = 0$ and $\eta_2 \neq 0$. System (2.2.1) is found to have three equilibria. We deduce criteria for the existence and stability of all equilibria. The stability conditions are then summarized in Table 2.4 and corroborated in Figure 2.3.

By setting the right-hand sides of System (2.2.1) equal to zero, the following three equilibria are found:

$$E^0 = (0,0) = \left(B_P^0, B_A^0\right)$$

$$E^1 = \left(\frac{K}{\gamma}, 0\right) = \left(B_P^1, B_A^1\right)$$
$$E^2 = \left(\frac{K(\eta_2 - \alpha_2)}{(\alpha_1 - \alpha_2\gamma)}, -\frac{\alpha_1 K(\eta_2 - \alpha_2)}{\alpha_2(\alpha_1 - \alpha_2\gamma)}\right) = \left(B_P^2, B_A^2\right)$$

Before considering the stability of the equilibria, one must know when and if each equilibrium is biologically feasible. Recall that the values for B_P and B_A that appear in E^i, where $i = 0, 1, 2$, represent population sizes. Hence, these values must all be non-negative.

E^0: Clearly, $B_P^0 = B_A^0 = 0$ are non-negative. Therefore, E^0 is always biologically feasible and always exists.

E^1: Clearly, $B_P^1 = \dfrac{K}{\gamma}$ and $B_A^1 = 0$ are non-negative. Therefore, E^1 is always biologically feasible and always exists.

E^2: Lastly, note $B_P^2 = -\dfrac{\alpha_1}{\alpha_2} B_A^2$. This means B_P^2 and B_A^2 are non-negative if and only if they are equal to zero, i.e. when $E^0 = E^2$. Thus, if $E^0 \neq E^2$, E^2 is never biologically feasible. For our purposes, this means E^2 never exists.

Moving forward, only E^0 and E^1 are eligible for analysis.

Next, we establish the stability conditions for the two equilibria E^0 and E^1. The following theorem concerns the local stability of the trivial equilibrium E^0.

Theorem 2.2.1. *The trivial equilibrium E^0 is always unstable.*

Proof. The Jacobian evaluated at E^0 is

$$J\left(E^0\right) = \begin{bmatrix} \alpha_1 & \eta_2 \\ 0 & \alpha_2 - \eta_2 \end{bmatrix}.$$

Thus,

$$det\left(J\left(E^0\right)\right) = \alpha_1(\alpha_2 - \eta_2)$$

and

$$tr\left(J\left(E^0\right)\right) = \alpha_1 + (\alpha_2 - \eta_2).$$

By the Routh-Hurwitz stability criterion [39], E^0 is stable when $det\left(J\left(E^0\right)\right) > 0$ and $tr\left(J\left(E^0\right)\right) < 0$. The above conditions are never satisfied simultaneously:

$$\text{Suppose } det\left(J\left(E^0\right)\right) = \alpha_1(\alpha_2 - \eta_2) > 0 \text{ and } tr\left(J\left(E^0\right)\right) = \alpha_1 + (\alpha_2 - \eta_2) < 0.$$
$$\text{Thus, } \alpha_2 - \eta_2 > 0 \text{ and } tr\left(J\left(E^0\right)\right) = \alpha_1 + (\alpha_2 - \eta_2) > 0.$$

A contradiction has been reached. In conclusion, the Routh-Hurwitz stability criterion is never satisfied, and E^0 is always unstable.

□

Next, we prove that the boundary equilibrium E^1 is always locally asymptotically stable.

Theorem 2.2.2. *The boundary equilibrium E^1 is always locally asymptotically stable.*

Proof. The Jacobian evaluated at E^1 is

$$J\left(E^1\right) = \begin{bmatrix} -\alpha_1 & -\alpha_1\gamma + \eta_2 \\ 0 & -\eta_2 \end{bmatrix}.$$

By the Routh-Hurwitz stability criterion [39], E^1 is stable when $det\left(J\left(E^1\right)\right) > 0$ and $tr\left(J\left(E^1\right)\right) < 0$. Clearly,

$$det\left(J\left(E^1\right)\right) = \alpha_1\eta_2 > 0$$

and

$$tr\left(J\left(E^1\right)\right) = -(\eta_2 + \alpha_1) < 0.$$

Thus, E^1 is always locally asymptotically stable. □

Furthermore, the above stability analysis is summarized in Table 2.4 and supported by the phase portraits in Figure 2.3.

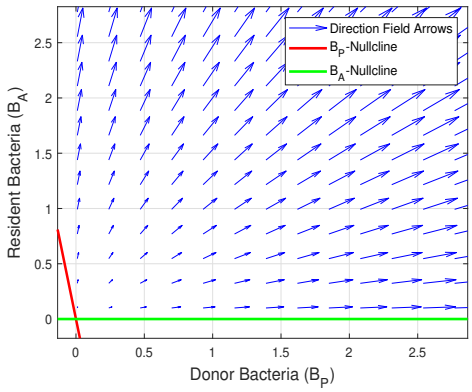

(a) $E^0 = (0, 0)$ unstable

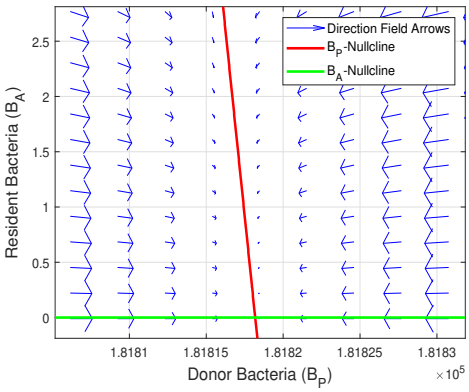

(b) $E^1 = \left(\frac{K}{\gamma}, 0\right)$ stable

Figure 2.3: Phase portraits of System (2.2.1) when $\eta_2 \neq 0$, and $\beta = 0$. The parameter values in (a) and (b) are $\alpha_1 = 3, \alpha_2 = 3.7848, K = 200,000, \gamma = 1.1$, and $\eta_2 = 0.4973$. E^0 is unstable, as shown by the direction field arrows moving away from $E^0 = (0, 0)$. E^1 is locally asymptotically stable, as shown by the direction field arrows moving toward $E^1 = \left(\frac{K}{\gamma}, 0\right)$.

Existence and Stability
E^0 exists and unstable
E^1 exists and stable
E^2 does not exist

Table 2.4: Existence and stability of the equilibria of System (2.2.1) when $\beta = 0$ and $\eta_2 \neq 0$.

2.2.3 Analysis of Conjugation Model ($\eta_1 = 0, \eta_2 = 0, \beta \neq 0$)

This subsection assumes $\eta_2 = 0$ and $\beta \neq 0$. System (2.2.1) is found to have four equilibria. We deduce the criteria for the existence and stability of all equilibria. The stability conditions are then summarized in Table 2.5 and corroborated in Figure 2.4.

By setting the right-hand sides of System (2.2.1) equal to zero, the following four equilibria are found:

$$E^0 = (0,0) = \left(B_P^0, B_A^0\right)$$
$$E^1 = \left(\frac{K}{\gamma}, 0\right) = \left(B_P^1, B_A^1\right)$$
$$E^2 = (0,K) = \left(B_P^2, B_A^2\right)$$
$$E^3 = \left(\frac{\alpha_2 K}{(\beta K - \alpha_1 + \alpha_2\gamma)}, -\frac{\alpha_1 K}{(\beta K - \alpha_1 + \alpha_2\gamma)}\right) = \left(B_P^3, B_A^3\right)$$

Before considering the stability of the equilibria, one must know when and if each equilibrium is biologically feasible. Recall that the values for B_P and B_A that appear in E^i, where $i = 0, 1, 2, 3$, represent population sizes. Hence, these values must all be non-negative.

E^0: Clearly, $B_P^0 = B_A^0 = 0$ are non-negative. Therefore, E^0 is always biologically feasible and always exists.

E^1: Clearly, $B_P^1 = \dfrac{K}{\gamma}$ and $B_A^1 = 0$ are non-negative. Therefore, E^1 is always biologically feasible and always exists.

E^2: Clearly, $B_P^2 = 0$ and $B_A^2 = K$ are non-negative. Therefore, E^2 is always biologically feasible and always exists.

E^3: Lastly, note $B_A^3 = -\dfrac{\alpha_1}{\alpha_2} B_P^3$. This means B_P^3 and B_A^3 are non-negative if and only if they are equal to zero, i.e. when $E^0 = E^3$. Thus, if $E^0 \neq E^3$, E^3 is never biologically feasible. For our purposes, this means E^3 never exists.

Moving forward, E^0, E^1, and E^2 are eligible for analysis.

Next, we establish the stability conditions for the three equilibria E^0, E^1, and E^2. The following theorem concerns the local stability of the trivial equilibrium E^0.

Theorem 2.2.3. *The trivial equilibrium E^0 is always unstable.*

Proof. The Jacobian evaluated at E^0 is

$$J\left(E^0\right) = \begin{bmatrix} \alpha_1 & 0 \\ 0 & \alpha_2 \end{bmatrix}.$$

By the Routh-Hurwitz stability criterion [39], E^0 is stable when $det\left(J\left(E^0\right)\right) > 0$ and $tr\left(J\left(E^0\right)\right) < 0$. However,

$$det\left(J\left(E^0\right)\right) = \alpha_1\alpha_2 > 0$$

and

$$tr\left(J\left(E^0\right)\right) = \alpha_1 + \alpha_2 > 0.$$

Thus, E^0 is always unstable. □

Next, we prove that the boundary equilibrium E^1 is always locally asymptotically stable.

Theorem 2.2.4. *The boundary equilibrium E^1 is always locally asymptotically stable.*

Proof. The Jacobian evaluated at E^1 is

$$J\left(E^1\right) = \begin{bmatrix} -\alpha_1 & \dfrac{-\alpha_1}{\gamma} + \dfrac{\beta K}{\gamma} \\ 0 & -\dfrac{\beta K}{\gamma} \end{bmatrix}.$$

By the Routh-Hurwitz stability criterion [39], E^1 is stable when $det\left(J\left(E^1\right)\right) > 0$ and $tr\left(J\left(E^1\right)\right) < 0$. Clearly,

$$det\left(J\left(E^1\right)\right) = \frac{\alpha_1\beta K}{\gamma} > 0$$

and

$$tr\left(J\left(E^1\right)\right) = -\alpha_1 - \frac{\beta K}{\gamma} < 0.$$

Thus, E^1 is always locally asymptotically stable. □

Next, we prove that the boundary equilibrium E^2 is always unstable.

Theorem 2.2.5. *The boundary equilibrium E^2 is always unstable.*

Proof. The Jacobian evaluated at E^2 is

$$J\left(E^2\right) = \begin{bmatrix} \beta K & 0 \\ -\alpha_2\gamma - \beta K & -\alpha_2 \end{bmatrix}.$$

By the Routh-Hurwitz stability criterion [39], E^2 is stable when $det\left(J\left(E^2\right)\right) > 0$ and $tr\left(J\left(E^2\right)\right) < 0$. However,

$$det\left(J\left(E^2\right)\right) = -\alpha_2\beta K < 0$$

and

$$tr\left(J\left(E^2\right)\right) = \beta K - \alpha_2.$$

Thus, E^2 is always unstable. □

Furthermore, the above stability analysis is summarized in Table 2.5 and supported by the phase portraits in Figure 2.4.

Existence and Stability
E^0 exists and unstable
E^1 exists and stable
E^2 exists and unstable
E^3 does not exist

Table 2.5: Existence and stability of the equilibria of System (2.2.1) when $\eta_2 = 0$, and $\beta \neq 0$.

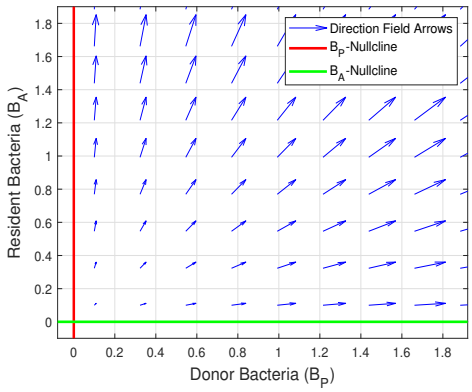

(a) $E^0 = (0, 0)$ unstable

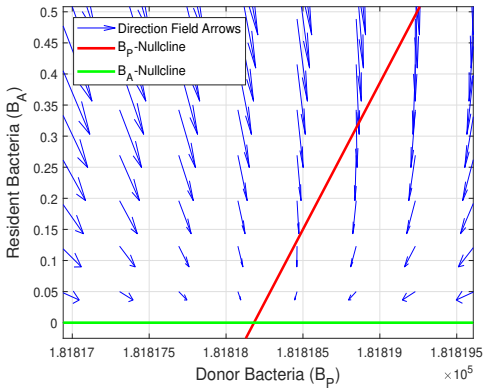

(b) $E^1 = \left(\frac{K}{\gamma}, 0\right)$ stable

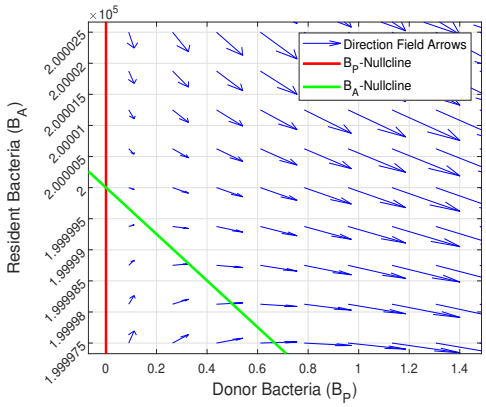

(c) $E^2 = (0, K)$ unstable

Figure 2.4: Phase portraits of System (2.2.1) when $\eta_2 = 0$, and $\beta \neq 0$. The parameter values in (a)-(c) are $\alpha_1 = 3, \alpha_2 = 3.7848, K = 200,000, \gamma = 1.1$, and $\beta = 0.00005$. E^0 and E^2 are unstable, as shown by the direction field arrows moving away from $E^0 = (0, 0)$ and $E^2 = (0, K)$. E^1 is locally asymptotically stable, as shown by the direction field arrows moving toward $E^1 = \left(\frac{K}{\gamma}, 0\right)$.

2.2.4 Analysis of Conjugation and Transformation Model ($\eta_1 = 0, \eta_2 \neq 0, \beta \neq 0$)

This subsection assumes $\eta_2, \beta \neq 0$. System (2.2.1) is found to have four equilibria. We deduce the criteria for the existence and stability of all equilibria. The stability conditions are then summarized in Table 2.6 and corroborated in Figure 2.5.

By setting the right-hand sides of System (2.2.1) equal to zero, the following four equilibria are found:

$$
\begin{aligned}
E^0 &= (0,0) = (B_P^0, B_A^0) \\
E^1 &= \left(\frac{K}{\gamma}, 0\right) = (B_P^1, B_A^1) \\
E^2 &= \left(-\frac{\eta_2}{\beta}, K + \frac{\eta_2\gamma}{\beta}\right) = (B_P^2, B_A^2) \\
E^3 &= \left(\frac{K(\alpha_2 - \eta_2)}{(\beta K - \alpha_1 + \alpha_2\gamma)}, -\frac{\alpha_1 K(\alpha_2 - \eta_2)}{\alpha_2(\beta K - \alpha_1 + \alpha_2\gamma)}\right) = (B_P^3, B_A^3)
\end{aligned}
$$

Before considering the stability of the equilibria, one must know when and if each equilibrium is biologically feasible. Recall that the values for B_P and B_A that appear in E^i, where $i = 0, 1, 2, 3$, represent population sizes. Hence, these values must all be non-negative.

E^0: Clearly, $B_P^0 = B_A^0 = 0$ are non-negative. Therefore, E^0 is always biologically feasible and always exists.

E^1: Clearly, $B_P^1 = \dfrac{K}{\gamma}$ and $B_A^1 = 0$ are non-negative. Therefore, E^1 is always biologically feasible and always exists.

E^2: Clearly, $B_A^2 = K + \dfrac{\eta_2\gamma}{\beta}$ is non-negative. However, $B_P^2 = -\dfrac{\eta_2}{\beta}$ is non-negative if and only if $\eta_2 = 0$, which violates our initial assumption of $\eta_2, \beta \neq 0$. Thus, if $\eta_2 \neq 0$, E^2 is never biologically feasible. For our purposes, this means E^2 never exists.

E^3: Lastly, note $B_P^4 = -\dfrac{\alpha_2}{\alpha_1} B_A^4$. This means B_P^3 and B_A^3 are non-negative if and only if they are equal to zero, i.e. when $E^0 = E^3$. Thus, if $E^0 \neq E^3$, E^3 is never biologically feasible. For our purposes, this means E^3 never exists.

Moving forward, E^0 and E^1 are eligible for analysis.

Next, we establish the stability conditions for the two equilibria E^0 and E^1. The following theorem concerns the local stability of the trivial equilibrium E^0.

Theorem 2.2.6. *The trivial equilibrium E^0 is always unstable.*

Proof. The Jacobian evaluated at E^0 is

$$J\left(E^0\right) = \begin{bmatrix} \alpha_1 & \eta_2 \\ 0 & \alpha_2 - \eta_2 \end{bmatrix}.$$

Thus,

$$det\left(J\left(E^0\right)\right) = \alpha_1(\alpha_2 - \eta_2)$$

and

$$tr\left(J\left(E^0\right)\right) = \alpha_1 + (\alpha_2 - \eta_2).$$

By the Routh-Hurwitz stability criterion [39], E^0 is stable when $det\left(J\left(E^0\right)\right) > 0$ and $tr\left(J\left(E^0\right)\right) < 0$. The above conditions are never satisfied simultaneously:

$$\text{Suppose } det\left(J\left(E^0\right)\right) = \alpha_1(\alpha_2 - \eta_2) > 0 \text{ and } tr\left(J\left(E^0\right)\right) = \alpha_1 + (\alpha_2 - \eta_2) < 0.$$
$$\text{Thus, } \alpha_2 - \eta_2 > 0 \text{ and } tr\left(J\left(E^0\right)\right) = \alpha_1 + (\alpha_2 - \eta_2) > 0.$$

A contradiction has been reached. In conclusion, the Routh-Hurwitz stability criterion is never satisfied, and E^0 is always unstable. □

Next, we prove that the boundary equilibrium E^1 is always locally asymptotically stable.

Theorem 2.2.7. *The boundary equilibrium E^1 is always locally asymptotically stable.*

Proof. The Jacobian evaluated at E^1 is

$$J\left(E^1\right) = \begin{bmatrix} -\alpha_1 & -\alpha_1\gamma + \eta_2 + \dfrac{\beta K}{\gamma} \\ 0 & -\eta_2 - \dfrac{\beta K}{\gamma} \end{bmatrix}.$$

By the Routh-Hurwitz stability criterion [39], E^0 is stable when $det\left(J\left(E^0\right)\right) > 0$ and $tr\left(J\left(E^0\right)\right) < 0$. Clearly,

$$det\left(J\left(E^1\right)\right) = \alpha_1\left(\eta_2 + \frac{\beta K}{\gamma}\right) > 0$$

and

$$tr\left(J\left(E^1\right)\right) = -\left(\eta_2 + \alpha_1 + \frac{\beta K}{\gamma}\right) < 0.$$

Thus, E^1 is always locally asymptotically stable. □

Furthermore, the above stability analysis is summarized in Table 2.6 and supported by the phase portraits in Figure 2.5.

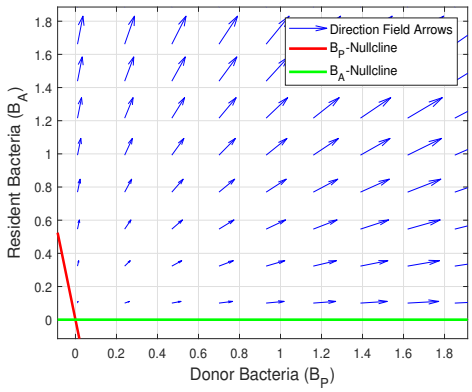

(a) $E^0 = (0, 0)$ unstable

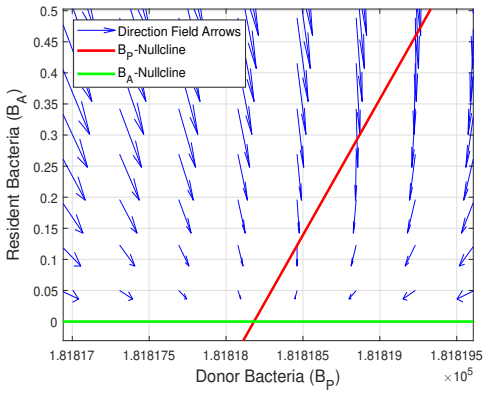

(b) $E^1 = \left(\frac{K}{\gamma}, 0\right)$ stable

Figure 2.5: Phase portraits of System (2.2.1). The parameter values in (a) and (b) are $\alpha_1 = 3, \alpha_2 = 3.7848, K = 200,000, \gamma = 1.1, \eta_2 = 0.4973$, and $\beta = 0.00005$. E^0 is unstable, as shown by the direction field arrows moving away from $E^0 = (0, 0)$. E^1 is locally asymptotically stable, as shown by the direction field arrows moving toward $E^1 = \left(\frac{K}{\gamma}, 0\right)$.

2.2.5 Numerical Simulations and Discussion

In this subsection, we discuss simulations of System (2.2.1), which were created using the Matlab® `ode45` solver. In this model, the only plasmid dynamic included is plasmid acquisition, which manifests in two different ways: transformation and

Existence and Stability
E^0 exists and unstable
E^1 exists and stable
E^2 does not exist
E^3 does not exist

Table 2.6: Existence and stability of the equilibria of System (2.2.1) when $\eta_2, \beta \neq 0$.

conjugation. However, conversion only happens in one direction: resident bacteria, B_A, can gain plasmids and become donor bacteria, B_P. This creates an uneven influx of plasmid-carrying

bacteria. It follows that the system will approach a steady state where only the plasmid-carrying donor bacteria, B_P, persist as inferred by the lone stability of

$$E^1 = \left(\frac{K}{\gamma}, 0\right) = \left(B_P^1, B_A^1\right)$$

across the three sub-models of System (2.2.1): $\eta_2 \neq 0$ and $\beta = 0$, $\eta_2 = 0$ and $\beta \neq 0$, and $\eta_2, \beta \neq 0$.

Note the overall outcome of simulations in Figure 2.6: $B_P = \frac{K}{\gamma}$ and $B_A = 0$. In (a),(c), and (e), the initial population sizes are identical and $\frac{1}{200}$ of the carrying capacity, K. However, in (b),(d), and (f), $B_P(0)$ is 100 times smaller, and $B_A(0)$ is 100 times bigger in comparison to (a),(c), and (e). Still, the outcome is identical. This will be the case for any initial condition with at least one initial positive population value. Furthermore, all numerical simulations of System (2.1.1) can be categorized into two outcomes:

1. If $B_P(0) = B_A(0) = 0$, then the system will remain at $E^0 = (0, 0) = \left(B_P^0, B_A^0\right)$.
2. If $\eta_2 = 0, \beta \neq 0$, $B_P(0) = 0$, and $B_A(0) = K$, then the system will remain at $B_P(0) = 0$ and $B_A(0) = K$.
3. Otherwise, the system will trend towards and stabilize at $E^1 = \left(\frac{K}{\gamma}, 0\right) = \left(B_P^1, B_A^1\right)$.

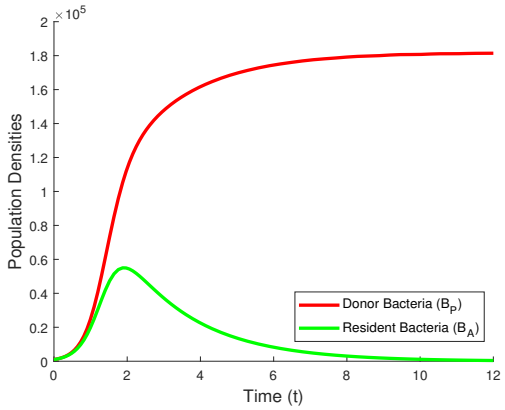

(a) $B_P(0) = 1000, B_A(0) = 1000$

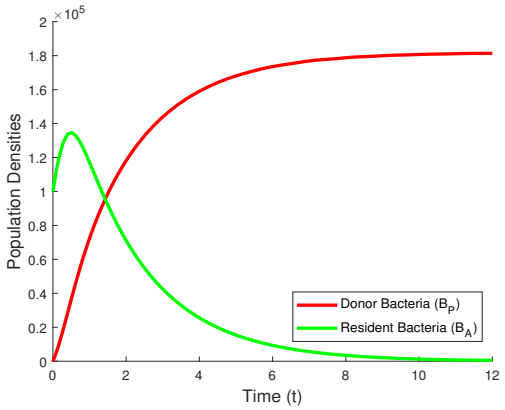

(b) $B_P(0) = 10, B_A(0) = 100000$

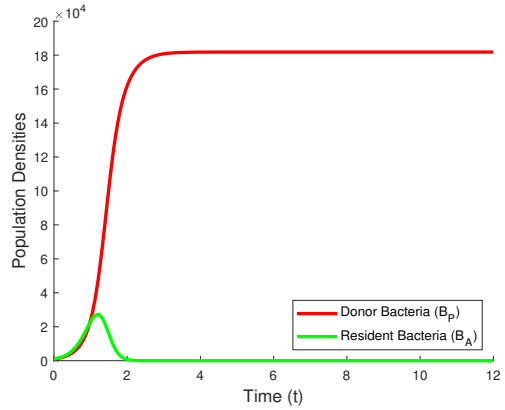

(c) $B_P(0) = 1000, B_A(0) = 1000$

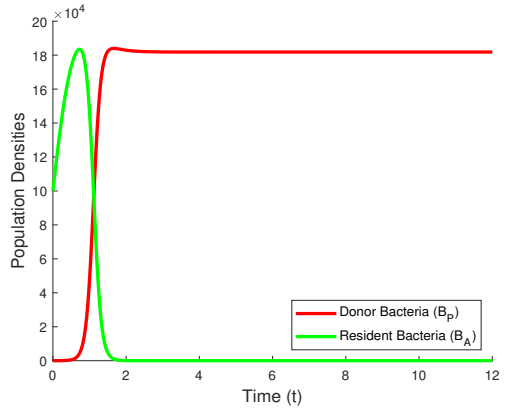

(d) $B_P(0) = 10, B_A(0) = 100000$

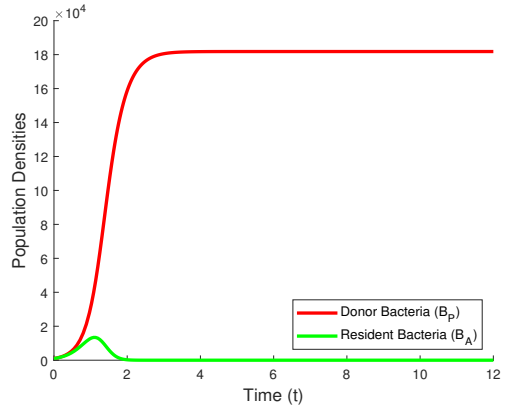

(e) $B_P(0) = 1000, B_A(0) = 1000$

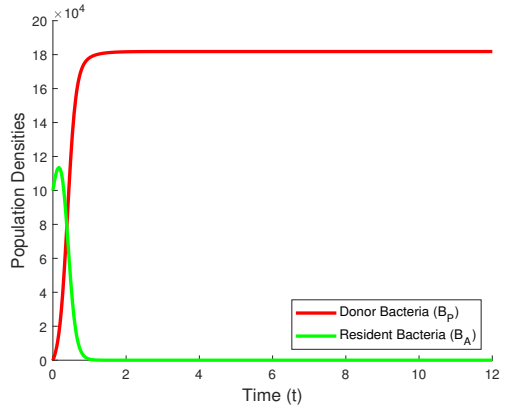

(f) $B_P(0) = 10, B_A(0) = 100000$

Figure 2.6: Numerical simulations of System (2.2.1). In (a)-(f), E^1 is locally asymptotically stable, and any remaining existing equilibria are unstable. In (a) and (b), $\beta = 0$. In (c) and (d), $\eta_2 = 0$. Otherwise, the parameter values are $\alpha_1 = 3, \alpha_2 = 3.7848, K = 200,000, \gamma = 1.1, \eta_2 = 0.4973$, and $\beta = 0.00005$.

2.3 Plasmid Loss and Acquisition Model

In this section, we will explore both plasmid loss and acquisition in a batch culture model. We will analyze the different combinations of System (2.1.1) and System (2.2.1). During this section, we always assume $\eta_1 \neq 0$.

2.3.1 Formulation of Plasmid Loss and Acquisition Model

We build off the previous models and incorporate both plasmid acquisition and loss. Below is the modified system of ordinary differential equations:

$$\begin{aligned}
\frac{dB_P}{dt} &= \underbrace{\alpha_1 B_P \left(1 - \frac{\gamma B_P + B_A}{K}\right)}_{\substack{\text{replication of} \\ \text{plasmid-carrying bacteria}}} - \underbrace{\eta_1 B_P}_{\substack{\text{plasmid} \\ \text{loss}}} + \underbrace{\eta_2 B_A}_{\text{transformation}} + \underbrace{\beta B_P B_A}_{\text{conjugation}}, \\
\frac{dB_A}{dt} &= \underbrace{\alpha_2 B_A \left(1 - \frac{\gamma B_P + B_A}{K}\right)}_{\substack{\text{replication of} \\ \text{plasmid-free bacteria}}} + \underbrace{\eta_1 B_P}_{\substack{\text{plasmid} \\ \text{loss}}} - \underbrace{\eta_2 B_A}_{\text{transformation}} - \underbrace{\beta B_P B_A}_{\text{conjugation}},
\end{aligned} \tag{2.3.1}$$

Table 2.7 lists the model parameters with their descriptions and units.

Variable/Parameter	Description	Units
B_P	Donor/plasmid-carrying bacteria	$cells/\mu L$
B_A	Resident/plasmid-free bacteria	$cells/\mu L$
α_1	Replication rate of donor bacteria	$1/hour$
α_2	Replication rate of resident bacteria	$1/hour$
K	Carrying capacity of the environment	$cells/\mu L$
γ	Relative capacity coefficient of B_P	–
η_1	Rate of conversion from donor to resident bacteria	$1/hour$
η_2	Rate of conversion from resident to donor bacteria	$1/hour$
β	Rate of bacterial conjugation	$\mu L/cells/hour$

Table 2.7: Model (2.3.1) parameters with their descriptions and units.

2.3.2 Analysis of Plasmid Loss and Transformation Model($\eta_1 \neq 0, \eta_2 \neq 0, \beta = 0$)

This subsection assumes $\eta_1, \eta_2 \neq 0$, and $\beta = 0$. The System (2.3.1) is found to have three equilibria. We deduce the criteria for the existence and stability of all equilibria. The stability conditions are then summarized in Table 2.8 and corroborated in Figure 2.7.

By setting the right-hand sides of System (2.3.1) equal to zero, the following three equilibria are found:

$$E^0 = (0,0) = \left(B_P^0, B_A^0\right),$$
$$E^1 = \left(\frac{K\eta_2}{\eta_1 + \eta_2\gamma}, \frac{K\eta_1}{\eta_1 + \eta_2\gamma}\right) = \left(B_P^1, B_A^1\right),$$
$$E^2 = \left(\frac{K(\alpha_1\eta_2 + \alpha_2\eta_1 - \alpha_1\alpha_2)}{\alpha_1(\alpha_1 - \alpha_2\gamma)}, -\frac{K(\alpha_1\eta_2 + \alpha_2\eta_1 - \alpha_1\alpha_2)}{\alpha_2(\alpha_1 - \alpha_2\gamma)}\right) = \left(B_P^2, B_A^2\right).$$

Before considering the stability of the equilibria, one must know when and if each equilibrium is biologically feasible. Recall that the values for B_P and B_A that appear in E^i, where $i = 0, 1, 2$, represent population sizes. Hence, these values must all be non-negative.

E^0: Clearly, $B_P^0 = B_A^0 = 0$ are non-negative. Therefore, E^0 is always biologically feasible and always exists.

E^1: Clearly, $B_P^1 = \dfrac{K\eta_2}{\eta_1 + \eta_2\gamma}$ and $B_A^1 = \dfrac{K\eta_1}{\eta_1 + \eta_2\gamma}$ are non-negative. Therefore, E^1 is always biologically feasible and always exists.

E^2: Lastly, note $B_A^2 = -\dfrac{\alpha_1}{\alpha_2}B_P^2$. This means B_P^2 and B_A^2 are non-negative if and only if they are equal to zero, i.e. when $E^0 = E^2$. Thus, if $E^0 \neq E^2$, E^2 is never biologically feasible. For our purposes, this means E^2 never exists.

Moving forward, only E^0 and E^1 are eligible for analysis.

Next, we establish the stability conditions for the two equilibria E^0 and E^1. The following theorem concerns the local stability of the trivial equilibrium E^0.

Theorem 2.3.1. *The trivial equilibrium E^0 is always unstable.*

Proof. The Jacobian evaluated at E^0 is

$$J\left(E^0\right) = \begin{bmatrix} \alpha_1 - \eta_1 & \eta_2 \\ \eta_1 & \alpha_2 - \eta_2 \end{bmatrix}.$$

Thus,

$$det\left(J\left(E^0\right)\right) = (\alpha_1 - \eta_1)(\alpha_2 - \eta_2) - \eta_1\eta_2 = \alpha_1(\alpha_2 - \eta_2) - \alpha_2\eta_1$$

and

$$tr\left(J\left(E^0\right)\right) = (\alpha_1 - \eta_1) + (\alpha_2 - \eta_2).$$

By the Routh-Hurwitz stability criterion [39], E^0 is stable when $det\left(J\left(E^0\right)\right) > 0$ and $tr\left(J\left(E^0\right)\right) < 0$. The above conditions are never satisfied simultaneously:

$$\begin{aligned} \text{Suppose } det\left(J\left(E^0\right)\right) &= (\alpha_1 - \eta_1)(\alpha_2 - \eta_2) - \eta_1\eta_2 = \alpha_1(\alpha_2 - \eta_2) - \alpha_2\eta_1 > 0 \\ \text{and } tr\left(J\left(E^0\right)\right) &= (\alpha_1 - \eta_1) + (\alpha_2 - \eta_2) < 0. \\ \text{This implies, } (\alpha_1 - \eta_1)(\alpha_2 - \eta_2) &> \eta_1\eta_2 > 0 \text{ and } \alpha_1(\alpha_2 - \eta_2) > \alpha_2\eta_1 > 0. \\ \text{Thus, } (\alpha_1 - \eta_1) &> 0 \text{ and } (\alpha_2 - \eta_2) > 0. \\ \text{Lastly, } tr\left(J\left(E^0\right)\right) &= (\alpha_1 - \eta_1) + (\alpha_2 - \eta_2) > 0. \end{aligned}$$

A contradiction has been reached. In conclusion, the Routh-Hurwitz stability criterion is never satisfied, and E^0 is always unstable. □

Next, we prove that the interior equilibrium E^1 is always locally asymptotically stable.

Theorem 2.3.2. *The interior equilibrium E^1 is always locally asymptotically stable.*

Proof. The Jacobian evaluated at E^1 is

$$J(E_1) = \begin{bmatrix} -\dfrac{\eta_1^2 + \alpha_1\gamma\eta_2 + \gamma\eta_1\eta_2}{\eta_1 + \gamma\eta_2} & \eta_2 - \dfrac{\alpha_1\eta_2}{\eta_1 + \gamma\eta_2} \\ \eta_1 - \dfrac{\alpha_2\gamma\eta_1}{\eta_1 + \gamma\eta_2} & -\eta_2 - \dfrac{\alpha_2\eta_1}{\eta_1 + \gamma\eta_2} \end{bmatrix}.$$

By the Routh-Hurwitz stability criterion [39], E^1 is stable when $det\left(J\left(E^1\right)\right) > 0$ and $tr\left(J\left(E^1\right)\right) < 0$. Clearly,

$$det(J(E^1)) = \alpha_2\eta_1 + \alpha_1\eta_2 > 0,$$

and

$$tr(J(E^1)) = -\frac{\alpha_2\eta_1 + \eta_1^2 + (1+\gamma)\eta_1\eta_2 + \gamma\eta_2(\alpha_1 + \eta_2)}{\eta_1 + \gamma\eta_2} < 0.$$

Thus, E^1 is locally asymptotically stable. □

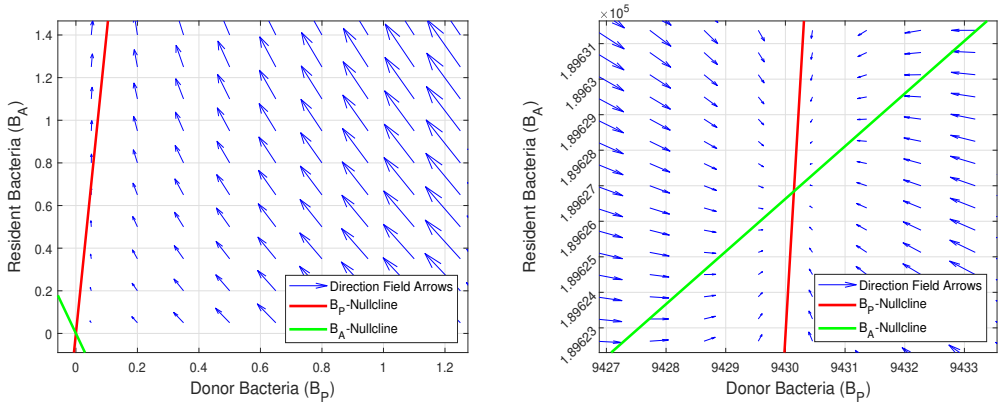

(a) $E^0 = (0,0)$ unstable

(b) $E^1 = \left(\frac{K\eta_2}{\eta_1 + \eta_2\gamma}, \frac{K\eta_1}{\eta_1 + \eta_2\gamma}\right)$ stable

Figure 2.7: Phase portraits of System (2.3.1) when $\eta_1, \eta_2 \neq 0$, and $\beta = 0$. The parameter values in (a) and (b) are $\alpha_1 = 3, \alpha_2 = 3.7848, K = 200,000, \gamma = 1.1, \eta_1 = 10$, and $\eta_2 = 0.4973$. E^0 is unstable, as shown by the direction field arrows moving away from $E^0 = (0,0)$. E^1 is locally asymptotically stable, as shown by the direction field arrows moving toward $E^1 = \left(\frac{K\eta_2}{\eta_1 + \eta_2\gamma}, \frac{K\eta_1}{\eta_1 + \eta_2\gamma}\right)$.

Furthermore, the above stability analysis is summarized in Table 2.8 and supported by the phase portraits in Figure 2.7.

Existence and Stability
E^0 exists and unstable
E^1 exists and stable
E^2 does not exist

Table 2.8: Existence and stability of the equilibria of System (2.3.1) when $\eta_1, \eta_2 \neq 0$, and $\beta = 0$.

2.3.3 Analysis of Plasmid Loss and Conjugation Model($\eta_1 \neq 0, \eta_2 = 0, \beta \neq 0$)

This subsection assumes $\eta_1, \beta \neq 0$, and $\eta_2 = 0$. System (2.3.1) is found to have four equilibria. We deduce the criteria for the existence and stability of all equilibria. The stability conditions are then summarized in Table 2.9 and corroborated in Figures 2.8 and 2.9.

By setting the right-hand sides of System (2.3.1) equal to zero, the following four equilibria are found:

$$E^0 = (0,0) = (B_P^0, B_A^0),$$

$$E^1 = (0,K) = (B_P^1, B_A^1),$$

$$E^2 = \left(\frac{\beta K - \eta_1}{\beta\gamma}, \frac{\eta_1}{\beta}\right) = (B_P^2, B_A^2),$$

$$E^3 = \left(\frac{\alpha_2 K(\alpha_1 - \eta_1)}{\alpha_1(\beta K - \alpha_1 + \alpha_2\gamma)}, -\frac{K(\alpha_1 - \eta_1)}{(\beta K - \alpha_1 + \alpha_2\gamma)}\right) = (B_P^3, B_A^3).$$

Before considering the stability of the equilibria, one must know when and if each equilibrium is biologically feasible. Recall that the values for B_P and B_A that appear in E^i, where $i = 0, 1, 2, 3$, represent population sizes. Hence, these values must all be non-negative.

E^0: Clearly, $B_P^0 = B_A^0 = 0$ are non-negative. Therefore, E^0 is always biologically feasible and always exists.

E^1: Clearly, $B_P^1 = 0$ and $B_A^1 = K$ are non-negative. Therefore, E^1 is always biologically feasible and always exists.

E^2: Clearly, $B_A^2 = \dfrac{\eta_1}{\beta}$ is non-negative. However, $B_P^2 = \dfrac{\beta K - \eta_1}{\beta\gamma}$ is non-negative if and only if $\beta K - \eta_1 > 0$. Therefore, E^2 is biologically feasible and exists if and only if $\beta K - \eta_1 > 0$.

E^3: Lastly, note $B_A^3 = -\dfrac{\alpha_1}{\alpha_2} B_P^3$. This means B_P^3 and B_A^3 are non-negative if and only if they are equal to zero, i.e. when $E^0 = E^3$. Thus, if $E^0 \neq E^3$, E^3 is never biologically feasible. For our purposes, this means E^3 never exists.

Moving forward, E^0 and E^1 are always eligible for analysis. However, E^2 is eligible for analysis only when $\beta K - \eta_1 > 0$.

Next, we establish the stability conditions for the three equilibria E^0, E^1, and E^2. The following theorem concerns the local stability of the trivial equilibrium E^0.

Theorem 2.3.3. *The trivial equilibrium E^0 is always unstable.*

Proof. The Jacobian evaluated at E^0 is

$$J\left(E^0\right) = \begin{bmatrix} \alpha_1 - \eta_1 & 0 \\ \eta_1 & \alpha_2 \end{bmatrix}.$$

Thus,

$$det\left(J\left(E^0\right)\right) = (\alpha_1 - \eta_1)\alpha_2$$

and

$$tr\left(J\left(E^0\right)\right) = (\alpha_1 - \eta_1) + \alpha_2.$$

By the Routh-Hurwitz stability criterion [39], E^0 is stable when $det\left(J\left(E^0\right)\right) > 0$ and $tr\left(J\left(E^0\right)\right) < 0$. The above conditions are never satisfied simultaneously:

$$\text{Suppose } det\left(J\left(E^0\right)\right) = (\alpha_1 - \eta_1)\alpha_2 > 0 \text{ and } tr\left(J\left(E^0\right)\right) = (\alpha_1 - \eta_1) + \alpha_2 < 0.$$

$$\text{Thus, } (\alpha_1 - \eta_1) > 0 \text{ and } tr\left(J\left(E^0\right)\right) = (\alpha_1 - \eta_1) + \alpha_2 > 0.$$

A contradiction has been reached. In conclusion, the Routh-Hurwitz stability criterion is never satisfied, and E^0 is always unstable. □

Next, we prove that the boundary equilibrium E^1 is locally asymptotically stable when $\beta K - \eta_1 < 0$.

Theorem 2.3.4. *The boundary equilibrium E^1 is locally asymptotically stable if and only if $\beta K - \eta_1 < 0$.*

Proof. The Jacobian evaluated at E^1 is

$$J(E_1) = \begin{bmatrix} \beta K - \eta_1 & 0 \\ \eta_1 - \gamma\alpha_2 & -\alpha_2 \end{bmatrix}.$$

By the Routh-Hurwitz stability criterion [39], E^1 is stable when $det\left(J\left(E^1\right)\right) > 0$ and $tr\left(J\left(E^1\right)\right) < 0$. Since $\beta K - \eta_1 < 0$, clearly

$$det\left(J\left(E^1\right)\right) = -(\beta K - \eta_1)\alpha_2 > 0$$

and

$$tr\left(J\left(E^1\right)\right) = (\beta K - \eta_1) - \alpha_2 < 0.$$

Thus, E^1 is locally asymptotically stable if and only if $\beta K - \eta_1 < 0$. □

Next, we prove that the interior equilibrium E^2 is locally asymptotically stable when $0 < \beta K - \eta_1$.

Theorem 2.3.5. *The boundary equilibrium E^2 is locally asymptotically stable if and only if $0 < \beta K - \eta_1$.*

Proof. The Jacobian evaluated at E^2 is

$$J(E_2) = \begin{bmatrix} \alpha_1\left(\frac{\eta_1}{K\beta} - 1\right) & \frac{(\beta K - \alpha_1)(\beta K - \eta_1)}{\beta\gamma K} \\ -\frac{\alpha_2\eta_1\gamma}{\beta K} & \eta_1\left(\frac{1}{\gamma} - \frac{\alpha_2}{\beta K}\right) - \frac{\beta K}{\gamma} \end{bmatrix}.$$

By the Routh-Hurwitz stability criterion [39], E^1 is stable when $det\left(J\left(E^1\right)\right) > 0$ and $tr\left(J\left(E^1\right)\right) < 0$. Since $0 < \beta K - \eta_1$, clearly

$$det\left(J\left(E^2\right)\right) = \frac{(\beta K - \eta_1)[\alpha_1(\beta K - \eta_1) + \alpha_2\eta_1\gamma]}{\beta\gamma K} > 0$$

and

$$tr\left(J\left(E^2\right)\right) = \frac{-\alpha_2\eta_1\gamma - \alpha_1\gamma(\beta K - \eta_1) - \beta K(\beta K - \eta_1)}{\beta\gamma K} < 0.$$

Thus, E^2 is locally asymptotically stable if and only if $0 < \beta K - \eta_1$. □

Existence and Stability	
$\beta K - \eta_1 < 0$	$0 < \beta K - \eta_1$
E^0 exists and unstable	E^0 exists and unstable
E^1 exists and stable	E^1 exists and unstable
E^2 does not exist	E^2 exists and stable
E^3 does not exist	E^3 does not exist

Table 2.9: Existence and stability conditions of the equilibria of System (2.3.1) when $\eta_1, \beta \neq 0$, and $\eta_2 = 0$.

Furthermore, the above stability analysis is summarized in Table 2.9 and supported by the phase portraits in Figures 2.8 and 2.9. As the model analysis indicates, the relationship between the parameters, β, η_1, and K, is instrumental in understanding the population dynamics of donor and resident bacteria. The stability analysis reveals two scenarios:

1. If the plasmid loss rate, η_1, is greater than the conjugation potential, βK, then the trivial equilibrium, $E^0 = (0, 0)$, is unstable, the boundary equilibrium, $E^1 = (0, K)$, is locally asymptotically stable, and the interior equilibrium, $E^2 = \left(\frac{\beta K - \eta_1}{\beta\gamma}, \frac{\eta_1}{\beta}\right)$, does not exist. In other words, if the plasmid loss is greater than the plasmid acquisition, only the plasmid-free resident bacteria,

B_A, will persist when introduced to a controlled and closed environment as inferred by Figure 2.8 and the lone stability of

$$E^1 = (B_P, B_A) = (0, K)\,.$$

2. If the plasmid loss rate, η_1, is less the conjugation potential, βK, then the trivial and boundary equilibrium, $E^0 = (0, 0)$ and $E^1 = (0, K)$, are unstable and the interior equilibrium, $E^2 = \left(\dfrac{\beta K - \eta_1}{\beta\gamma}, \dfrac{\eta_1}{\beta}\right)$, is locally asymptotically stable. In other words, if the plasmid loss is less than the plasmid acquisition, both the donor and resident bacteria, B_P and B_A, will persist when introduced to a controlled and closed environment as inferred by Figure 2.9 and the lone stability of

$$E^2 = \left(\frac{\beta K - \eta_1}{\beta\gamma}, \frac{\eta_1}{\beta}\right).$$

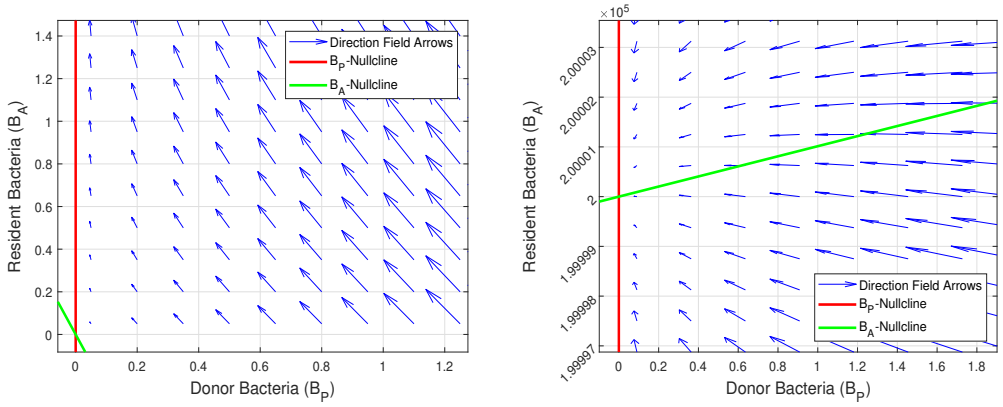

(a) $E^0 = (0, 0)$ always unstable (b) $E^1 = (0, K)$ stable when $\beta K - \eta_1 < 0$

Figure 2.8: Phase portraits of System (2.3.1) when $\eta_1, \beta \neq 0, \eta_2 = 0$, and $\beta K - \eta_1 < 0$. In (a) and (b), the parameter values are $\alpha_1 = 3, \alpha_2 = 3.7848, K = 200,000, \gamma = 1.1, \eta_1 = 10, \eta_2 = 0.4973$, and $\beta = 0.00001$. E^0 is unstable, as shown by the direction field arrows moving away from $E^0 = (0, 0)$. E^1 is locally asymptotically stable because $\beta K - \eta_1 < 0$ when $\beta = 0.00001$, as shown by the direction field arrows moving toward $E^1 = (0, K)$.

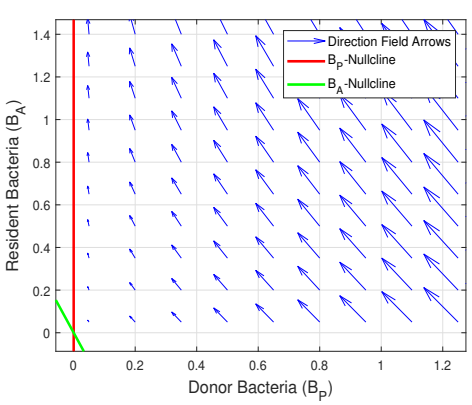

(a) $E^0 = (0, 0)$ always unstable

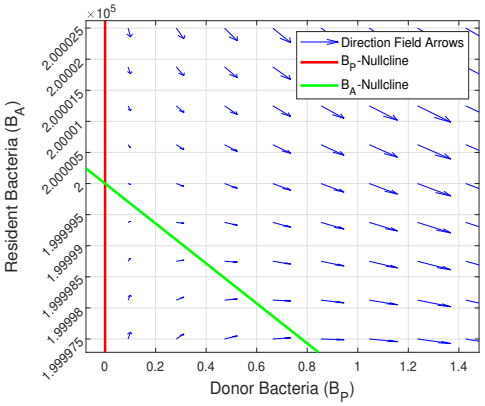

(b) $E^1 = (0, K)$ unstable when $0 < \beta K - \eta_1$

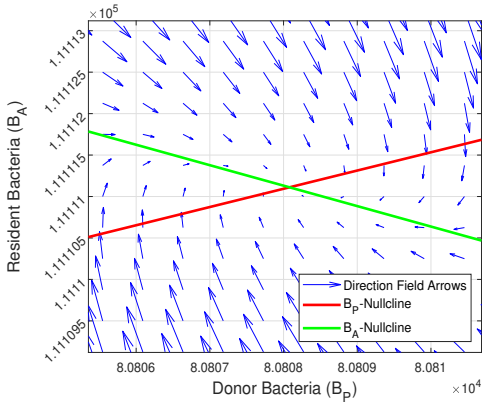

(c) $E^2 = \left(\dfrac{\beta K - \eta_1}{\beta\gamma}, \dfrac{\eta_1}{\beta}\right)$ stable when $0 < \beta K - \eta_1$

Figure 2.9: Phase portraits of System (2.3.1) when $\eta_1, \beta \neq 0, \eta_2 = 0$, and $0 < \beta K - \eta_1$. In (a)-(c), the parameter values are $\alpha_1 = 3, \alpha_2 = 3.7848, K = 200,000, \gamma = 1.1, \eta_1 = 10, \eta_2 = 0.4973$, and $\beta = 0.00009$. E^0 is unstable, as shown by the direction field arrows moving away from $E^0 = (0, 0)$. E^1 is unstable because $0 < \beta K - \eta_1$ when $\beta = 0.00009$, as shown by the direction field arrows moving away from $E^1 = (0, K)$. E^2 is locally asymptotically stable because $0 < \beta K - \eta_1$ when $\beta = 0.00009$, as shown by the direction field arrows moving toward $E^2 = \left(\dfrac{\beta K - \eta_1}{\beta\gamma}, \dfrac{\eta_1}{\beta}\right)$.

In the stability analysis above, we found that the long-term behavior of System (2.3.1) when $\eta_1, \beta \neq 0,$ and $\eta_2 = 0$ depends on parameter values. We will conduct a more detailed numerical investigation of the system's behavior by examining how

each equilibrium changes with variations in each, β and η_1. We create one-parameter bifurcation diagrams by varying each parameter separately, as shown in Figure 2.10:

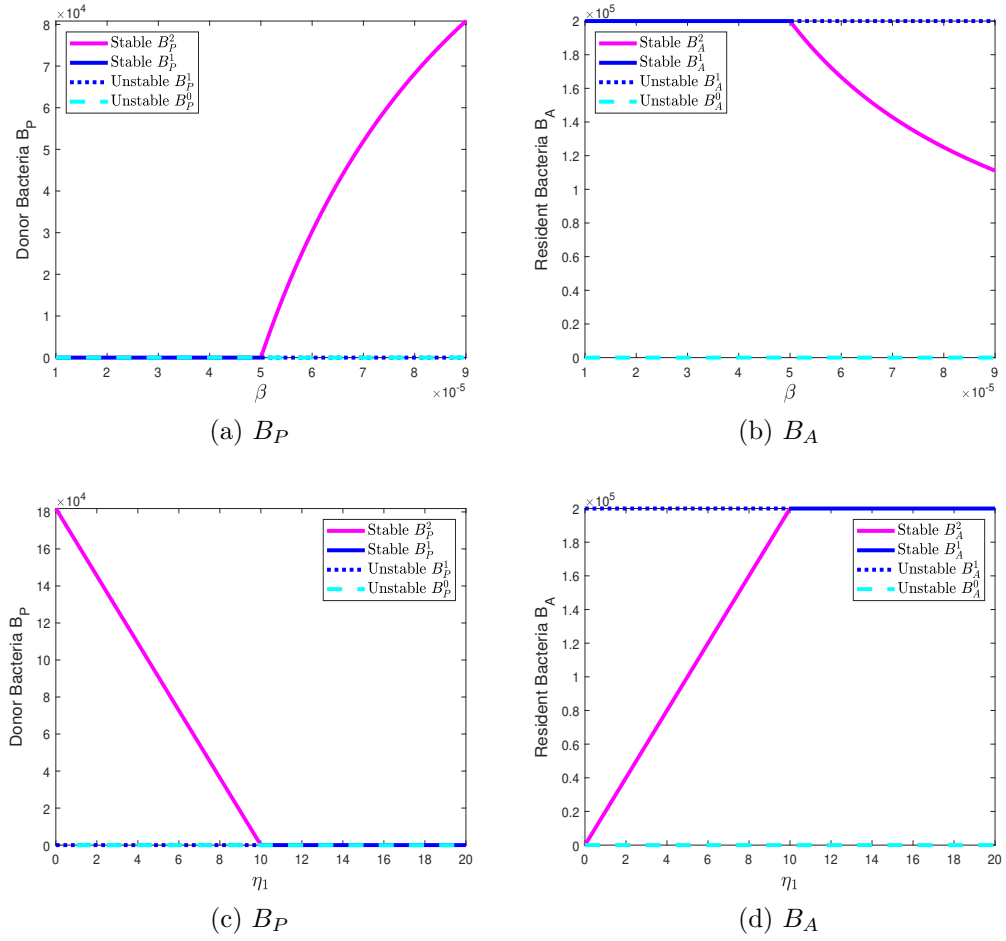

(a) B_P (b) B_A

(c) B_P (d) B_A

Figure 2.10: Bifurcation diagrams of System (2.3.1), when $\eta_1, \beta \neq 0,$ and $\eta_2 = 0$, for the donor bacteria B_P in (a) and (c), and resident bacteria B_A in (b) and (d). In (a)-(d), $\alpha_1 = 3, \alpha_2 = 3.7848, K = 200,000$, and $\gamma = 1.1$. In (a) and (b), $\eta_1 = 10$ and the steady-state values are plotted as a function of β as it changes in $[1 \times 10^{-5}, 9 \times 10^{-5}]$. In (c) and (d), $\beta_1 = 5 \times 10^{-5}$ and the steady-state values are plotted as a function of η_1 as it changes in $[0, 20]$. In the diagrams, solid lines show stable states, and dashed or dotted lines show unstable states. The trivial equilibrium, E^0, is always unstable. The boundary equilibrium, E^1, is locally asymptotically stable when $\beta < 5 \times 10^{-5}$ or equivalently, when $10 < \eta_1$. Otherwise, E^1 is unstable. The interior equilibrium, E^2, is locally asymptotically stable when $5 \times 10^{-5} < \beta$ or equivalently, when $\eta_1 < 10$. Otherwise, E^2 does not exist.

We hold all model parameters constant and adjust a single parameter within the biologically meaningful intervals of $(1 \times 10^{-5}, 9 \times 10^{-5})$ for β in 2.10 (a)-(b), or $(0, 20)$ for η_1 in 2.10 (c)-(d). The bifurcation occurs at $\beta = 5 \times 10^{-5}$, or equivalently, $\eta_1 = 10$.

As shown in the diagrams, if $\beta < 5 \times 10^{-5}$ or $\eta_1 > 10$, System (2.3.1) ($\eta_1, \beta \neq 0$, and $\eta_2 = 0$) only has two equilibria, E^0 and E^1, with only E^1 being locally asymptotically stable. This represents the persistence of resident bacteria and complete plasmid elimination. On the other hand, if $\beta > 5 \times 10^{-5}$ or $\eta_1 < 10$, there are three equilibria, E^0, E^1, and E^2, with only E^2 being locally asymptotically stable. This scenario represents the co-existence and persistence of resident and donor bacteria and the successful establishment of plasmids in the system.

2.3.4 Analysis of Plasmid Loss, Conjugation, and Transformation Model ($\eta_1 \neq 0, \eta_2 \neq 0, \beta \neq 0$)

This subsection assumes $\eta_1, \eta_2, \beta \neq 0$. System (2.3.1) is found to have four equilibria. We deduce criteria for the existence and stability of all equilibria. The stability conditions are then summarized in Table 2.10 and corroborated in Figure 3.1.

By setting the right-hand sides of System (2.3.1) equal to zero, the following four equilibria are found:

$$E^0 = (0,0) = \left(B_P^0, B_A^0\right),$$
$$E^1 = \left(B_P^1, B_A^1\right),$$
$$E^2 = \left(B_P^2, B_A^2\right),$$
$$E^3 = \left(\frac{K(\alpha_1\eta_2 + \alpha_2\eta_1 - \alpha_1\alpha_2)}{\alpha_1(\alpha_1 - \alpha_2\gamma - K\beta)}, -\frac{K(\alpha_1\eta_2 + \alpha_2\eta_1 - \alpha_1\alpha_2)}{\alpha_2(\alpha_1 - \alpha_2\gamma - K\beta)}\right) = \left(B_P^3, B_A^3\right),$$

where

$$B_P^1 = \frac{K\beta - \eta_1 - \gamma\eta_2 + \sqrt{(K\beta - \eta_1 - \gamma\eta_2)^2 + 4\beta K\gamma\eta_2}}{2\beta\gamma},$$
$$B_A^1 = \frac{K\beta + \eta_1 + \gamma\eta_2 - \sqrt{(K\beta + \eta_1 + \gamma\eta_2)^2 - 4\beta K\eta_1}}{2\beta},$$

and

$$B_P^2 = \frac{K\beta - \eta_1 - \gamma\eta_2 - \sqrt{(K\beta - \eta_1 - \gamma\eta_2)^2 + 4\beta K\gamma\eta_2}}{2\beta\gamma},$$
$$B_A^2 = \frac{K\beta + \eta_1 + \gamma\eta_2 + \sqrt{(K\beta + \eta_1 + \gamma\eta_2)^2 - 4\beta K\eta_1}}{2\beta}.$$

Before considering the stability of the equilibria, one must know when and if each equilibrium is biologically feasible. Recall that the values for B_P and B_A that appear in E^i, where $i = 0, 1, 2, 3$, represent population sizes. Hence, these values must all be non-negative.

E^0: Clearly, $B_P^0 = B_A^0 = 0$ are non-negative. Therefore, E^0 is always biologically feasible and always exists.

E^1: Notice that B_P^1's denominator, $2\beta\gamma$, is positive. Therefore, B_P^1 is non-negative if and only if B_P^1's numerator is non-negative. Notice

$$(K\beta - \eta_1 - \gamma\eta_2)^2 < (K\beta - \eta_1 - \gamma\eta_2)^2 + 4K\beta\gamma\eta_2$$
$$-(K\beta - \eta_1 - \gamma\eta_2) \leq |K\beta - \eta_1 - \gamma\eta_2| < \sqrt{(K\beta - \eta_1 - \gamma\eta_2)^2 + 4K\beta\gamma\eta_2}$$
$$0 < (K\beta - \eta_1 - \gamma\eta_2) + \sqrt{(K\beta - \eta_1 - \gamma\eta_2)^2 + 4K\beta\gamma\eta_2}$$

and so B_P^1's numerator and, consequently, B_P^1 are non-negative.

Notice that B_A^1's denominator, 2β, is positive. Therefore, B_A^1 is non-negative if and only if B_A^1's numerator is non-negative. Notice

$$(K\beta + \eta_1 + \gamma\eta_2)^2 > (K\beta + \eta_1 + \gamma\eta_2)^2 - 4K\beta\eta_1$$
$$K\beta + \eta_1 + \gamma\eta_2 = |K\beta + \eta_1 + \gamma\eta_2| > \sqrt{(K\beta + \eta_1 + \gamma\eta_2)^2 - 4K\beta\eta_1}$$

$$K\beta + \eta_1 + \gamma\eta_2 - \sqrt{(K\beta + \eta_1 + \gamma\eta_2)^2 - 4K\beta\eta_1} > 0$$

and so B_A^1's numerator and, consequently, B_A^1 are non-negative. Thus, E^1 is always biologically feasible and always exists.

E^2: Notice that B_P^2's denominator, $2\beta\gamma$, is positive. Therefore, B_P^2 is non-negative if and only if B_P^2's numerator is non-negative. However, notice

$$(K\beta - \eta_1 - \gamma\eta_2)^2 < (K\beta - \eta_1 - \gamma\eta_2)^2 + 4K\beta\gamma\eta_2$$
$$K\beta - \eta_1 - \gamma\eta_2 \leq |K\beta - \eta_1 - \gamma\eta_2| < \sqrt{(K\beta - \eta_1 - \gamma\eta_2)^2 + 4K\beta\gamma\eta_2}$$
$$K\beta - \eta_1 - \gamma\eta_2 - \sqrt{(K\beta - \eta_1 - \gamma\eta_2)^2 + 4K\beta\gamma\eta_2} < 0$$

and so B_P^2's numerator and, consequently, B_P^2 are negative. Thus, E^2 is never biologically feasible and never exists.

E^3: Lastly, note $B_A^3 = -\frac{\alpha_1}{\alpha_1} B_P^3$. This means B_P^3 and B_A^3 are non-negative if and only if they are equal to zero, i.e. when $E^0 = E^3$. Thus, if $E^0 \neq E^3$, E^3 is never biologically feasible. For our purposes, this means E^3 never exists.

Moving forward, only E^0 and E^1 are eligible for analysis.

Next, we establish the stability conditions for the two equilibria E^0 and E^1. The following theorem concerns the local stability of the trivial equilibrium E^0.

Theorem 2.3.6. *The trivial equilibrium E^0 is always unstable.*

Proof. The Jacobian evaluated at E^0 is

$$J\left(E^0\right) = \begin{bmatrix} \alpha_1 - \eta_1 & \eta_2 \\ \eta_1 & \alpha_2 - \eta_2 \end{bmatrix}.$$

Thus,

$$det\left(J\left(E^0\right)\right) = (\alpha_1 - \eta_1)(\alpha_2 - \eta_2) - \eta_1\eta_2 = \alpha_1(\alpha_2 - \eta_2) - \alpha_2\eta_1$$

and

$$tr\left(J\left(E^0\right)\right) = (\alpha_1 - \eta_1) + (\alpha_2 - \eta_2).$$

By the Routh-Hurwitz stability criterion [39], E^0 is stable when $det\left(J\left(E^0\right)\right) > 0$ and $tr\left(J\left(E^0\right)\right) < 0$. The above conditions are never satisfied simultaneously:

$$\text{Suppose } det\left(J\left(E^0\right)\right) = (\alpha_1 - \eta_1)(\alpha_2 - \eta_2) - \eta_1\eta_2 = \alpha_1(\alpha_2 - \eta_2) - \alpha_2\eta_1 > 0$$
$$\text{and } tr\left(J\left(E^0\right)\right) = (\alpha_1 - \eta_1) + (\alpha_2 - \eta_2) < 0.$$
$$\text{This implies, } (\alpha_1 - \eta_1)(\alpha_2 - \eta_2) > \eta_1\eta_2 > 0 \text{ and } \alpha_1(\alpha_2 - \eta_2) > \alpha_2\eta_1 > 0.$$
$$\text{Thus, } (\alpha_1 - \eta_1) > 0 \text{ and } (\alpha_2 - \eta_2) > 0.$$
$$\text{Lastly, } tr\left(J\left(E^0\right)\right) = (\alpha_1 - \eta_1) + (\alpha_2 - \eta_2) > 0.$$

A contradiction has been reached. In conclusion, the Routh-Hurwitz stability criterion is never satisfied, and E^0 is always unstable. □

Next, we prove that the interior equilibrium E^1 is always locally asymptotically stable.

Theorem 2.3.7. *The interior equilibrium E^1 is always locally asymptotically stable.*

Proof. The Jacobian evaluated at E^1 is

$$J\left(E^1\right) = \begin{bmatrix} \beta B_A^1 - \frac{\alpha_1}{K}B_A^1 - 2\frac{\alpha_1\gamma}{K}B_P^1 + \alpha_1 - \eta_1 & \left(\beta - \frac{\alpha_1}{K}\right)B_P^1 + \eta_2 \\ \\ \left(-\beta - \frac{\alpha_2\gamma}{K}\right)B_A^1 + \eta_1 & -\beta B_P^1 - \frac{\alpha_2\gamma}{K}B_P^1 - 2\frac{\alpha_2}{K}B_A^1 + \alpha_2 - \eta_2 \end{bmatrix}.$$

By the Routh-Hurwitz stability criterion [39], E^1 is stable when $det\left(J\left(E^1\right)\right) > 0$ and $tr\left(J\left(E^1\right)\right) < 0$. Clearly

$$det\left(J\left(E^1\right)\right) = \frac{\sqrt{(\eta_1 + \gamma\eta_2 - K\beta)^2 + 4K\beta\gamma\eta_2}}{K}\left(\alpha_1 B_P^1 + \alpha_2 B_A^1\right) > 0$$

and

$$tr\left(J\left(E^1\right)\right) = \frac{1}{2}X - \beta B_P^1 - \frac{\alpha_1\gamma}{K}B_P^1 - \frac{\alpha_2}{K}B_A^1 - \eta_2 < 0$$

since

$$X = K\beta - \eta_1 + \gamma\eta_2 - \sqrt{(K\beta - \eta_1 + \gamma\eta_2)^2 + 4\gamma\eta_1\eta_2} < 0,$$

as shown below:

$$(K\beta - \eta_1 + \gamma\eta_2)^2 < (K\beta - \eta_1 + \gamma\eta_2)^2 + 4\gamma\eta_1\eta_2$$
$$K\beta - \eta_1 + \gamma\eta_2 \leq |K\beta - \eta_1 + \gamma\eta_2| < \sqrt{(K\beta - \eta_1 + \gamma\eta_2)^2 + 4\gamma\eta_1\eta_2}$$
$$X = K\beta - \eta_1 + \gamma\eta_2 - \sqrt{(K\beta - \eta_1 + \gamma\eta_2)^2 + 4\gamma\eta_1\eta_2} < 0.$$

Thus, E^1 is always locally asymptotically stable. □

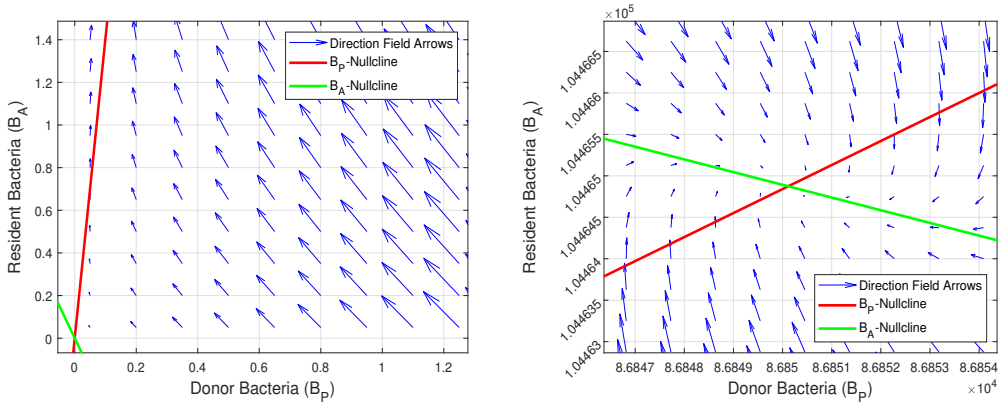

(a) $E^0 = (0, 0)$ unstable

(b) $E^1 = \left(B_P^1, B_A^1\right)^*$ stable

Figure 2.11: Phase portraits of System (2.3.1) when $\eta_1, \eta_2, \beta \neq 0$. In (a) and (b), the parameter values are $\alpha_1 = 3, \alpha_2 = 3.7848, K = 200,000, \gamma = 1.1, \eta_1 = 10, \eta_2 = 0.4973$, and $\beta = 0.00009$. E^0 is unstable, as shown by the direction field arrows moving away from $E^0 = (0, 0)$. E^1 is locally asymptotically, as shown by the direction field arrows moving toward $E^1 = \left(\frac{K\beta - \eta_1 - \gamma\eta_2 + \sqrt{(K\beta - \eta_1 - \gamma\eta_2)^2 + 4\beta K\gamma\eta_2}}{2\beta\gamma}, \frac{K\beta + \eta_1 + \gamma\eta_2 - \sqrt{(K\beta + \eta_1 + \gamma\eta_2)^2 - 4\beta K\eta_1}}{2\beta}\right)$.

Furthermore, the above stability analysis is summarized in Table 2.10 and supported by the phase portraits in Figure 3.1.

Existence and Stability
E^0 exists and unstable
E^1 exists and stable
E^2 does not exist
E^3 does not exist

Table 2.10: Existence and stability of the equilibria of System (2.3.1) when $\eta_1, \eta_2, \beta \neq 0$.

2.3.5 Numerical Simulations and Discussion

In this subsection, we discuss simulations of System (2.3.1), which were created using the Matlab® `ode45 or ode89` solvers. In this model, there are two plasmid dynamics, plasmid loss, and plasmid acquisition, which can manifest in two different ways: transformation and conjugation. Hence, conversion happens in both directions.

1. Resident bacteria, B_A, can gain plasmids and become donor bacteria, B_P.
2. Donor bacteria, B_P, can lose their plasmids and become resident bacteria, B_A.

This creates the possibility of balance within the system. It makes sense that the system usually approaches a steady state where both the plasmid-carrying donor bacteria, B_P, and the plasmid-free resident bacteria, B_A, persist as inferred by Figure 2.12 and the stability of

$$E^1 = \left(\frac{K\eta_2}{\eta_1 + \eta_2\gamma}, \frac{K\eta_1}{\eta_1 + \eta_2\gamma}\right) \text{ when } \eta_1, \eta_2 \neq 0 \text{ and } \beta = 0 \text{ in 2.12 (a)-(b)},$$
$$E^2 = \left(\frac{\beta K - \eta_1}{\beta\gamma}, \frac{\eta_1}{\beta}\right) \text{ when } \eta_1, \beta \neq 0 \text{ and } \eta_2 = 0 \text{ and } 0 < K\beta - \eta_1 \text{ in 2.12 (c)-(d)},$$
$$E^1 = \left(B_P^1, B_A^1\right) \text{ when } \eta_1, \eta_2, \beta \neq 0 \text{ in 2.12 (e)-(f)},$$

where

$$B_P^1 = \frac{K\beta - \eta_1 - \gamma\eta_2 + \sqrt{(K\beta - \eta_1 - \gamma\eta_2)^2 + 4\beta K\gamma\eta_2}}{2\beta\gamma},$$
$$B_A^1 = \frac{K\beta + \eta_1 + \gamma\eta_2 - \sqrt{(K\beta + \eta_1 + \gamma\eta_2)^2 - 4\beta K\eta_1}}{2\beta}.$$

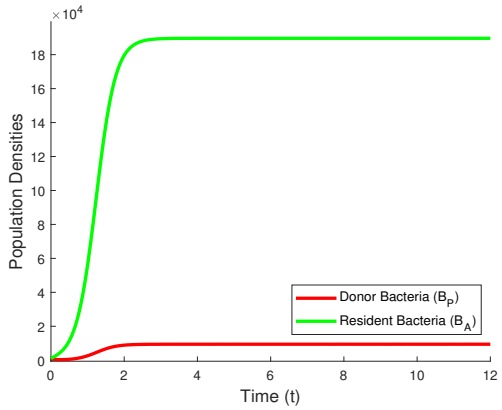

(a) $B_P(0) = 1000, B_A(0) = 1000$

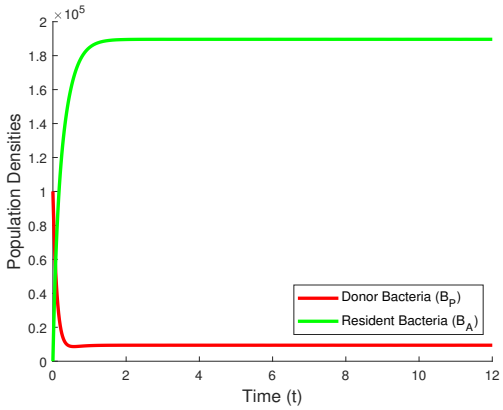

(b) $B_P(0) = 100000, B_A(0) = 10$

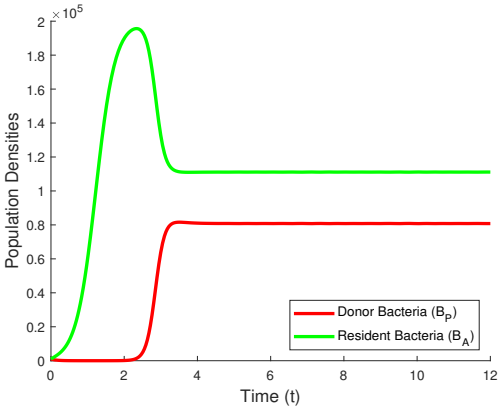

(c) $B_P(0) = 1000, B_A(0) = 1000$

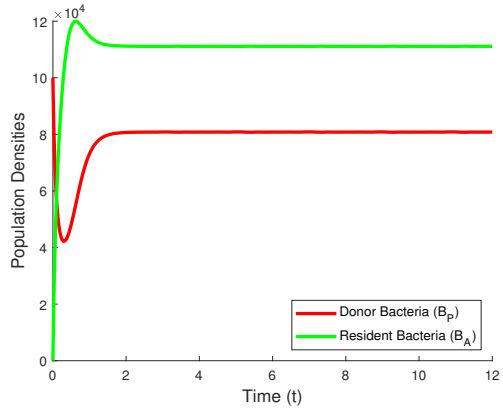

(d) $B_P(0) = 100000, B_A(0) = 10$

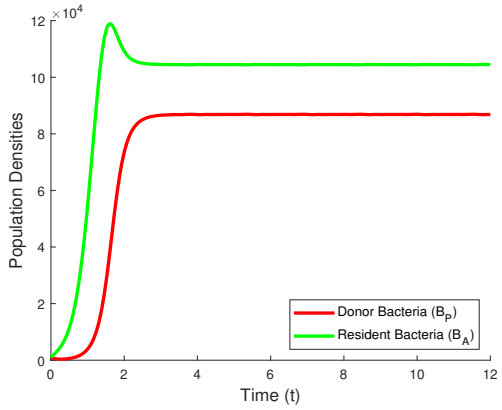

(e) $B_P(0) = 1000, B_A(0) = 1000$

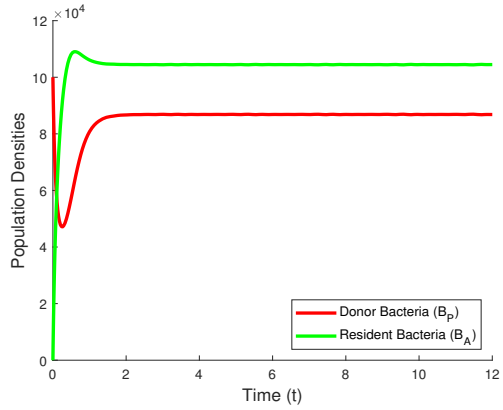

(f) $B_P(0) = 100000, B_A(0) = 10$

Figure 2.12: Numerical simulations of System (2.3.1). In (a) and (b), $\beta = 0$. In (c) and (d), $\eta_2 = 0$. Otherwise, the parameter values are $\alpha_1 = 3, \alpha_2 = 3.7848, K = 200,000, \gamma = 1.1, \eta_1 = 10, \eta_2 = 0.4973$, and $\beta = 0.00009$.

However, when $\eta_2 = 0$ and $K\beta - \eta_1 < 0$ the stable equilibrium becomes

$$E^1 = (0, K),$$

as shown by Figure 2.13 (a)-(b). Furthermore, this shows a scenario where the plasmid-carrying donor bacteria, B_P, can be eliminated in this double-dynamic system. In contrast, the plasmid-free resident bacteria, B_A, always persists in System (2.3.1).

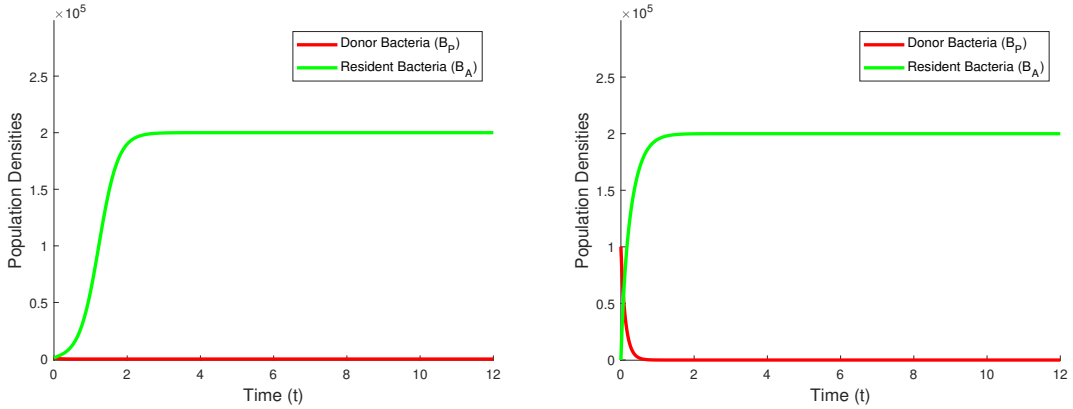

(a) $B_P(0) = 1000, B_A(0) = 1000$ (b) $B_P(0) = 100000, B_A(0) = 10$

Figure 2.13: Numerical simulations of System (2.3.1) when $\eta_1, \beta \neq 0$, and $\eta_2 = 0$. In (a) and (b), the parameter values are $\alpha_1 = 3, \alpha_2 = 3.7848, K = 200,000, \gamma = 1.1, \eta_1 = 10$, and $\beta = 0.00001$.

Note the overall outcome of all simulations in Figure 2.12: $B_P > 0$ and $B_A > 0$, i.e., co-existence. In (a), (c), and (e), the initial population sizes are identical and $\frac{1}{200}$ of the carrying capacity, K. However, in (b), (d), and (f), $B_P(0)$ is 100 times bigger, and $B_A(0)$ is 100 times smaller in comparison to (a), (c), and (e). Still, all outcomes are similar in Figure 2.12.

Now, note the overall outcome of simulations in Figure 2.13: $B_P = 0$ and $B_A = K$. In (a), the initial population sizes are identical and $\frac{1}{200}$ of the carrying capacity, K. However, in (b), $B_P(0)$ is 100 times bigger, and $B_A(0)$ is 100 times smaller in comparison to (a). Still, the outcome is identical.

Most of the time, any initial condition with at least one positive value will lead to co-existence, as pictured in Figure 2.12. However, if $\eta_2 = 0$ and $\beta K - \eta_1 < 0$, any initial condition with at least one positive value will lead to the persistence of B_A and extinction of B_P, as pictured in Figure 2.13. In summary, all numerical simulations of System (2.3.1) can be categorized into three outcomes:

1. If $B_P(0) = B_A(0) = 0$, then the system will remain at $E^0 = (0, 0) = \left(B_P^0, B_A^0\right)$.
2. If $\eta_1, \beta \neq 0, \eta_2 = 0$, $\beta K - \eta_1 < 0$, and $B_P(0) > 0$ or $B_A(0) > 0$

   OR

   $\eta_1, \beta \neq 0, \eta_2 = 0, B_P(0) = 0$, and $B_A(0) = K$,

   the system will trend towards and stabilize at $B_P = 0$ and $B_A = K$.
3. Otherwise, the system will trend towards and stabilize at co-existence where $B_P > 0$ and $B_A > 0$.

It's important to consider how to keep plasmid-carrying donor bacteria, B_P, in the system when $\eta_2 = 0$, and $\beta K - \eta_1 < 0$. In other words, how can we maintain donor bacteria when the system naturally eliminates all plasmids? If B_P is administered like a medicine, how many "doses" does it take to maintain a certain level of B_P in the system? How do the pertinent parameters, K, β, and η_1 affect these dosages?

The peaks of B_P in Figure 2.14 represent the "doses" required to maintain $B_P > \dfrac{K}{4}$ over the span of 2 hours. In Figure 2.14 (a), the doses seem farther apart as time progresses. Recall the conjugation term in System (2.3.1), $\beta B_P B_A$, and note an increase in B_A increases plasmid acquisition, which, in turn, increases plasmid-carrying donor bacteria, B_P. Thus, an increase in B_A can help temporarily delay the elimination of the plasmid-carrying donor population, B_P. Since B_A initially increases rapidly, B_P elimination slows, and dosages become farther apart. The dosage frequency later stabilizes alongside B_A's growth.

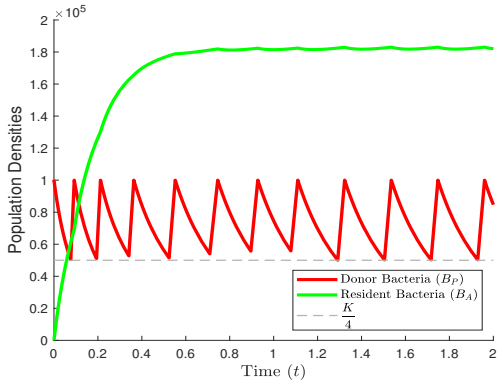

(a) 12 doses

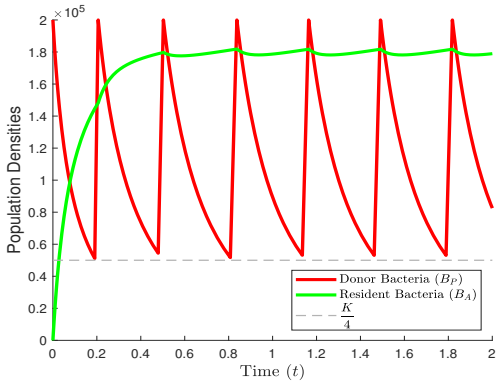

(b) $B_P(0) = K$; 7 doses

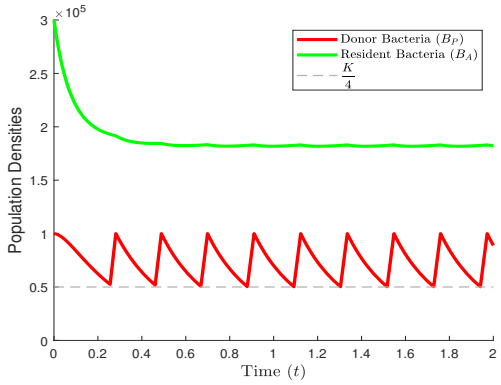

(c) $B_A(0) = \frac{3K}{2}$; 10 doses

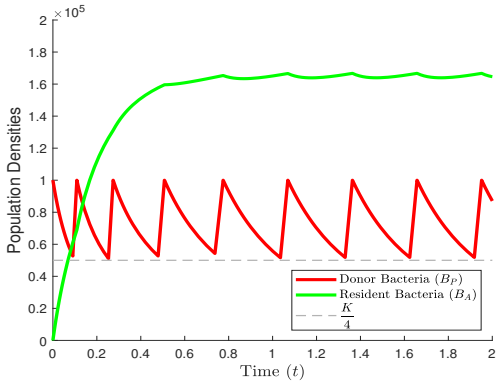

(d) $\eta_1 = 10.1$; 9 doses

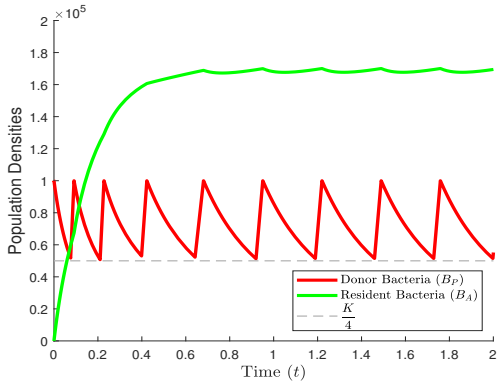

(e) $\beta = 5.9 \times 10^{-5}$; 9 doses

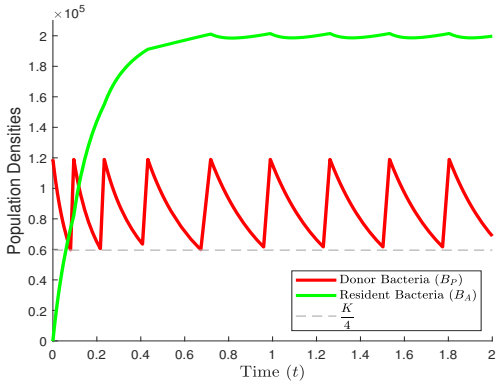

(f) $K = 238000$; 9 doses

Figure 2.14: Numerical simulations of System (2.3.1) when $\eta_1, \beta \neq 0, \eta_2 = 0$, and $\beta K - \eta_1 < 0$. Unless otherwise stated above, the parameter values and initial conditions in (a)-(f) are $\alpha_1 = 3, \alpha_2 = 3.7848, \gamma = 1.1, \eta_1 = 12, \beta = 5 \times 10^{-5}, K = 200,000, B_P(0) = \frac{K}{2}$, and $B_A = 10$. The initial condition for B_P is routinely reset to ensure $B_P > \frac{K}{4}$.

In Figure 2.14 (b), increasing the dosage from $\frac{K}{2}$ in (a) to K in (b) reduces the number of doses necessary to maintain $B_P > \frac{K}{4}$ because higher dosages of B_P take longer to eliminate.

In Figure 2.14 (c), $B_A(0) = \frac{3K}{2}$ is $30,000$ times greater than $B_A(0) = 10$ in (a). Similar to the previous rationale, since $B_A(0)$ is initially much greater, B_P elimination slows, and doses are initially farther apart than those initially seen in (a). Thus, greater initial population sizes can allow for an initial lower dose frequency.

In Figure 2.14 (d), $\eta_1 = 10.1$ is smaller than $\eta_1 = 12$ in (a). Recall the plasmid loss term in System (2.3.1), $\eta_1 B_P$, and note a smaller η_1 decreases plasmid loss and, in turn, increases plasmid-carrying donor bacteria, B_P. Thus, doses can decrease and maintain the same minimum level of B_P with a lower η_1.

In Figure 2.14 (e), $\beta = 5.9 \times 10^{-5}$ is greater than $\beta = 5 \times 10^{-5}$ in (a). Recall the conjugation term in System (2.3.1), $\beta B_P B_A$, and note a greater β increases plasmid acquisition and, in turn, increases plasmid-carrying donor bacteria, B_P. Thus, doses can decrease and maintain the same minimum level of B_P with a greater β.

In Figure 2.14 (f), $K = 238,000$ is greater than $K = 200,000$ in (a). Recall the conjugation term in System (2.3.1), $\beta B_P B_A$, and note a larger K increases both B_P and B_A, which increases plasmid acquisition and, in turn, further increases plasmid-carrying donor bacteria, B_P. Thus, doses can decrease and maintain the same minimum level of B_P with a greater K.

Below are ways to decrease the required doses and maintain B_P above an arbitrary minimum value.

$\left(B_P(t_i)^{\uparrow}\right)$ An increase ($\uparrow$) of B_P in each dosage at times, t_i, will decrease ($\downarrow$) the doses required.

$\left(B_A(0)^{\uparrow}\right)$ An increase ($\uparrow$) in $B_A(0)$, the initial amount of B_A introduced into the system, will decrease ($\downarrow$) the doses required.

$(\eta_{1\downarrow})$ A decrease ($\downarrow$) in η_1, the plasmid loss rate, will decrease ($\downarrow$) the doses required.

$(\beta^{\uparrow})$ An increase ($\uparrow$) in β, the bacterial conjugation rate, will decrease ($\downarrow$) the doses required.

$(K^{\uparrow})$ An increase ($\uparrow$) in K, the carrying capacity, will decrease ($\downarrow$) the doses required.

Incorporating the above recommendations into Figure 2.14 (a) reduces the number of doses required to a third of the original amount, as shown in Figure 2.15.

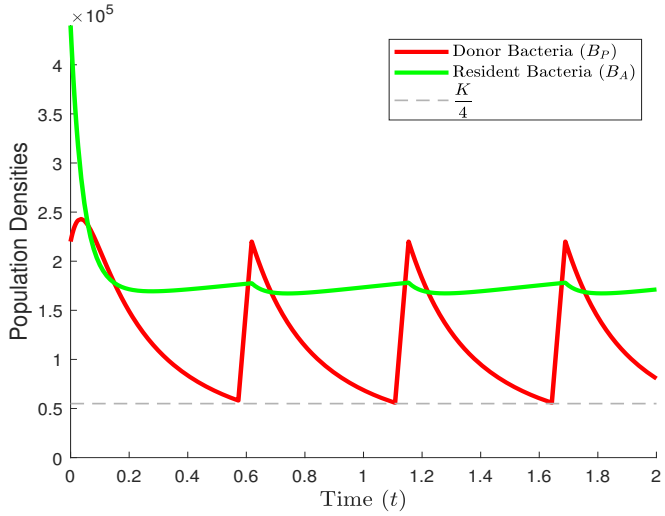

(a) 4 doses

Figure 2.15: Numerical simulation of System (2.3.1) when $\eta_1, \beta \neq 0, \eta_2 = 0$, and $\beta K - \eta_1 < 0$. The parameter values and initial conditions in (a) are $\alpha_1 = 3, \alpha_2 = 3.7848, \gamma = 1.1, \eta_1 = 11.25, \beta = 5.5 \times 10^{-5}, K = 220,000, B_P(0) = K$, and $B_A = 2K$. The initial condition for B_P is routinely reset to ensure $B_P > \dfrac{K}{4}$.

CHAPTER 3

Batch Culture and Chemostat Models of Dormancy-Capable-Microorganisms

This chapter will explore a variety of dormancy-capable microorganisms in both batch culture and chemostat settings.

3.1 Batch Culture Model of Dormancy-Capable-Bacteria and Plasmids in the Gut Micriobiome

This section will explore dormancy, plasmid loss, and acquisition in a batch culture model. Evidence shows that bacteria commonly found in gut microbiomes can enter dormant states [9, 23, 53]. Of particular relevancy, *E. coli* has been shown to become dormant and was used in the murine gut microbiome experiments referenced in Chapter 2. We will build off the most general plasmid model System (2.3.1) and incorporate dormancy.

3.1.1 Formulation of Dormancy-Capable-Bacteria and Plasmids in a Batch Culture Model

We build off the previous Model (2.3.1) and incorporate dormant plasmid-free resident bacteria, B_D, where dormancy is modeled as a first-order conversion between active-resident bacteria, B_A, and dormant-resident bacteria, B_D. Below is the modified system of ordinary differential equations:

$$
\begin{aligned}
\frac{dB_P}{dt} &= \underbrace{\alpha_1 B_P\Big(1-\frac{\gamma B_P+B_A}{K}\Big)}_{\text{growth}} - \underbrace{\eta_1 B_P}_{\text{plasmid loss}} + \underbrace{\eta_2 B_A}_{\text{transformation}} + \underbrace{\beta B_P B_A}_{\text{conjugation}},\\
\frac{dB_A}{dt} &= \underbrace{\alpha_2 B_A\Big(1-\frac{\gamma B_P+B_A}{K}\Big)}_{\text{growth}} + \underbrace{\eta_1 B_P}_{\text{plasmid loss}} - \underbrace{\eta_2 B_A}_{\text{transformation}} - \underbrace{\beta B_P B_A}_{\text{conjugation}}\\
&\quad - \underbrace{\delta_1 B_A}_{\text{conversion to } B_D} + \underbrace{\delta_2 B_D}_{\text{conversion to } B_A}\\
\frac{dB_D}{dt} &= \underbrace{\delta_1 B_A}_{\text{conversion to } B_D} - \underbrace{\delta_2 B_D}_{\text{conversion to } B_A},
\end{aligned}
\tag{3.1.1}
$$

In batch cultures, an organism resides in a regulated environment with a finite amount of a predetermined nutrient, and therefore, additional nutrients and organisms cannot enter the closed system [8]. Because of their dormant state, dormant-resident bacteria, B_D, do not reproduce or utilize nutrients. Donor bacteria, B_P, and active-resident bacteria, B_A, remain active, grow, and reproduce, hence taking up nutrients. The plasmid dynamics are identical to the previous Model (2.3.1). Furthermore, the conversion rate from active-resident bacteria to dormant-resident bacteria is δ_1, and from dormant-resident bacteria to active-resident bacteria is δ_2. Both of these conversion rates are assumed to be constant. Table 3.1 lists the model parameters with their descriptions and units.

3.1.2 Analysis of Plasmid Loss, Conjugation, and Transformation Model with Dormancy ($\eta_1 \neq 0, \eta_2 \neq 0, \beta \neq 0$)

In this subsection, System (3.1.1) is found to have four equilibria. Criteria for the existence and stability of all equilibria are deduced. The stability conditions are then summarized in Table 3.2 and corroborated in Figure 3.2.

Variable/Parameter	Description	Units
B_P	Donor/plasmid-carrying bacteria	$cells/\mu L$
B_A	Resident/plasmid-free bacteria	$cells/\mu L$
α_1	Replication rate of donor bacteria	$1/hour$
α_2	Replication rate of resident bacteria	$1/hour$
K	Carrying capacity of the environment	$cells/\mu L$
γ	Relative capacity coefficient of B_P	–
η_1	Rate of conversion from donor to resident bacteria	$1/hour$
η_2	Rate of conversion from resident to donor bacteria	$1/hour$
β	Rate of bacterial conjugation	$\mu L/cells/hour$
δ_1	Rate of conversion from active to dormant	day^{-1}
δ_2	Rate of conversion from dormant to active	day^{-1}

Table 3.1: Model (3.1.1) parameters with their descriptions and units.

By setting the right-hand sides of System (3.1.1) equal to zero, the following four equilibria are found:

$$E^0 = (0,0,0) = \left(B_P^0, B_A^0, B_D^0\right),$$
$$E^1 = \left(B_P^1, B_A^1, B_D^1\right),$$
$$E^2 = \left(B_P^2, B_A^2, B_D^2\right),$$
$$E^3 = \left(B_P^3, B_A^3, B_D^3\right),$$

where

$$B_P^1 = \frac{K\beta - \eta_1 - \gamma\eta_2 + \sqrt{(K\beta - \eta_1 - \gamma\eta_2)^2 + 4\beta K\gamma\eta_2}}{2\beta\gamma},$$
$$B_A^1 = \frac{K\beta + \eta_1 + \gamma\eta_2 - \sqrt{(K\beta + \eta_1 + \gamma\eta_2)^2 - 4\beta K\eta_1}}{2\beta},$$
$$B_D^1 = \frac{\delta_1}{\delta_2}B_A^1,$$
$$B_P^2 = \frac{K\beta - \eta_1 - \gamma\eta_2 - \sqrt{(K\beta - \eta_1 - \gamma\eta_2)^2 + 4\beta K\gamma\eta_2}}{2\beta\gamma},$$
$$B_A^2 = \frac{K\beta + \eta_1 + \gamma\eta_2 + \sqrt{(K\beta + \eta_1 + \gamma\eta_2)^2 - 4\beta K\eta_1}}{2\beta},$$
$$B_D^2 = \frac{\delta_1}{\delta_2}B_A^2,$$
$$B_P^3 = \frac{K(\alpha_1\eta_2 + \alpha_2\eta_1 - \alpha_1\alpha_2)}{\alpha_1(\alpha_1 - \alpha_2\gamma - \beta K)},$$

$$B_A^3 = -\frac{\alpha_1}{\alpha_2} B_P^3,$$
$$B_D^3 = \frac{\delta_1}{\delta_2} B_A^3.$$

Before considering the stability of the equilibria, one must know when and if each equilibrium is biologically feasible. Recall that the values for B_P, B_A, and B_D that appear in E^i, where $i = 0, 1, 2, 3$, represent population sizes. Hence, these values must all be non-negative.

E^0: Clearly, $B_P^0 = B_A^0 = B_D^0 = 0$ are non-negative. Therefore, E^0 is always biologically feasible and always exists.

E^1: Notice that B_P^1's denominator, $2\beta\gamma$, is positive. Therefore, B_P^1 is non-negative if and only if B_P^1's numerator is non-negative. Notice

$$\begin{aligned} (K\beta - \eta_1 - \gamma\eta_2)^2 &< (K\beta - \eta_1 - \gamma\eta_2)^2 + 4K\beta\gamma\eta_2 \\ -(K\beta - \eta_1 - \gamma\eta_2) \leq |K\beta - \eta_1 - \gamma\eta_2| &< \sqrt{(K\beta - \eta_1 - \gamma\eta_2)^2 + 4K\beta\gamma\eta_2} \\ 0 &< (K\beta - \eta_1 - \gamma\eta_2) + \sqrt{(K\beta - \eta_1 - \gamma\eta_2)^2 + 4K\beta\gamma\eta_2} \end{aligned}$$

and so B_P^1's numerator and, consequently, B_P^1 are non-negative.

Notice that B_A^1's denominator, 2β, is positive. Therefore, B_A^1 is non-negative if and only if B_A^1's numerator is non-negative. Notice

$$\begin{aligned} (K\beta + \eta_1 + \gamma\eta_2)^2 &> (K\beta + \eta_1 + \gamma\eta_2)^2 - 4K\beta\eta_1 \\ K\beta + \eta_1 + \gamma\eta_2 = |K\beta + \eta_1 + \gamma\eta_2| &> \sqrt{(K\beta + \eta_1 + \gamma\eta_2)^2 - 4K\beta\eta_1} \\ K\beta + \eta_1 + \gamma\eta_2 - \sqrt{(K\beta + \eta_1 + \gamma\eta_2)^2 - 4K\beta\eta_1} &> 0 \end{aligned}$$

and so B_A^1's numerator and, consequently, B_A^1 are non-negative.

Lastly, $B_D^1 = \frac{\delta_1}{\delta_2} B_A^1$ is non-negative because B_A^1 is non-negative. Thus, E^1 is always biologically feasible and always exists.

E^2: Notice that B_P^2's denominator, $2\beta\gamma$, is positive. Therefore, B_P^2 is non-negative if and only if B_P^2's numerator is non-negative. Notice

$$\begin{aligned}(K\beta-\eta_1-\gamma\eta_2)^2 &< (K\beta-\eta_1-\gamma\eta_2)^2+4K\beta\gamma\eta_2\\ K\beta-\eta_1-\gamma\eta_2 \le |K\beta-\eta_1-\gamma\eta_2| &< \sqrt{(K\beta-\eta_1-\gamma\eta_2)^2+4K\beta\gamma\eta_2}\\ K\beta-\eta_1-\gamma\eta_2-\sqrt{(K\beta-\eta_1-\gamma\eta_2)^2+4K\beta\gamma\eta_2} &< 0\end{aligned}$$

and so B_P^2's numerator and, consequently, B_P^2 are negative. Thus, E^2 is never biologically feasible and never exists.

E^3: Lastly, note $-\dfrac{\alpha_1}{\alpha_1}B_P^3 = B_A^3 = \dfrac{\delta_2}{\delta_1}B_D^3$. This means B_P^3, B_A^3, and B_D^3 are all non-negative if and only if they are all equal to zero, i.e., when $E^0 = E^3$. Thus, if $E^0 \neq E^3$, E^3 is never biologically feasible. For our purposes, this means E^3 never exists.

Moving forward, only E^0 and E^1 are eligible for analysis.

Here, we establish the stability conditions for the equilibria E^0 and E^1. The following theorem regards the local stability of the trivial equilibrium E^0.

Theorem 3.1.1. *The trivial equilibrium E^0 is always unstable.*

Proof. The Jacobian evaluated at E^0 is

$$\begin{bmatrix}\alpha_1-\eta_1 & \eta_2 & 0\\ \eta_1 & \alpha_2-\eta_2-\delta_1 & \delta_2\\ 0 & \delta_1 & -\delta_2\end{bmatrix}.$$

The characteristic polynomial of $J(E^0)$ is

$$0 = x^3 + a_1x^2 + a_2x + a_3,$$

where

$$a_1 = -\alpha_1+\eta_1-\alpha_2+\eta_2+\delta_1+\delta_2,$$

$$a_2 = (-\alpha_1 + \eta_1)(-\alpha_2 + \eta_2 + \delta_1 + \delta_2) + \delta_2(-\alpha_2 + \eta_2) - \eta_1\eta_2,$$

$$a_3 = \delta_2(-\alpha_2 + \eta_2)(-\alpha_1 + \eta_1) - \delta_2\eta_1\eta_2.$$

By the Routh-Hurwitz stability criterion [39], E^0 is stable if and only if $a_1 > 0, a_3 > 0$ and $a_1a_2 - a_3 > 0$. The above conditions are never satisfied simultaneously:

$$\text{Suppose } a_1 = -\alpha_1 + \eta_1 - \alpha_2 + \eta_2 + \delta_1 + \delta_2 > 0, a_1a_2 - a_3 > 0,$$

$$\text{and } a_3 = \delta_2\left[(-\alpha_2 + \eta_2)(-\alpha_1 + \eta_1) - \eta_1\eta_2\right] > 0.$$

$$\text{This implies, } (-\alpha_1 + \eta_1)(-\alpha_2 + \eta_2) > \eta_1\eta_2 > 0 \text{ and } \alpha_1(\alpha_2 - \eta_2) > \alpha_2\eta_1 > 0.$$

$$\text{Thus, } (\alpha_1 - \eta_1) > 0 \text{ and } (\alpha_2 - \eta_2) > 0.$$

$$\text{This implies, } -\alpha_2 + \eta_2 + \delta_1 + \delta_2 > \alpha_1 - \eta_1 > 0$$

$$\text{and } a_2 = (-\alpha_1 + \eta_1)(-\alpha_2 + \eta_2 + \delta_1 + \delta_2) + \delta_2(-\alpha_2 + \eta_2) - \eta_1\eta_2 < 0.$$

$$\text{Lastly, } a_1a_2 - a_3 < 0.$$

A contradiction has been reached. In conclusion, the Routh-Hurwitz stability criterion is never satisfied, and E^0 is always unstable. □

Next, we prove that the interior equilibrium E^1 is locally asymptotically stable.

Theorem 3.1.2. *The interior equilibrium E^1 is always locally asymptotically stable.*

Proof. The Jacobian evaluated at E^1 is $J(E^1) =$

$$\begin{bmatrix} \alpha_1 - \frac{2\alpha_1\gamma}{K}B_P^1 - \eta_1 + B_A^1\left(\beta - \frac{\alpha_1}{K}\right) & \eta_2 + B_P^1\left(\beta - \frac{\alpha_1}{K}\right) & 0 \\ \eta_1 - B_A^1\left(\frac{\alpha_2\gamma}{K} + \beta\right) & \alpha_2 - \eta_2 - \delta_1 - B_P^1\left(\beta + \frac{\alpha_2\gamma}{K}\right) - \frac{2\alpha_2}{K}B_A^1 & \delta_2 \\ 0 & \delta_1 & -\delta_2 \end{bmatrix}.$$

Thus, the characteristic polynomial of $J(E^1)$ is

$$0 = x^3 + a_1x^2 + a_2x + a_3$$

where

$$
\begin{aligned}
a_1 &= \delta_1 + \delta_2 + \frac{C}{2} + \frac{B}{2\gamma} + \frac{\alpha_1 P}{2\beta K} + \frac{\alpha_2 A}{2\beta K}, \\
a_2 &= \frac{(\delta_1+\delta_2)C}{2} + \frac{\delta_2 B}{\eta_2\gamma} + \frac{\alpha_1(\delta_1+\delta_2)P}{2\beta K} + \frac{\alpha_2\delta_2 A}{2\beta K} + \frac{a_3}{\delta_2}, \\
a_3 &= \frac{\delta_2\sqrt{(K\beta-\eta_1-\gamma\eta_2)^2+4\beta K\gamma\eta_2}}{2\beta K}\left(\frac{\alpha_1 P}{\gamma}+\alpha_2 A\right).
\end{aligned}
$$

By the Routh-Hurwitz stability criterion [39], E^1 is stable if and only if $a_1 > 0, a_3 > 0$ and $a_1 a_2 - a_3 > 0$. Note

$$
\begin{aligned}
a_1 &= \delta_1 + \delta_2 + \frac{C}{2} + \frac{B}{2\gamma} + \frac{\alpha_1 P}{2\beta K} + \frac{\alpha_2 A}{2\beta K} > 0, \\
a_3 &= \frac{\delta_2\sqrt{(K\beta-\eta_1-\gamma\eta_2)^2+4\beta K\gamma\eta_2}}{2\beta K}\left(\frac{\alpha_1 P}{\gamma}+\alpha_2 A\right) > 0,
\end{aligned}
$$

and

$$
\begin{aligned}
a_1 a_2 - a_3 =& \left(\delta_1 + \frac{C}{2} + \frac{B}{2\gamma} + \frac{\alpha_1 P}{2\beta K} + \frac{\alpha_2 A}{2\beta K}\right) a_2 \\
&+ \delta_2\left(\frac{(\delta_1+\delta_2)C}{2} + \frac{\delta_2 B}{\eta_2\gamma} + \frac{\alpha_1(\delta_1+\delta_2)P}{2\beta K} + \frac{\alpha_2\delta_2 A}{2\beta K}\right) > 0
\end{aligned}
$$

since

$$
\begin{aligned}
A &= K\beta + \eta_1 + \gamma\eta_2 - \sqrt{(K\beta+\eta_1+\gamma\eta_2)^2 - 4\beta K\eta_1} > 0, \\
P &= K\beta - \eta_1 - \gamma\eta_2 + \sqrt{(K\beta-\eta_1-\gamma\eta_2)^2 + 4\beta K\gamma\eta_2} > 0, \\
B &= K\beta - \eta_1 + \gamma\eta_2 + \sqrt{(K\beta-\eta_1+\gamma\eta_2)^2 + 4\gamma\eta_1\eta_2} > 0, \\
C &= -K\beta + \eta_1 - \gamma\eta_2 + \sqrt{(-K\beta+\eta_1-\gamma\eta_2)^2 + 4\gamma\eta_1\eta_2} > 0
\end{aligned}
$$

as shown below:

$$
\begin{aligned}
(K\beta+\eta_1+\gamma\eta_2)^2 &> (K\beta+\eta_1+\gamma\eta_2)^2 - 4\beta K\eta_1 \\
K\beta+\eta_1+\gamma\eta_2 = |K\beta+\eta_1+\gamma\eta_2| &> \sqrt{(K\beta+\eta_1+\gamma\eta_2)^2 - 4\beta K\eta_1} \\
A = K\beta+\eta_1+\gamma\eta_2 - \sqrt{(K\beta-\eta_1-\gamma\eta_2)^2 - 4\beta K\eta_1} &> 0,
\end{aligned}
$$

$$(K\beta - \eta_1 - \gamma\eta_2)^2 < (K\beta - \eta_1 - \gamma\eta_2)^2 + 4\beta K\gamma\eta_2$$

$$-(K\beta - \eta_1 - \gamma\eta_2) \leq |K\beta - \eta_1 - \gamma\eta_2| < \sqrt{(K\beta - \eta_1 - \gamma\eta_2)^2 + 4\beta K\gamma\eta_2}$$

$$P = K\beta - \eta_1 - \gamma\eta_2 + \sqrt{(K\beta - \eta_1 - \gamma\eta_2)^2 + 4\beta K\gamma\eta_2} > 0,$$

$$(K\beta - \eta_1 + \gamma\eta_2)^2 < (K\beta - \eta_1 + \gamma\eta_2)^2 + 4\gamma\eta_1\eta_2$$

$$-(K\beta - \eta_1 + \gamma\eta_2) \leq |K\beta - \eta_1 + \gamma\eta_2| < \sqrt{(K\beta - \eta_1 + \gamma\eta_2)^2 + 4\gamma\eta_1\eta_2}$$

$$B = K\beta - \eta_1 + \gamma\eta_2 + \sqrt{(K\beta - \eta_1 + \gamma\eta_2)^2 + 4\gamma\eta_1\eta_2} > 0,$$

and

$$(-K\beta + \eta_1 - \gamma\eta_2)^2 < (-K\beta + \eta_1 - \gamma\eta_2)^2 + 4\gamma\eta_1\eta_2$$

$$-(-K\beta + \eta_1 - \gamma\eta_2) \leq |-K\beta + \eta_1 - \gamma\eta_2| < \sqrt{(-K\beta + \eta_1 - \gamma\eta_2)^2 + 4\gamma\eta_1\eta_2}$$

$$C = -K\beta + \eta_1 - \gamma\eta_2 + \sqrt{(-K\beta + \eta_1 - \gamma\eta_2)^2 + 4\gamma\eta_1\eta_2} > 0,$$

since

$$(K\beta + \eta_1 + \gamma\eta_2)^2 - 4\beta K\eta_1 =$$

$$(K\beta - \eta_1 - \gamma\eta_2)^2 + 4\beta K\gamma\eta_2 =$$

$$(K\beta - \eta_1 + \gamma\eta_2)^2 + 4\gamma\eta_1\eta_2 =$$

$$(-K\beta + \eta_1 - \gamma\eta_2)^2 + 4\gamma\eta_1\eta_2 > 0.$$

Thus, E^1 is always locally asymptotically stable. □

Existence and Stability
E^0 exists and unstable
E^1 exists and stable
E^2 does not exist
E^3 does not exist

Table 3.2: Existence and stability of the equilibria of System (3.1.1).

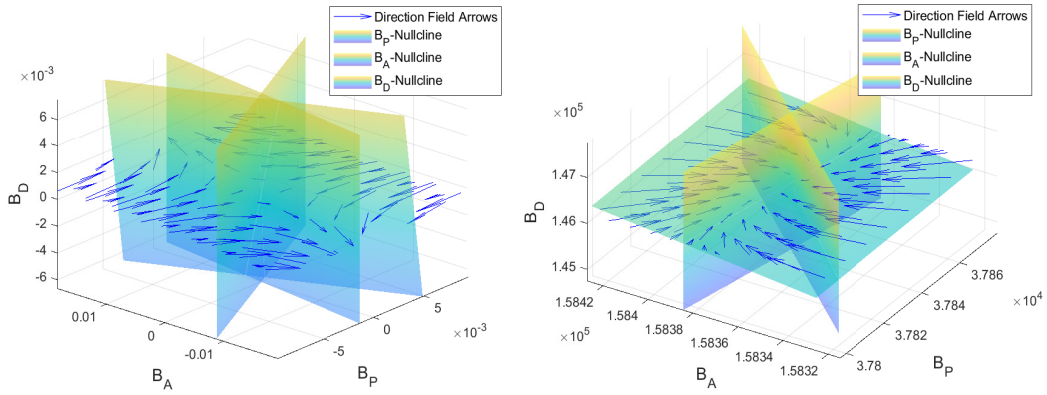

(a) $E^0 = (0, 0, 0)$ unstable

(b) $E^1 = \left(B_P^1, B_A^1, B_D^1\right)$ stable

Figure 3.1: Phase portraits of System (2.3.1). In (a) and (b), the parameter values are $\alpha_1 = 3, \alpha_2 = 3.7848, K = 200,000, \gamma = 1.1, \eta_1 = 10, \eta_2 = 0.4973, \beta = 0.00005, \delta_1 = 1.2$, and $\delta_2 = 1.3$. E^0 is unstable, as shown by the direction field arrows moving away from $E^0 = (0, 0, 0)$. E^1 is locally asymptotically, as shown by the direction field arrows moving toward $E^1 = \left(\frac{K\beta-\eta_1-\gamma\eta_2+\sqrt{(K\beta-\eta_1-\gamma\eta_2)^2+4\beta K\gamma\eta_2}}{2\beta\gamma}, \frac{K\beta+\eta_1+\gamma\eta_2-\sqrt{(K\beta+\eta_1+\gamma\eta_2)^2-4\beta K\eta_1}}{2\beta}, \frac{\delta_1}{\delta_2}B_A^1\right)$.

3.1.3 Numerical Simulations and Discussion

In this subsection, we discuss simulations of System (3.1.1), which were created using the Matlab® `ode45` solver. The results are almost exactly those of System (2.3.1). The only difference is our third additional population, B_D, now mirrors the

behavior of B_A. This is highlighted when the equilibrium and stability are seen side by side as shown next. The equilibrium for our general dormancy System (3.1.1) are

$$E^0 = (0, 0, 0)\,,$$
$$E^1 = \left(B_P^1, B_A^1, B_D^1\right),$$

where

$$B_P^1 = \frac{K\beta - \eta_1 - \gamma\eta_2 + \sqrt{(K\beta - \eta_1 - \gamma\eta_2)^2 + 4\beta K\gamma\eta_2}}{2\beta\gamma},$$
$$B_A^1 = \frac{K\beta + \eta_1 + \gamma\eta_2 - \sqrt{(K\beta + \eta_1 + \gamma\eta_2)^2 - 4\beta K\eta_1}}{2\beta},$$
$$B_D^1 = \frac{\delta_1}{\delta_2} B_A^1,$$

and for our general plasmid System (2.3.1) are

$$E^0 = (0, 0)\,,$$
$$E^1 = \left(B_P^1, B_A^1\right),$$

where

$$B_P^1 = \frac{K\beta - \eta_1 - \gamma\eta_2 + \sqrt{(K\beta - \eta_1 - \gamma\eta_2)^2 + 4\beta K\gamma\eta_2}}{2\beta\gamma},$$
$$B_A^1 = \frac{K\beta + \eta_1 + \gamma\eta_2 - \sqrt{(K\beta + \eta_1 + \gamma\eta_2)^2 - 4\beta K\eta_1}}{2\beta}.$$

Furthermore, the tables summarizing the stability of Systems (2.3.1) and (3.1.1) are identical.

This shows that including first-order conversion to model dormancy in System (2.3.1) does not affect the original dynamics. Future research should explore different ways dormancy can affect plasmid dynamics: this can be accomplished by adding complex plasmid and dormancy dynamics to Model (3.1.1).

Existence and Stability
E^0 exists and unstable
E^1 exists and stable
E^2 does not exist
E^3 does not exist

Table 3.3: Existence and stability of the equilibria of Systems (2.3.1) and (3.1.1).

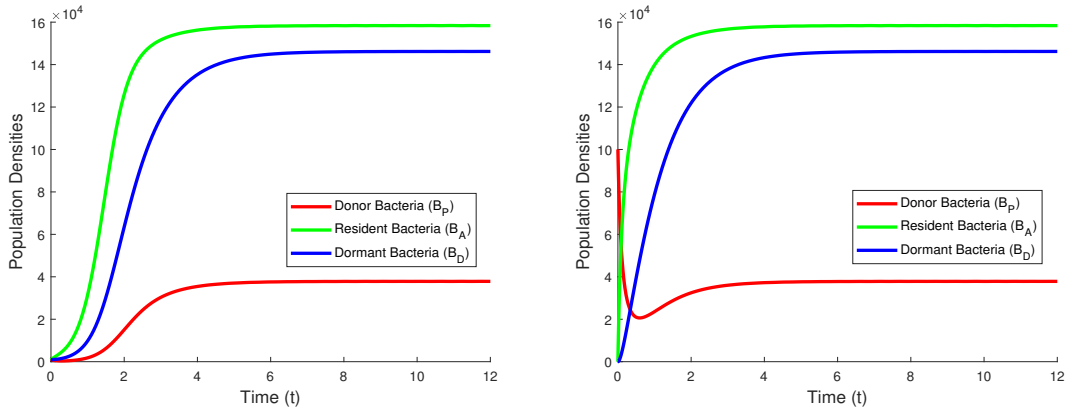

(a) $B_P(0) = 1000, B_A(0) = 1000, B_D(0) = 1000$ (b) $B_P(0) = 100000, B_A(0) = 10, B_D(0) = 10$

Figure 3.2: Numerical simulations of System (3.1.1). In (a) and (b), E^0 is unstable and E^1 is locally asymptotically stable with parameter values $\alpha_1 = 3, \alpha_2 = 3.7848, K = 200,000, \gamma = 1.1, \eta_1 = 10, \eta_2 = 0.4973, \beta = 0.00005, \delta_1 = 1.2$, and $\delta_2 = 1.3$.

Note the overall outcome of both simulations in Figure 3.2: $B_P = \frac{K\beta-\eta_1-\gamma\eta_2+\sqrt{(K\beta-\eta_1-\gamma\eta_2)^2+4\beta K\gamma\eta_2}}{2\beta\gamma}, B_A = \frac{K\beta+\eta_1+\gamma\eta_2-\sqrt{(K\beta+\eta_1+\gamma\eta_2)^2-4\beta K\eta_1}}{2\beta}$ and $B_D = \frac{\delta_1}{\delta_2}B_A^1$. In (a), the initial population sizes are identical and $\frac{1}{200}$ of the carrying capacity, K. However, in (b), $B_P(0)$ is 100 times bigger, and both $B_A(0)$ and $B_D(0)$ are 100 times smaller in comparison to (a). Still, the outcomes are identical. This will be the case for any initial condition with at least one positive value. Furthermore, all numerical simulations of System (3.1.1) can be categorized into two outcomes:

1. If $B_P(0) = B_A(0) = 0$, then the system will remain at $E^0 = (0,0,0) = (B_P^0, B_A^0, B_D^0)$.
2. Otherwise, the system will trend towards and stabilize at $E^1 = \left(\frac{K\beta-\eta_1-\gamma\eta_2+\sqrt{(K\beta-\eta_1-\gamma\eta_2)^2+4\beta K\gamma\eta_2}}{2\beta\gamma}, \frac{K\beta+\eta_1+\gamma\eta_2-\sqrt{(K\beta+\eta_1+\gamma\eta_2)^2-4\beta K\eta_1}}{2\beta}, \frac{\delta_1}{\delta_2}B_A^1\right) = (B_P^1, B_A^1, B_D^1)$.

3.2 Batch Culture Model of Dormancy-Capable-Golden Algae and Conserved Nutrient Recycling

Prymnesium parvum is a unicellular species of phytoplankton often referred to as golden algae. While this alga may be harmless at times, *P. parvum* is one of several algae species known to grow excessively and release lethal toxins. The scientific community refers to this phenomenon as a harmful algal bloom. These toxins can annihilate local aquatic populations, compromise water sources, and harm or even kill humans and animals [49, 54]. Rightfully, *P. parvum* has the attention of many scientists, governments, and environmental protection agencies and organizations. In hopes of assisting, the analysis below aims to deepen the understanding of the population dynamics of golden algae.

The model presented modifies previous zooplankton and phytoplankton models to fit *P. parvum* [32, 33, 15, 44, 26, 45]. Specifically, a batch culture model provides some understanding of the dormancy of golden alga [56]. However, the model does not take into account mortality; thus, its applicability is limited. The batch culture model introduced below focuses only on the population dynamics of golden algae. Hence, the main features of this golden algae model are the documented dormancy of golden alga [20] and the extensive phenomenon of nutrient recycling [13].

In this section, we use a model of ordinary differential equations to represent the population dynamics of *P. parvum*. The initial model is reduced in order by one, resulting in both a trivial and non-trivial equilibrium. A complete stability analysis is conducted and numerical simulations are provided to support the theoretical results.

3.2.1 Formulation of Dormancy-Capable-Golden Algae and Conserved Nutrient Recycling in a Batch Culture Model

The following model is a direct extension of Ventura et al.'s batch culture model [56], with the addition of a death term and Martines et al.'s nutrient recycling term [32]. A system of three ordinary differential equations is constructed to represent the population dynamics of golden algae in a batch culture:

$$\begin{aligned}
\frac{dR}{dt} &= \underbrace{-\frac{\mu_{max} RM}{K+R} q}_{\text{consumption by M}} + \underbrace{\lambda M q}_{\text{recycled nutrients from death of M}}, \\
\frac{dM}{dt} &= \underbrace{\frac{\mu_{max} RM}{K+R}}_{\text{growth of M}} - \underbrace{\lambda M}_{\text{death of M}} - \underbrace{\delta M}_{\text{conversion to N}} + \underbrace{\gamma N}_{\text{conversion to M}}, \qquad (3.2.1) \\
\frac{dN}{dt} &= \underbrace{\delta M}_{\text{conversion to N}} - \underbrace{\gamma N}_{\text{conversion to M}}.
\end{aligned}$$

Here, R represents the nutrient concentration available in the closed system. "Motile algae" refers to metabolically active *P. parvum*, where M represents motile algae density, while "non-motile algae" refers to dormant *P. parvum*, where N represents non-motile algae density. In batch cultures, an organism resides in a regulated environment with a finite amount of a predetermined nutrient, and therefore, additional nutrients and organisms cannot enter the closed system [8]. Because of their dormant state, non-motile algae do not reproduce and do not utilize nutrients. Motile algae remain active, grow, and reproduce, hence, taking up nutrients in the process. Algal growth

is understood to be limited by nutrient supplies [55]. Historically, models have utilized the Monod function [36],

$$\frac{\mu_{max} R}{K + R},$$

to represent the relationship between nutrient use and *P. parvum* growth [21]; this model does the same. Here, μ_{max} is the maximal growth rate of motile algae as $R \to \infty$, and K is the half-saturation constant for motile algae. The constant parameter q denotes the portion of nutrient necessary per individual *P. parvum* cell. The conversion rate from motile algae to non-motile algae is δ, and from non-motile algae to motile algae is γ. Both of these conversion rates are assumed to be constant. Since non-motile algae reside in a protective-cyst-like state, they have an assumed negligible mortality rate. However, motile algae lack this protection and naturally perish at a constant rate λ. As mentioned earlier, nutrient recycling emerges in multiple related models [32, 44, 26, 45], but this model takes direct inspiration from Martines et al.'s recycling term [32]. Thus, nutrients contained in dead motile algae are recycled back into the system at the rate $\lambda M q$. It is worth noting that q appears in both the consumption term,

$$-\frac{\mu_{max} R M}{K + R} q,$$

and the recycling term, $\lambda M q$. While other models incorporate different parameters for these terms [44, 26, 45], q does appear in all of Martines et al.'s consumption and recycling terms [32]. Furthermore, utilizing q for these terms facilitates the reduction of order of System (3.2.1) and the analysis of System (3.2.2). Table 3.4 lists all variables and parameters mentioned and their units.

3.2.1.1 Reduction of Order

It is worth noting that System (3.2.1) can be reduced to a system of two differential equations. The total amount of nutrients in the system, T, is comprised of

Variable/Parameter	Description	Units
R	Nutrient concentration	μmol/mL
M	Motile algae density	cells/mL
N	Non-motile algae density	cells/mL
γ	Rate of conversion from non-motile to motile algae	day^{-1}
δ	Rate of conversion from motile to non-motile algae	day^{-1}
K	Half-saturation constant for motile algae	μmol/mL
μ_{max}	Maximal growth rate of motile algae	day^{-1}
λ	Death rate of motile algae	day^{-1}
q	Nutrient quota of motile algae	μmol/cell

Table 3.4: Model (3.2.1) parameters and variables with their description and units.

the nutrient concentration in the system, R, and the nutrient concentration present in both types of algae, Mq and Nq. Thus,

$$T = R + Mq + Nq$$

and

$$\frac{dT}{dt} = \frac{dR}{dt} + \frac{dM}{dt}q + \frac{dN}{dt}q.$$

Direct substitution yields $\dfrac{dT}{dt} = 0$. This implies T is constant. Hence,

$$R = T - Mq - Nq$$

can be used to eliminate the equation:

$$\frac{dR}{dt} = -\frac{\mu_{max}RM}{K+R}q + \lambda Mq.$$

After substitution, the resulting reduced system is given by:

$$\begin{aligned} \frac{dM}{dt} &= \underbrace{\frac{\mu_{max}M(T-Mq-Nq)}{K+T-Mq-Nq}}_{\text{growth of M}} - \underbrace{\lambda M}_{\text{death of M}} - \underbrace{\delta M}_{\text{conversion to N}} + \underbrace{\gamma N}_{\text{conversion to M}}, \\ \frac{dN}{dt} &= \underbrace{\delta M}_{\text{conversion to N}} - \underbrace{\gamma N}_{\text{conversion to M}}. \end{aligned} \tag{3.2.2}$$

3.2.2 Analysis of Dormancy and Conserved Nutrient Recycling in a Batch Culture Model

In this subsection, the reduced System (3.2.2) is found to have two equilibria. Criteria for the existence and stability of both equilibria are deduced. The stability conditions are then summarized in Table 3.5 and corroborated in Figure 3.4.

By setting the right-hand sides of System (3.2.2) equal to zero, the following two equilibria are found:

$$E^0 = \left(M^0, N^0\right) = (0,0),$$
$$E^* = (M^*, N^*) = \left(\gamma\frac{\lambda K + T(\lambda - \mu_{max})}{q(\delta+\gamma)(\lambda-\mu_{max})}, \delta\frac{\lambda K + T(\lambda - \mu_{max})}{q(\delta+\gamma)(\lambda-\mu_{max})}\right).$$

Before considering the stability of the equilibria, one must know when and if each equilibrium is biologically feasible. Recall that the values for M and N that appear in E^0 and E^* represent population sizes and the value for R, given by

$$R = T - Mq - Nq,$$

represents the nutrient concentration in the system. Hence, these values must all be non-negative.

E^0: Clearly, $M^0 = N^0 = 0$ and $R^0 = T - M^0q - M^0q = T$ are non-negative. Therefore, E^0 is always biologically feasible and always exists.

E^*: Note $R^* = T - M^*q - M^*q = \dfrac{-\lambda K}{\lambda - \mu_{max}}$. Thus, R^* is non-negative if and only if

$$\lambda - \mu_{max} < 0.$$

Now, note $M^* = \dfrac{\delta}{\gamma}N^*$. Thus, M^* is non-negative if and only if N^* is non-negative. Since $\gamma, \delta, q > 0$, both M^* and N^* are non-negative if and only if $\dfrac{\lambda K + T(\lambda - \mu_{max})}{\lambda - \mu_{max}}$ is non-negative. Since $\lambda - \mu_{max} < 0$, M^* and N^* are non-negative if and only if

$$\lambda K + T(\lambda - \mu_{max}) < 0.$$

Note the two above conditions can be combined. Therefore, E^* is biologically feasible and exists when $\lambda < \frac{\mu_{max}T}{K+T} < \mu_{max}$.

Moving forward, E^0 is always eligible for analysis. However, E^* is eligible for analysis only when $\lambda < \frac{\mu_{max}T}{K+T} < \mu_{max}$.

Next, we establish the stability conditions for the two equilibria E^0 and E^*. The following theorem concerns the local stability of the trivial equilibrium E^0.

Theorem 3.2.1. *The trivial equilibrium E^0 is locally asymptotically stable if and only if $\lambda > \frac{\mu_{max}T}{K+T}$.*

Proof. The Jacobian evaluated at E^0 is

$$J\left(E^0\right) = \begin{bmatrix} -\lambda - \delta + \frac{\mu_{max}T}{K+T} & \gamma \\ \delta & -\gamma \end{bmatrix}.$$

By the Routh-Hurwitz stability criterion [39], E^0 is stable when $det\left(J\left(E^0\right)\right) > 0$ and $tr\left(J\left(E^0\right)\right) < 0$. Clearly,

$$det\left(J\left(E^0\right)\right) = \gamma\left(\lambda - \frac{\mu_{max}T}{K+T}\right) > 0$$

and

$$tr\left(J\left(E^0\right)\right) = -(\delta+\gamma) + \left(-\lambda + \frac{\mu_{max}T}{K+T}\right) < 0.$$

Thus, E^0 is locally asymptotically stable if and only if $\lambda > \frac{\mu_{max}T}{K+T}$. □

Next, we prove that the interior equilibrium E^* is locally asymptotically stable when it exists, $\lambda < \frac{\mu_{max}T}{K+T}$.

Theorem 3.2.2. *The interior equilibrium E^* is locally asymptotically stable if and only if $\lambda < \frac{\mu_{max}T}{K+T}$.*

Proof. The Jacobian evaluated at E^* is

$$J(E^*) = \begin{bmatrix} -\delta - q\dfrac{(\lambda-\mu_{max})^2}{\mu_{max}K}M^* & \gamma - \dfrac{(\lambda-\mu_{max})^2}{\mu_{max}K}M^* \\ \delta & -\gamma \end{bmatrix}.$$

By the Routh-Hurwitz stability criterion [39], E^* is stable when $det\,(J(E^*)) > 0$ and $tr\,(J(E^*)) < 0$. Clearly,

$$det\,(J(E^*)) = q\gamma\frac{(\lambda-\mu_{max})^2}{\mu_{max}K}M^* + \delta\frac{(\lambda-\mu_{max})^2}{\mu_{max}K}M^* > 0$$

and

$$tr\,(J(E^*)) = -\left(\delta + \gamma + q\frac{(\lambda-\mu_{max})^2}{\mu_{max}K}M^*\right) < 0.$$

Thus, E^* is locally asymptotically stable if and only if $\lambda < \dfrac{\mu_{max}T}{K+T}$. □

Furthermore, the above stability analysis is summarized in Table 3.5 and supported by the phase portraits in Figure 3.4. As indicated by the model analysis, the relationship between the death rate, λ, and the growth term, $\dfrac{\mu_{max}T}{K+T}$, is instrumental in understanding the population dynamics of *P. parvum*. The stability analysis reveals two scenarios:

1. If the death rate is less than the growth term, $\lambda < \dfrac{\mu_{max}T}{K+T}$, then the trivial equilibrium is unstable, and the non-trivial equilibrium is locally asymptotically stable. In other words, if the overall death is less than the overall growth, both types of algae will persist when introduced to a controlled and closed environment as inferred by Figure 3.4 (a) and the stability of

$$E^* = (M^*, N^*) = \left(\gamma\frac{\lambda K + T(\lambda-\mu_{max})}{q(\delta+\gamma)(\lambda-\mu_{max})}, \delta\frac{\lambda K + T(\lambda-\mu_{max})}{q(\delta+\gamma)(\lambda-\mu_{max})}\right).$$

2. If the death rate is greater than the growth term, $\lambda > \dfrac{\mu_{max}T}{K+T}$, then the trivial equilibrium is locally asymptotically stable, and the non-trivial equilibrium does not exist. In other words, if the overall death is greater than the overall

growth, both types of algae will die off when introduced to a controlled and closed environment as inferred by Figure 3.4 (b) and the stability of

$$E^0 = (M^*, N^*) = (0, 0)\,.$$

Existence and Stability	
$\lambda < \dfrac{\mu_{max} T}{K + T}$	$\dfrac{\mu_{max} T}{K + T} < \lambda$
E^0 exists and unstable	E^0 exists and stable
E^* exists and stable	E^* does not exist

Table 3.5: Existence and local stability conditions of the equilibria of System (3.2.2)

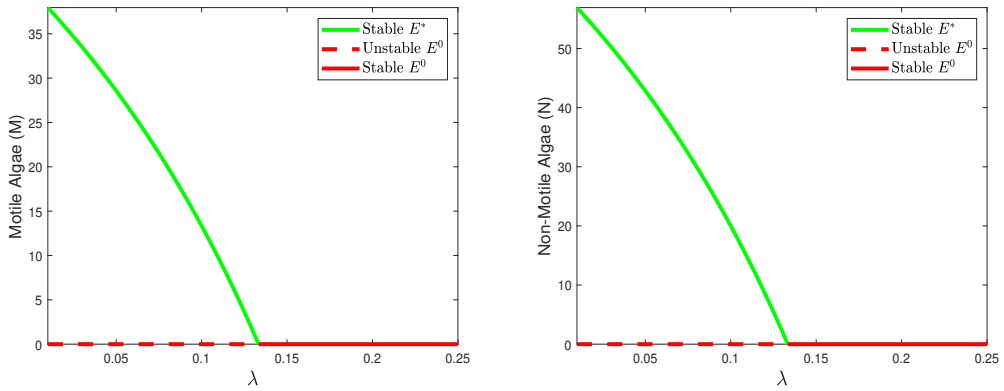

(a) B_P (b) B_A

Figure 3.3: Bifurcation diagrams of System (3.2.2) for the motile algae M in (a), and non-motile algae N in (b). The parameter values are $\mu_{max} = 0.4$, $q = 0.05$, $T = 5$, $\delta = 0.3$, $\gamma = 0.2$ and $K = 10$. In (a) and (b), the steady-state values are plotted as a function of λ as it changes in $[0.01, 0.25]$. In the diagrams, solid lines show stable states, and dashed lines show unstable states. The trivial equilibrium, E^0, is locally asymptotically stable when $\lambda > 0.1\overline{3}$. Otherwise, E^0 is unstable. The interior equilibrium, E^*, is locally asymptotically stable when $\lambda < 0.1\overline{3}$. Otherwise, E^* does not exist.

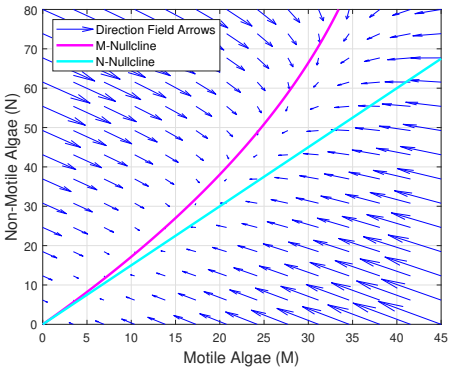

(a) $E^0 = (0,0)$ stable when $\dfrac{\mu_{max}T}{K+T} < \lambda$

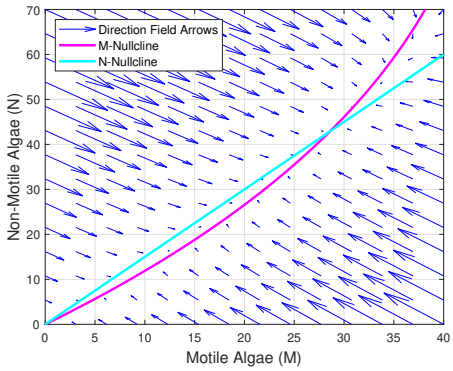

(b) $E^* = (M^*, N^*)$ stable and $E^0 = (0,0)$ unstable when $\lambda < \dfrac{\mu_{max}T}{K+T}$

Figure 3.4: Phase portraits of System (3.2.2). In (a) and (b), the parameter values are $\mu_{max} = 0.4$, $q = 0.05$, $T = 5$, $\delta = 0.3$, $\gamma = 0.2$ and $K = 10$. In (a), E^0 is locally asymptotically stable, and E^* does not exist because $\lambda > \dfrac{\mu_{max}T}{K+T}$ when $\lambda = 0.15$, as shown by the direction field arrows moving toward the single nullcline intersection at $E^0 = (0,0)$. In (b), E^* is locally asymptotically stable, and E^0 is unstable because $\lambda < \dfrac{\mu_{max}T}{K+T}$ when $\lambda = 0.05$, as shown by the direction field arrows moving toward $E^* = (M^*, N^*) = \left(\gamma\dfrac{\lambda K + T(\lambda - \mu_{max})}{q(\delta+\gamma)(\lambda-\mu_{max})}, \delta\dfrac{\lambda K + T(\lambda - \mu_{max})}{q(\delta+\gamma)(\lambda-\mu_{max})}\right)$ and away from $E^0 = (0,0)$.

In the stability analysis above, we found that the long-term behavior of System (3.2.2) depends on parameter values. We will conduct a more detailed numerical investigation of the system's behavior by examining how each equilibrium point changes with variations in λ. We will create a one-parameter bifurcation diagram by varying λ, as illustrated in Figure 3.3. We will hold all model parameters constant and adjust λ within the biologically meaningful interval of $(0.01, 0.25)$. The bifurcation occurs at $\lambda = \dfrac{\mu_{max}T}{K+T} = \dfrac{2}{15} = 0.1\overline{3}$.

As shown in the diagrams, if $\lambda > 0.1\overline{3}$, System (3.2.2) has a single locally asymptotically stable equilibria, E^0. This represents the extinction of both motile

and non-motile algae. On the other hand, if $\lambda < 0.1\overline{3}$, there are two equilibria, E^0 and E^*, with only E^* being locally asymptotically stable. This scenario represents the co-existence and persistence of both motile and non-motile algae.

3.2.3 Numerical Simulations and Discussion

In this subsection, we discuss simulations of System (3.2.2), which were created using the Matlab® `ode45` solver.In this model, two main algae dynamics are in play: death and growth. It follows that the relationship between the death rate, λ, and the growth term, $\frac{\mu_{max}T}{K+T}$, is fundamental in understanding the population dynamics of *P. parvum*. There are two existence and stability conditions:

1. The death rate is greater than the growth term, $\lambda > \frac{\mu_{max}T}{K+T}$.
2. The death rate is less than the growth term, $\lambda < \frac{\mu_{max}T}{K+T}$.

This creates the possibility of complete extinction when $\lambda > \frac{\mu_{max}T}{K+T}$ inferred by Figure 3.5 (a)-(b) and the lone stability of

$$E^0 = (0, 0)$$

and the possibility of mutual persistence when $\lambda < \frac{\mu_{max}T}{K+T}$ inferred by Figure 3.5 (c)-(d) and the lone stability of

$$E^1 = \left(\gamma\frac{\lambda K + T(\lambda - \mu_{max})}{q(\delta+\gamma)(\lambda-\mu_{max})}, \delta\frac{\lambda K + T(\lambda - \mu_{max})}{q(\delta+\gamma)(\lambda-\mu_{max})}\right).$$

Note the overall outcome of simulations in Figure 3.5 (a)-(b): $M = N = 0$. In 3.5 (a), the initial population sizes, $M(0) = N(0) = 10$, are identical and small. However, in 3.5 (b), the initial population sizes, $M(0) = N(0) = 100$, are 10 times bigger in comparison to 3.5 (a). Still, the outcomes are identical in Figures 3.5 (a)-(b).

Now, note the overall outcome of simulations in Figure 3.5 (c)-(d): $M = \gamma\frac{\lambda K + T(\lambda - \mu_{max})}{q(\delta+\gamma)(\lambda-\mu_{max})}$ and $N = \delta\frac{\lambda K + T(\lambda - \mu_{max})}{q(\delta+\gamma)(\lambda-\mu_{max})}$. In 3.5 (c), the initial population sizes, $M(0) = N(0) = 10$, are identical and small. However, in 3.5 (d), the

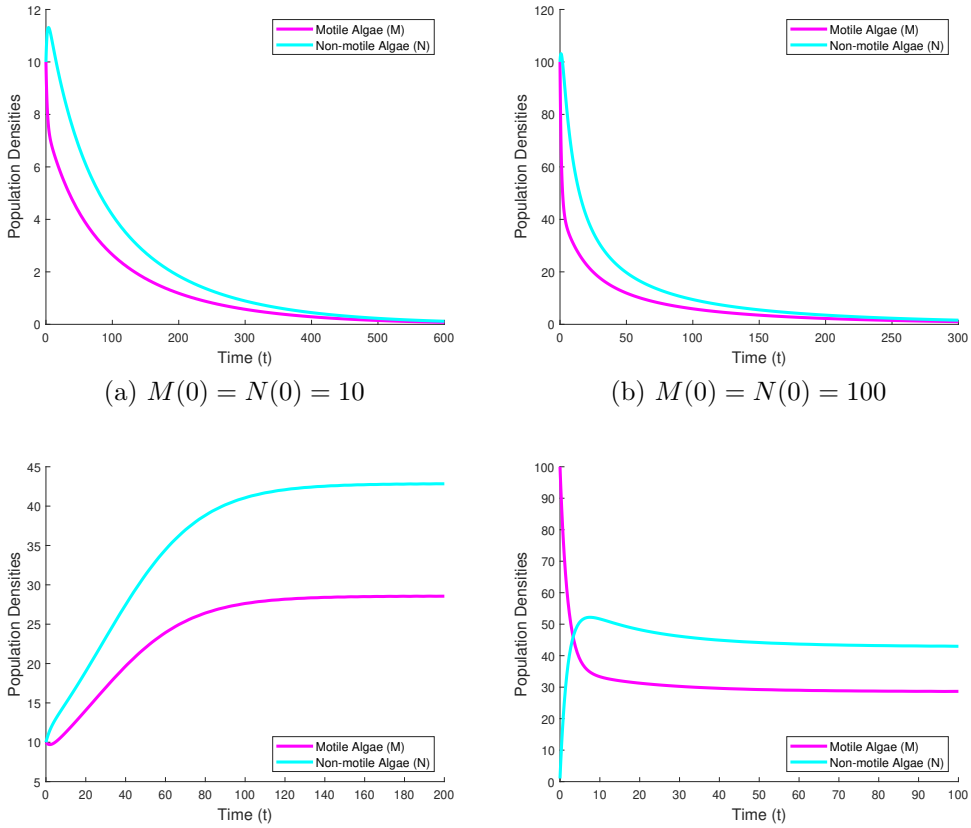

(a) $M(0) = N(0) = 10$ (b) $M(0) = N(0) = 100$

(c) $M(0) = N(0) = 10$ (d) $M(0) = 100, N(0) = 1$

Figure 3.5: Numerical simulations of System (3.2.2). In (a)-(d), the parameter values are $\mu_{max} = 0.4$, $q = 0.05$, $T = 5$, $\delta = 0.3$, $\gamma = 0.2$ and $K = 10$. In (a)-(b), $\lambda = 0.15$ and $\lambda > \dfrac{\mu_{max} T}{K + T}$. In (c)-(d), $\lambda = 0.05$ and $\lambda < \dfrac{\mu_{max} T}{K + T}$.

initial population size $M(0) = 100$ is 10 times bigger and $N(0) = 1$ is 10 times smaller in comparison to 3.5 (c). Still, the outcomes are identical in Figures 3.5 (c)-(d)

In this model, the existence and stability conditions largely dictate the behavior of the simulations. If the death rate is greater than the growth term, $\lambda > \dfrac{\mu_{max} T}{K + T}$, any initial condition will result in the extinction of both M and N, as pictured in Figures 3.5 (a)-(b). However, if the death rate is less than the growth term, $\lambda < \dfrac{\mu_{max} T}{K + T}$, any initial condition with at least one positive value will lead to the persistence of both

M and N, as pictured in Figures 3.5 (c)-(d). In summary, all numerical simulations of System (3.2.2) can be categorized into three outcomes:

1. If $M(0) = N(0) = 0$, then the system will remain at
   $E^0 = (0,0) = \left(M^0, N^0\right)$.
2. If $M(0) = \gamma \dfrac{\lambda K + T(\lambda - \mu_{max})}{q(\delta+\gamma)(\lambda - \mu_{max})}$ and $N(0) = \delta \dfrac{\lambda K + T(\lambda - \mu_{max})}{q(\delta+\gamma)(\lambda - \mu_{max})}$, then the system will remain at $E^* = \left(\gamma \dfrac{\lambda K + T(\lambda - \mu_{max})}{q(\delta+\gamma)(\lambda - \mu_{max})}, \delta \dfrac{\lambda K + T(\lambda - \mu_{max})}{q(\delta+\gamma)(\lambda - \mu_{max})}\right) = (M^*, N^*)$.
3. If $\lambda > \dfrac{\mu_{max} T}{K+T}$, the system will trend towards and stabilize at $E^0 = (0,0) = \left(M^0, N^0\right)$.
4. Otherwise, the system will trend towards and stabilize at
   $E^* = \left(\gamma \dfrac{\lambda K + T(\lambda - \mu_{max})}{q(\delta+\gamma)(\lambda - \mu_{max})}, \delta \dfrac{\lambda K + T(\lambda - \mu_{max})}{q(\delta+\gamma)(\lambda - \mu_{max})}\right) = (M^*, N^*)$.

3.3 Chemostat Model of Dormancy-Capable-Microorganisms and Nutrient Recycling

This section constructs a new chemostat model for dormancy-capable microorganisms while simultaneously generalizing the nutrient recycling term in the previous *P. parvum* Model (3.2.1). A chemostat is an apparatus that sustains a homogeneous environment through continuous inflow and outflow; compared to batch culture models, chemostat models can represent more realistic biological problems [51]. Furthermore, nutrients are not always conserved through nutrient recycling; nutrients can be lost, conserved, or acquired through nutrient cycling [28]. There are many other chemostat models that incorporate nutrient recycling but do not incorporate dormancy [6, 5, 18, 32, 43, 45, 46, 59, 56]. The mathematical model below consists of a system of nonlinear ordinary differential equations incorporating first-order conversion between active and dormant states of dormancy-capable microorganisms, a chemostat-like environment, and nutrient recycling at different efficiencies.

3.3.1 Formulation of Dormancy-Capable-Microorganisms and Nutrient Recycling in a Chemostat Model

The three nonlinear ordinary differential equations below constitute the new mathematical model:

$$\begin{aligned}
\frac{dR}{dt} &= \underbrace{DR_{in}}_{\text{input}} - \underbrace{DR}_{\text{dilution}} - \underbrace{q_1\mu(R)M}_{\text{consumption}} + \underbrace{q_2\lambda M}_{\text{nutrient recycling}}, \\
\frac{dM}{dt} &= \underbrace{\mu(R)M}_{\text{growth}} - \underbrace{\lambda M}_{\text{death}} - \underbrace{\delta M}_{\text{conversion}} + \underbrace{\gamma N}_{\text{conversion}} - \underbrace{DM}_{\text{dilution}}, \qquad (3.3.1) \\
\frac{dN}{dt} &= \underbrace{\delta M}_{\text{conversion}} - \underbrace{\gamma N}_{\text{conversion}} - \underbrace{DN}_{\text{dilution}}.
\end{aligned}$$

In Model (3.3.1), the variable R corresponds to the concentration of limiting nutrients in the system. The term "active cell" pertains to a metabolically active microorganism, where the density of the active population is denoted by M. Similarly, "dormant cell" pertains to a metabolically inactive microorganism, where N represents the density of the dormant population. As stated above, a chemostat undergoes continuous inflow and outflow of any combination of nutrients, byproducts, microorganisms, etc. All components in the chemostat flow out of the system at a constant dilution rate, D [38]. However, only the limiting nutrient flows into this system at the constant rate R_{in}. The active population, M, naturally grows and multiplies, depleting R as it does. In the literature, the Monod function,

$$\mu(R) = \frac{\mu_{max}R}{K+R},$$

often represents the above relationship between nutrient use and microbial growth [36]. For purposes of this model, μ_{max} is the maximal growth rate of active microorganisms as $R \to \infty$, and K is the half-saturation constant for active microorganisms. Dormant

microorganisms do not multiply and do not deplete the nutrient concentration; thus, N does not elicit a growth function like M.

The positive constant q_1 is the quota of nutrients required per individual microorganism [32]. The constant conversion rate from active to dormant microorganisms is δ and from dormant to active microorganisms is γ. This first-order conversion is routinely utilized as a first step when modeling dormancy [3, 35, 37, 47, 50, 56]. Because dormancy is a protective state, there is an assumed negligible mortality rate for N. However, active microorganisms are still vulnerable to their surroundings; thus, they perish at a constant rate λ. The product λq_2 is the nutrient recycle rate after the death of M. Here,

$$0 \leq q_2 \leq q_1,$$

where q_2 represents the quota of nutrients successfully recycled into the nutrient concentration per individual microorganism. This inequality implies only nutrients residing within a dead microorganism can be recycled back into R. In other words, this model assumes nutrients can be lost or conserved, but not acquired.

Remark 3.3.1. Amidst diverse microorganisms and complex biological processes, all manifestations of dormancy involve a minimum of two cellular states: active and inactive. Utilizing M and N to represent the populations of these two states, respectively, enables Model (3.3.1) to represent dormancy at a fundamental level across its different manifestations.

3.3.2 Analysis of Dormancy and Nutrient Recycling in a Chemostat Model

In this subsection, the reduced System (3.3.1) is found to have two equilibria. Criteria for the existence and stability of both equilibria are deduced. The stability conditions are then summarized in Table 3.7 and corroborated in Figure 3.6.

Variable/Parameter	Description	Units
R	Nutrient concentration	μmol/mL
M	Active population density	cells/mL
N	Dormant population density	cells/mL
R_{in}	Concentration of substrate in feed	μmol/mL
D	Dilution rate	day^{-1}
γ	Rate of conversion from dormant to active	day^{-1}
δ	Rate of conversion from active to dormant	day^{-1}
K	Half-saturation constant for active	μmol/mL
μ_{max}	Maximal growth rate of active	day^{-1}
λ	Death rate of active	day^{-1}
q_1	Nutrient quota of active	μmol/cell
q_2	Nutrient quota of recycled nutrients	μmol/cell

Table 3.6: Model (3.3.1) parameters and variables with their description and units.

By setting the right-hand sides of System (3.2.2) equal to zero, the following two equilibria are found:

$$E^0 = \left(R^0, M^0, N^0\right) = (R_{in}, 0, 0),$$
$$E^* = \left(R^*, M^*, N^*\right),$$

where

$$R^* = \mu^{-1}\left(D + \lambda + \frac{D\delta}{D+\gamma}\right),$$
$$M^* = \frac{D\left(R_{in} - R^*\right)}{q_1\left(D + \lambda + \frac{D\delta}{D+\gamma}\right) - q_2\lambda},$$
$$N^* = \frac{\delta}{D+\gamma}M^*, \text{ and}$$
$$\mu^{-1}(\hat{\mu}) = \frac{\hat{\mu}K}{\mu_{max} - \hat{\mu}}$$

Before considering the stability of the equilibria, one must know when and if each equilibrium is biologically feasible. Recall that the values for M and N that appear in E^0 and E^* represent population sizes. Hence, these values must all be non-negative.

E^0: Clearly, $M^0 = N^0 = 0$ and $R^0 = R_{in}$ are non-negative. Therefore, E^0 is always biologically feasible and always exists.

E^*: Note $N^* = \dfrac{\delta}{D+\gamma} M^*$. Thus, N^* is non-negative if and only if M^* is non-negative. Since $\gamma, \delta, D > 0$, both M^* and N^* are non-negative if and only if $\dfrac{D\left(R_{in} - R^*\right)}{q_1\left(D + \frac{D\delta}{D+\gamma}\right) + (q_1 - q_2)\lambda}$ is non-negative. Since $q_2 \leq q_1$, M^*'s denominator is positive. Thus, M^* and N^* are non-negative if and only if M^*'s numerator is non-negative, i.e., when $R_{in} > R^*$, which is equivalent to

$$\mu(R_{in}) > D + \lambda + \frac{D\delta}{D+\gamma}.$$

Now, consider R^*. R^* is non-negative if and only if $\dfrac{\left(D + \lambda + \frac{D\delta}{D+\gamma}\right) K}{\mu_{max} - \left(D + \lambda + \frac{D\delta}{D+\gamma}\right)}$ is non-negative. Clearly, R^*'s numerator is positive. Thus, R^* is non-negative if and only if R^*'s denominator is non-negative, i.e., when

$$\mu_{max} > D + \lambda + \frac{D\delta}{D+\gamma}.$$

Since $\mu_{max} > \mu(R_{in}) = \dfrac{\mu_{max} R_{in}}{K + R_{in}}$, the two above existence conditions are satisfied when

$$\mu_{max} > \mu(R_{in}) > D + \lambda + \frac{D\delta}{D+\gamma}.$$

Therefore, E^* is biologically feasible and exists when

$$\mu(R_{in}) > D + \lambda + \frac{D\delta}{D+\gamma}.$$

Moving forward, E^0 is always eligible for analysis. However, E^* is eligible for analysis only when $\mu(R_{in}) > D + \lambda + \dfrac{D\delta}{D+\gamma}$.

Next, we establish the stability conditions for the two equilibria E^0 and E^*. The following theorem is in regard to the local stability of the boundary equilibrium E^0.

Theorem 3.3.1. *The boundary equilibrium E^0 is locally asymptotically stable if and only if $R_{in} < R^*$.*

Proof. The Jacobian evaluated at E^0 is

$$J\left(E^0\right) = \begin{bmatrix} -D & -\mu(R_{in})q_1 + \lambda q_2 & 0 \\ 0 & \mu(R_{in}) - \lambda - \delta - D & \gamma \\ 0 & \delta & -\gamma - D \end{bmatrix}.$$

Thus, the characteristic polynomial of $J\left(E^0\right)$ is

$$x^3 + a_1^0 x^2 + a_2^0 x + a_3^0 = 0,$$

where

$$\begin{aligned} a_1^0 &= -trace\left(J\left(E^0\right)\right) = 2D + \gamma + \left[D + \lambda + \delta - \mu\left(R_{in}\right)\right], \\ a_2^0 &= Da_1^0 + \frac{a_3^0}{D} - D^2, \\ a_3^0 &= -det\left(J\left(E^0\right)\right) = D\left(D + \gamma\right)\left[D + \lambda + \frac{D\delta}{D + \gamma} - \mu\left(R_{in}\right)\right]. \end{aligned}$$

By the Routh-Hurwitz stability criterion [39], E^0 is stable when $a_1^0 > 0, a_3^0 > 0$ and $a_1^0 a_2^0 - a_3^0 > 0$. Note $R_{in} < R^*$ implies $0 < D + \lambda + \frac{D\delta}{D+\gamma} - \mu(R_{in}) < D + \lambda + \delta - \mu(R_{in})$. Thus,

$$\begin{aligned} a_1^0 &= 2D + \gamma + \left[D + \lambda + \delta - \mu\left(R_{in}\right)\right] > 0, \text{ and} \\ a_3^0 &= D\left(D + \gamma\right)\left[D + \lambda + \frac{D\delta}{D + \gamma} - \mu\left(R_{in}\right)\right] > 0. \end{aligned}$$

Lastly, $a_1^0 - D = D + \gamma + \left[D + \lambda + \delta - \mu\left(R_{in}\right)\right] > 0$ implies $\frac{a_1}{D} > 1$ and

$$a_1^0 a_2^0 - a_3^0 = Da_1^0\left(a_1^0 - D\right) + a_3^0\left(\frac{a_1^0}{D} - 1\right) > 0.$$

Thus, E^0 is locally asymptotically stable when $R_{in} < R^*$. □

Next, we prove that the interior equilibrium E^* is locally asymptotically stable if and only if $R_{in} > R^*$.

Theorem 3.3.2. *The interior equilibrium, E^*, is locally asymptotically stable if and only if $R_{in} > R^*$.*

Proof. The Jacobian evaluated at E^* is

$$J(E^*) = \begin{bmatrix} -D - q_1 M^* \dfrac{\mu_{max} K}{(K+R^*)^2} & -q_1\left(D + \dfrac{D\delta}{D+\gamma}\right) + (q_2 - q_1)\lambda & 0 \\ M^* \dfrac{\mu_{max} K}{(K+R^*)^2} & -\dfrac{\delta\gamma}{D+\gamma} & \gamma \\ 0 & \delta & -\gamma - D \end{bmatrix}.$$

Thus, the characteristic polynomial of $J(E^*)$ is

$$0 = x^3 + a_1 x^2 + a_2 x + a_3$$

where

$$\begin{aligned} a_1 &= -trace\left(J\left(E^0\right)\right) = 2D + \gamma + \frac{\delta\gamma}{D+\gamma} + q_1 M^* \frac{\mu_{max} K}{(K+R^*)^2}, \\ a_2 &= \left(D + \gamma + \frac{\delta\gamma}{D+\gamma}\right)\left(D + q_1 M^* \frac{\mu_{max} K}{(K+R^*)^2}\right) + \frac{a_3}{D+\gamma}, \\ a_3 &= -det\left(J\left(E^0\right)\right) = (D+\gamma) M^* \frac{\mu_{max} K}{(K+R^*)^2}\left(q1\left(D + \frac{D\delta}{D+\gamma}\right) + (q_1 - q_2)\lambda\right). \end{aligned}$$

By the Routh-Hurwitz stability criterion [39], E^* is stable if and only if $a_1 > 0, a_3 > 0$ and $a_1 a_2 - a_3 > 0$. Since $q_1 \geq q_2$ and $M^*, R^* > 0$,

$$\begin{aligned} a_1 &= 2D + \gamma + \frac{\delta\gamma}{D+\gamma} + q_1 M^* \frac{\mu_{max} K}{(K+R^*)^2} > 0, \\ a_2 &= \left(D + \gamma + \frac{\delta\gamma}{D+\gamma}\right)\left(D + q_1 M^* \frac{\mu_{max} K}{(K+R^*)^2}\right) + \frac{a_3}{D+\gamma} > 0, \\ a_3 &= (D+\gamma) M^* \frac{\mu_{max} K}{(K+R^*)^2}\left(q1\left(D + \frac{D\delta}{D+\gamma}\right) + (q_1 - q_2)\lambda\right) > 0, \end{aligned}$$

and

$$\begin{aligned} a_1 a_2 - a_3 = a_1 &\left(D + \gamma + \frac{\delta\gamma}{D+\gamma}\right)\left(D + q_1 M^* \frac{\mu_{max} K}{(K+R^*)^2}\right) \\ &+ \frac{a_3}{D+\gamma}\left(D + \frac{\delta\gamma}{D+\gamma} + q_1 M^* \frac{\mu_{max} K}{(K+R^*)^2}\right) > 0. \end{aligned}$$

Thus, E^* is locally asymptotically stable if and only if$R_{in} > R^*$. □

Existence and Stability	
$\mu\left(R_{in}\right) > D+\lambda+\dfrac{D\delta}{D+\gamma}$	$\mu\left(R_{in}\right) < D+\lambda+\dfrac{D\delta}{D+\gamma}$
E^0 exists and unstable	E^0 exists and stable
E^* exists and stable	E^* does not exist

Table 3.7: Existence and local stability conditions of the equilibria of System (3.3.1).

Furthermore, the above stability analysis is summarized in Table 3.7 and supported by the phase portraits in Figure 3.6. As indicated by the model analysis, the relationship between the dilution, death, and conversion rates $(D, \lambda, \delta, \gamma)$ and the growth term, $\mu(R_{in})$ is instrumental in understanding the population dynamics. The stability analysis reveals two scenarios:

1. If the elimination term, $D+\lambda+\dfrac{D\delta}{D+\gamma}$, is less than the growth term $\mu(R_{in})$, then the trivial equilibrium is unstable, and the non-trivial equilibrium is locally asymptotically stable. This implies that if the overall elimination is less than the overall growth, both the active and dormant populations will persist when introduced to a chemostat as inferred by Figure 3.6 (b) and the lone stability of

$$E^* = \left(\mu^{-1}\left(D+\lambda+\frac{D\delta}{D+\gamma}\right), \frac{D(R_{in}-R^*)}{q_1(D+\frac{D\delta}{D+\gamma})+(q_1-q_2)\lambda}, \frac{\delta}{D+\gamma}M^*\right)$$
$$= (R^*, M^*, N^*)\,.$$

2. If the elimination term, $D+\lambda+\dfrac{D\delta}{D+\gamma}$, is greater than the growth term $\mu(R_{in})$, then the trivial equilibrium is locally asymptotically stable, and the non-trivial equilibrium does not exist. This implies that when the overall elimination exceeds the overall growth, the microorganism will die off upon introduction to a chemostat as inferred by Figure 3.6 (c) and the lone stability of

$$E^0 = (R_{in}, 0, 0) = (R^*, M^*, N^*).$$

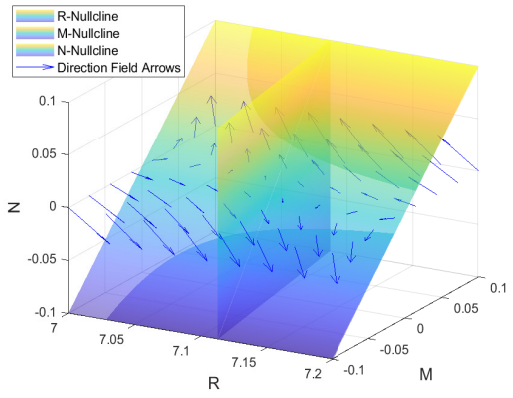

(a) $E^0 = (0, 0, 0)$ unstable when $\mu(R_{in}) > D + \lambda + \dfrac{D\delta}{D+\gamma}$

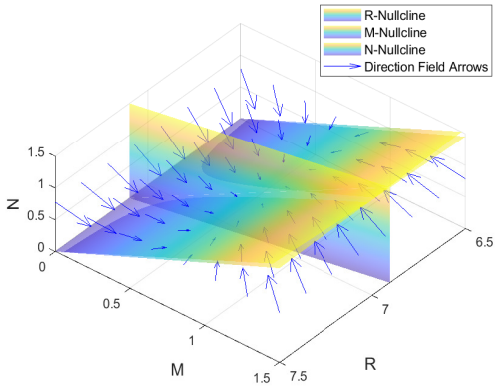

(b) $E^* = (R^*, M^*, N^*)$ stable when $\mu(R_{in}) > D + \lambda + \dfrac{D\delta}{D+\gamma}$

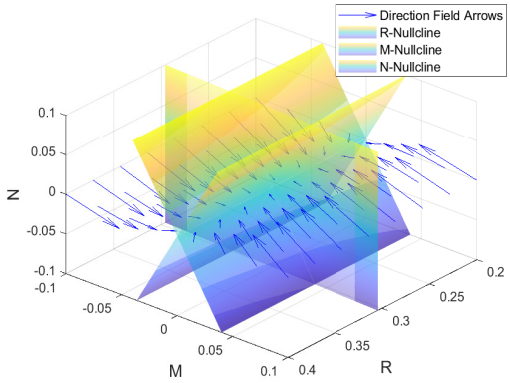

(c) $E^0 = (0, 0, 0)$ stable when $\mu(R_{in}) < D + \lambda + \dfrac{D\delta}{D+\gamma}$

Figure 3.6: Phase portraits of System (3.3.1). In (a)-(c), the parameter values are $\mu_{max} = 0.4, q_1 = 0.05, q_2 = 0.03, K = 1, \gamma = 0.2, \delta = 0.3, \lambda = 0.15$, and $D = 0.1$. In (a), E^0 is unstable because $\mu(R_{in}) > D + \lambda + \dfrac{D\delta}{D+\gamma}$ when $R_{in} = 0.3$, as shown by the direction field arrows moving away from $E^0 = (0, 0, 0)$. In (b), E^1 is locally asymptotically stable because $\mu(R_{in}) > D + \lambda + \dfrac{D\delta}{D+\gamma}$ when $R_{in} = 0.3$, as shown by the direction field arrows moving toward $E^* = \left(\mu^{-1}\left(D + \lambda + \dfrac{D\delta}{D+\gamma}\right), \dfrac{D(R_{in} - R^*)}{q_1(D + \frac{D\delta}{D+\gamma}) + (q_1 - q_2)\lambda}, \dfrac{\delta}{D+\gamma}M^*\right)$. In (c), E^0 is locally asymptotically stable because $\mu(R_{in}) < D + \lambda + \dfrac{D\delta}{D+\gamma}$ when $R_{in} = 7.1$, as shown by the direction field arrows moving toward $E^0 = (0, 0, 0)$.

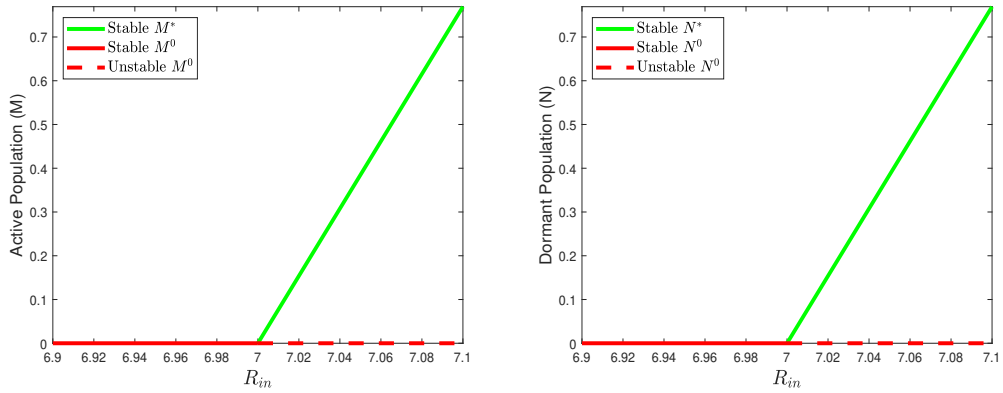

(a) B_P (b) B_A

Figure 3.7: Bifurcation diagrams of System (3.3.1) for the active population M in (a), and dormant population N in (b). The parameter values are $\mu_{max} = 0.4, q_1 = 0.05, q_2 = 0.03, K = 1, \gamma = 0.2, \delta = 0.3, \lambda = 0.15$, and $D = 0.1$. In (a) and (b), the steady-state values are plotted as a function of R_{in} as it changes in $[6.9, 7.1]$. In the diagrams, solid lines show stable states, and dashed lines show unstable states. The trivial equilibrium, E^0, is locally asymptotically stable when $R_{in} < 7$. Otherwise, E^0 is unstable. The interior equilibrium, E^*, exists and is locally asymptotically stable when $R_{in} > 7$. Otherwise, E^* does not exist.

Remark 3.3.2. When the constant dilution rate is equal to zero, $D = 0$, the chemostat model (3.3.1) can represent a batch culture model with dormancy and nutrient recycling. Setting $D = 0$ and $q_1 = q_2$ results in the batch culture Model (3.2.1). Setting $D = 0$ and $q_1 > q_2$ results in a batch culture where all equilibria require $M^* = N^* = 0$, i.e., in a closed system where nutrients are lost through nutrient recycling, neither M nor N persist under any conditions.

In the stability analysis above, we found that the long-term behavior of System (3.2.2) depends on parameter values. We will conduct a more detailed numerical investigation of the system's behavior by examining how each equilibrium point changes with variations in R_{in}. We will create a one-parameter bifurcation diagram by varying R_{in}, as illustrated in Figure 3.7. We will hold all model parameters

constant and adjust R_{in} within the biologically meaningful interval of $(6.9, 7.1)$. The bifurcation occurs at $R_{in} = 7$.

As shown in the diagrams, if $R_{in} < 7$, System (3.3.1) has a single locally asymptotically stable equilibrium, E^0. This represents the extinction of both active and dormant microorganisms. On the other hand, if $R_{in} > 7$, there are two equilibria, E^0 and E^*, with only E^* being locally asymptotically stable. This scenario represents the co-existence and persistence of both active and dormant microorganisms.

3.3.3 Numerical Simulations and Discussion

In this subsection, we discuss simulations of System (3.3.1), which were created using the Matlab® `ode45` solver. In this model, two main population dynamics are in play: elimination and growth. It follows that the relationship between the elimination term, $D + \lambda + \dfrac{D\delta}{D+\gamma}$, and the growth term, $\dfrac{\mu_{max} R_{in}}{K + R_{in}}$, is fundamental in understanding the population dynamics of dormancy-capable-microorganisms in a chemostat setting. There are two existence and stability conditions:

1. The elimination term is greater than the growth term,
   $\mu(R_{in}) < D + \lambda + \dfrac{D\delta}{D+\gamma}$.
2. The elimination term is less than the growth term,
   $\mu(R_{in}) > D + \lambda + \dfrac{D\delta}{D+\gamma}$.

This creates the possibility of complete extinction when $\mu(R_{in}) < D + \lambda + \dfrac{D\delta}{D+\gamma}$ inferred by Figure 3.8 (a)-(d) and the lone stability of

$$E^0 = (0, 0, 0)$$

and the possibility of mutual persistence when $\mu(R_{in}) > D + \lambda + \dfrac{D\delta}{D+\gamma}$ inferred by Figure 3.9 (a)-(d) and the lone stability of

$$E^* = \left(\mu^{-1}\left(D + \lambda + \frac{D\delta}{D+\gamma} \right), \frac{D(R_{in} - R^*)}{q_1(D + \frac{D\delta}{D+\gamma}) + (q_1 - q_2)\lambda}, \frac{\delta}{D+\gamma} M^* \right).$$

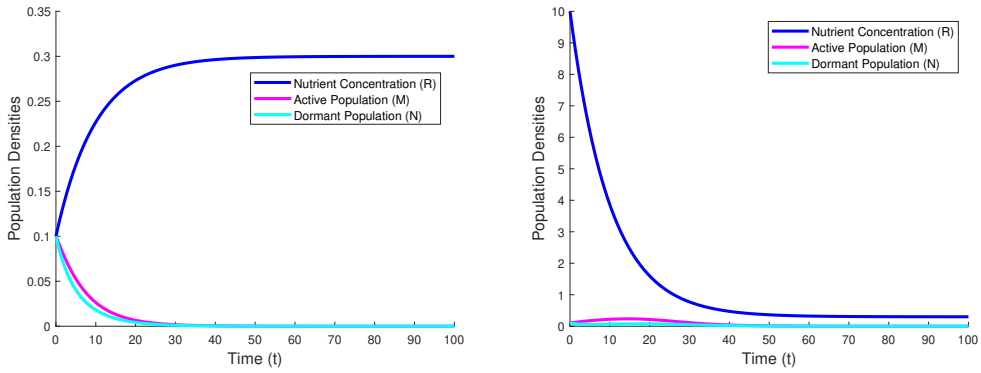

(a) $R(0) = M(0) = N(0) = 0.1$

(b) $R(0) = 10, M(0) = N(0) = 0.1$

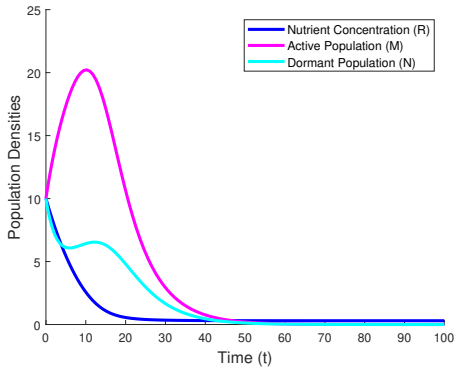

(c) $R(0) = M(0) = N(0) = 10$

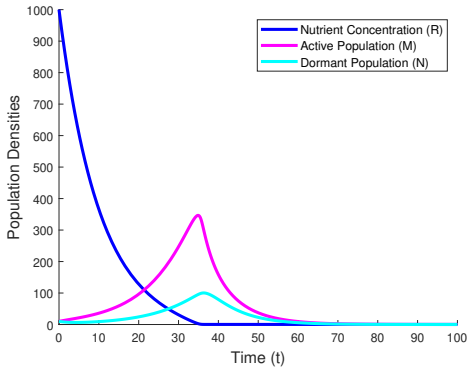

(d) $R(0) = 1000, M(0) = N(0) = 10$

Figure 3.8: Numerical simulations of System (3.2.2). In (a)-(d), the parameter values are $\mu_{max} = 0.4, q_1 = 0.05, q_2 = 0.03, K = 1, \gamma = 0.2, \delta = 0.1, \lambda = 0.15, R_{in} = 0.3$ and $D = 0.1$ and $\mu(R_{in}) < D + \lambda + \dfrac{D\delta}{D+\gamma}$.

Note the overall outcome of simulations in Figure 3.8 (a)-(d): $R = R_{in}, M = N = 0$. In (a)-(b), the initial population sizes, $M(0) = N(0) = 0.1$, are identical and small. However, in (b), the initial nutrient concentration, $R(0) = 10$, is 100 times

bigger in comparison to (a), where $R(0) = 0.1$. In (c)-(d), the initial population sizes, $M(0) = N(0) = 10$, are identical and larger. However, in (d), the initial nutrient concentration, $R(0) = 1000$, is 100 times bigger in comparison to (a), where $R(0) = 10$. Still, the outcomes are identical in (a)-(d).

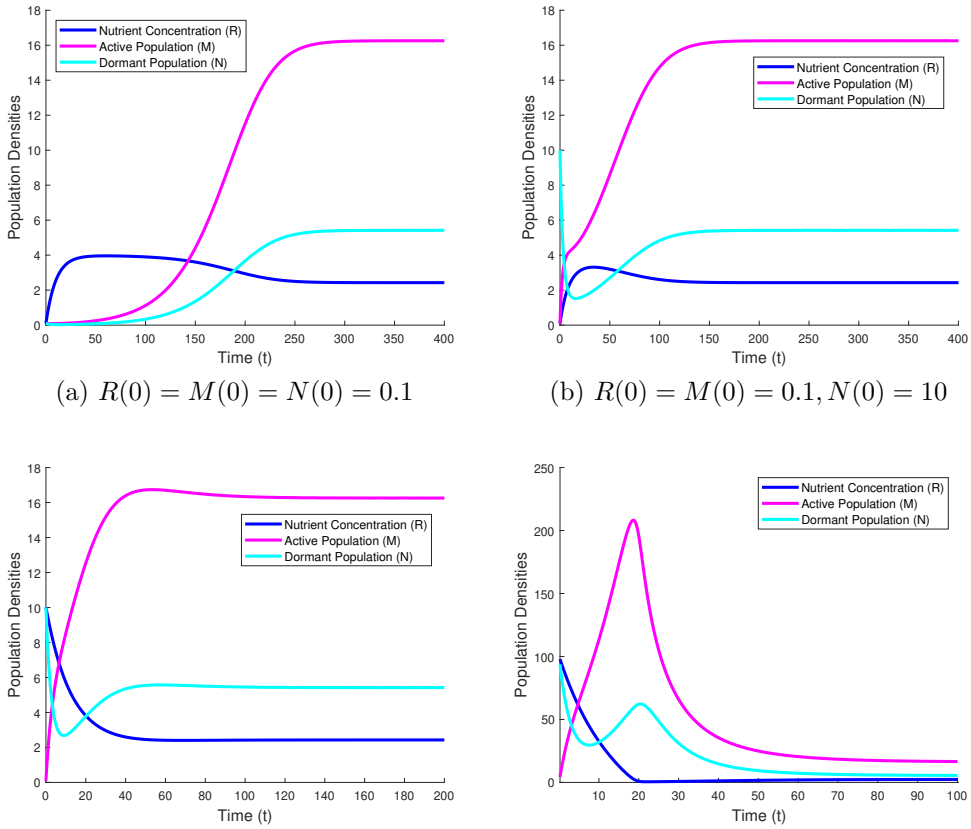

(a) $R(0) = M(0) = N(0) = 0.1$ (b) $R(0) = M(0) = 0.1, N(0) = 10$

(c) $R(0) = N(0) = 10, M(0) = 0.1$ (d) $R(0) = N(0) = 100, M(0) = 0.1$

Figure 3.9: Numerical simulations of System (3.2.2). In (a)-(d), the parameter values are $\mu_{max} = 0.4, q_1 = 0.05, q_2 = 0.03, K = 1, \gamma = 0.2, \delta = 0.1, \lambda = 0.15, R_{in} = 4$ and $D = 0.1$ and $\mu(R_{in}) > D + \lambda + \dfrac{D\delta}{D+\gamma}$.

Now, note the overall outcome of simulations in Figure 3.9 (a)-(d):

$$R = \mu^{-1}\left(D + \lambda + \frac{D\delta}{D+\gamma}\right), M = \frac{D(R_{in} - R^*)}{q_1(D + \frac{D\delta}{D+\gamma}) + (q_1 - q_2)\lambda},$$

$N = \dfrac{\delta}{D+\gamma}\dfrac{D(R_{in}-R^*)}{q_1(D+\frac{D\delta}{D+\gamma})+(q_1-q_2)\lambda}$. In (a)-(d), the initial population size for $M(0) = 0.1$ is noticeably small. However, in (a)-(d), the initial population size for N and the nutrient concentration gradually increase to $0.1, 10$, and 100. Regardless of the initial amount of nutrients or dormant microorganisms, the active population, M, remained the greatest, as shown by the identical outcomes in (a)-(d).

In this model, the existence and stability conditions largely dictate the behavior of the simulations. If the elimination term is greater than the growth term, $\mu(R_{in}) < D+\lambda+\dfrac{D\delta}{D+\gamma}$, any initial condition will result in the extinction of both M and N, as pictured in Figure 3.8 (a)-(d). However, if the elimination term is less than the growth term, $\mu(R_{in}) > D+\lambda+\dfrac{D\delta}{D+\gamma}$, any initial condition with at least one positive value will lead to the persistence of both M and N, as pictured in Figures 3.9 (a)-(d). In summary, all numerical simulations of System (3.2.2) can be categorized into three outcomes:

1. If $M(0) = N(0) = 0$, then the system will remain at
   $E^0 = (R(0), 0, 0) = \left(R^0, M^0, N^0\right)$.
1. If $M(0) = \mu^{-1}\left(D+\lambda+\dfrac{D\delta}{D+\gamma}\right)$ and $N(0) = \dfrac{D(R_{in}-R^*)}{q_1(D+\frac{D\delta}{D+\gamma})+(q_1-q_2)\lambda}, \dfrac{\delta}{D+\gamma}M^*$, then the system will remain at
   $E^* = \left(\mu^{-1}\left(D+\lambda+\dfrac{D\delta}{D+\gamma}\right), \dfrac{D(R_{in}-R^*)}{q_1(D+\frac{D\delta}{D+\gamma})+(q_1-q_2)\lambda}, \dfrac{\delta}{D+\gamma}M^*\right)$.
3. If $\mu(R_{in}) < D+\lambda+\dfrac{D\delta}{D+\gamma}$, the system will trend towards and stabilize at
   $E^0 = (R_{in}, 0, 0) = \left(R^0, M^0, N^0\right)$.
4. Otherwise, the system will trend towards and stabilize at
   $E^* = \left(\mu^{-1}\left(D+\lambda+\dfrac{D\delta}{D+\gamma}\right), \dfrac{D(R_{in}-R^*)}{q_1(D+\frac{D\delta}{D+\gamma})+(q_1-q_2)\lambda}, \dfrac{\delta}{D+\gamma}M^*\right)$.

Next, we perform a series of numerical simulations to explore different biological scenarios arising from the batch culture ($D = 0$) and chemostat ($D \neq 0$) models

originating from Model (3.3.1). Specifically, the effects of altering the dilution rate and the in-flowing nutrient concentration, D and R_{in}, are depicted in Figure (3.10).

3.10 (a): In Figure 3.10 (a), $\mu(R_{in}) < D + \lambda + \dfrac{D\delta}{D+\gamma}$, which corresponds to a stable E^0 and complete extinction in a batch culture model setting ($D = 0$) [34].

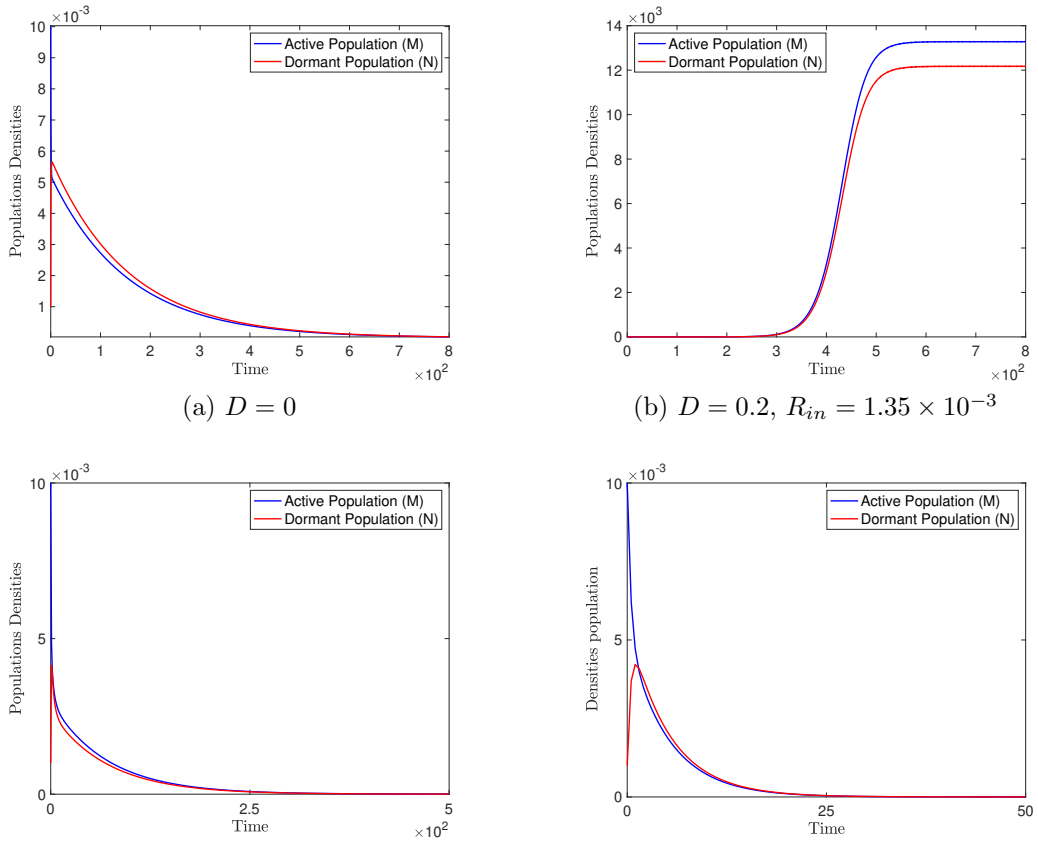

(a) $D = 0$

(b) $D = 0.2$, $R_{in} = 1.35 \times 10^{-3}$

(c) $D = 0.25$, $R_{in} = 1.35 \times 10^{-3}$

(d) $D = 0.2$, $R_{in} = 1.35 \times 10^{-4}$

Figure 3.10: Effects of the dilution rate D and the concentration of the limiting nutrient supplied in the in-flowing medium R_{in} on the system outcome, for model parameter values $q_1 = 10^{-8}, K = 10^{-3}, q_2 = 10^{-9}, \lambda = 0.1, \delta = 1.1, \gamma = 1, \mu_{max} = 0.95$, and $D = 0$ (batch culture model) in (a), $D = 0.2$ with $R_{in} = 1.35 \times 10^{-3}$ (chemostat model) in (b), $D = 0.25$ with $R_{in} = 1.35 \times 10^{-3}$ (chemostat model) in (c), and $D = 0.2$ with $R_{in} = 1.35 \times 10^{-4}$ (chemostat model) in (d).

3.10 (b) Introducing even a small non-zero dilution rate $D = 0.2$ and $R_{in} = 1.35 \times 10^{-3}$ in 3.10 (b), completely transforms the population dynamics. Now, in a chemostat setting, E^* is stable, indicating the persistence of both active and dormant populations.

3.10 (c) However, further increasing the dilution rate to $D = 0.25$ and maintaining $R_{in} = 1.35 \times 10^{-3}$ in 3.10 (c), results in a too high of a dilution in the chemostat, affecting the stability condition once again. Therefore, returning back to a stable E^0 and complete extinction in a chemostat setting ($D \neq 0$).

3.10 (d) Lastly, in Figure 3.10(d), $D = 0.2$, as in Figure (3.10) (b), but $R_{in} = 1.35 \times 10^{-4}$ is much smaller than in Figures3.10 (b)-(c). R_{in} is insufficient to sustain the population, again resulting in a stable E^0 and complete extinction in a chemostat setting ($D \neq 0$).

The effects of altering the dilution rate and the in-flowing nutrient concentration, D and R_{in}, are also depicted in Figure 3.11:

3.11 (a): In Figure 3.11 (a), $\mu(R_{in}) > D + \lambda + \dfrac{D\delta}{D+\gamma}$, which corresponds to a stable E^* and the persistence of both active and dormant populations in a batch culture model setting ($D = 0$) [34].

3.11 (b) Introducing a non-zero dilution rate $D = 10^{-4}$ and $R_{in} = 1.35 \times 10^{-4}$ in 3.11 (b), does not affect the population dynamics at all. Now, in a chemostat setting, E^* is still stable, indicating the persistence of both active and dormant populations.

3.11 (c) However, further increasing the dilution rate to $D = 10^{-1}$ and maintaining $R_{in} = 1.35 \times 10^{-4}$ in 3.11 (c), results in a too high of a dilution in the chemostat, affecting the stability condition. Therefore, this results in a stable E^0 and complete extinction in a chemostat setting ($D \neq 0$).

3.11 (d) Lastly, in Figure 3.11(d), $D = 10^{-1}$, as in Figure (3.11) (c), but $R_{in} = 1.35 \times 10^{-2}$ is much higher than in Figures3.11 (b)-(c). There is now sufficient R_{in} to sustain

both populations, resulting in a stable E^* and the persistence of both active and dormant populations in a chemostat setting ($D \neq 0$).

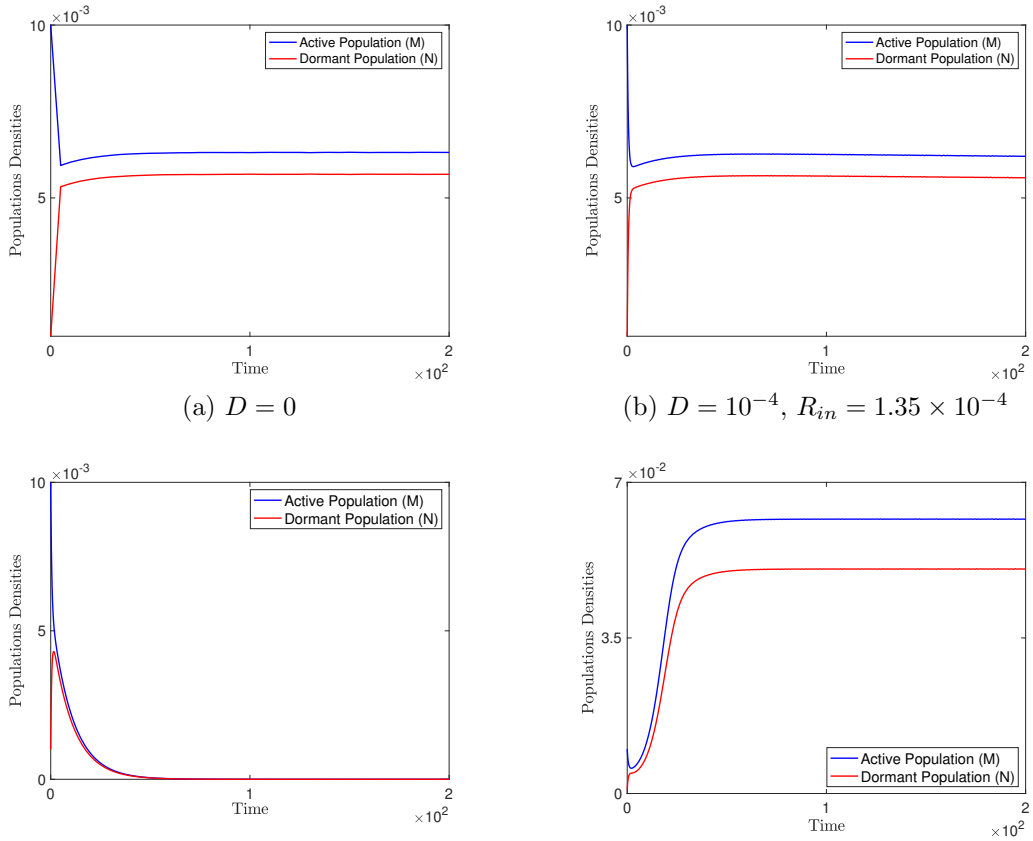

(a) $D = 0$ (b) $D = 10^{-4}$, $R_{in} = 1.35 \times 10^{-4}$

(c) $D = 10^{-1}$, $R_{in} = 1.35 \times 10^{-4}$ (d) $D = 10^{-1}$, $R_{in} = 1.35 \times 10^{-2}$

Figure 3.11: Effects of the dilution rate D and the concentration of the limiting nutrient supplied in the in-flowing medium R_{in} on the system outcome, for model parameter values $q_1 = 10^{-2}, K = 10^{-2}, q_2 = 10^{-2}, \lambda = 10^{-9}, \delta = 0.9, \gamma = 1, \mu_{max} = 0.98$, and $D = 0$ (batch culture model) in (a), $D = 10^{-4}$ with $R_{in} = 1.35 \times 10^{-4}$ (chemostat model) in (b), $D = 10^{-1}$ with $R_{in} = 1.35 \times 10^{-4}$ (chemostat model) in (c), and $D = 10^{-1}$ with $R_{in} = 1.35 \times 10^{-2}$ (chemostat model) in (d).

Since the chemostat Model (3.3.1) is able to distinguish between similar yet different environments, different combinations of the dilution rate D and the in-flowing nutrient concentration R_{in} can alter the stability of the steady states of the system.

Specifically, the numerical simulations in Figures 3.10 (a) and 3.11(a) show the two possible outcomes when $D = 0$. In contrast, the numerical simulations presented in Figures 3.10 (b)-(d) and 3.11 (b)-(d) demonstrate the adaptability of the chemostat model ($D \neq 0$) compared to the batch culture model ($D = 0$).

CHAPTER 4

Conclusion

All the plasmid sub-models in Chapter 2, except one, have straightforward stability results. They stabilize at their designated stable equilibrium value regardless of their parameter values. The sub-model with the most nuance, Model (2.3.1) where $\eta_2 = 0$ and $\beta, \eta_1 \neq 0$, is the only one with nuance.

In actuality, gut microbiomes often successfully eliminate newly introduced plasmids. This model allows for just that whenever $K\beta - \eta_1 < 0$ or equivalently, when $K < \frac{\eta_1}{\beta}$. This means whenever the carrying capacity is decreased by either smaller space or less nutrient (increased competition), there is more likelihood that $E^1 = (0, K)$ will be stable or that the plasmid-carrying donor bacteria, B_P, will be eliminated. Furthermore, note $\frac{\eta_1}{\beta}$ is a ratio between plasmid loss and plasmid acquisition via conjugation. Naturally, plasmid-carrying bacteria, B_P, are more likely to be eliminated as plasmid loss increases. Similarly, plasmid-carrying bacteria, B_P, are more likely to be eliminated as plasmid acquisition via conjugation decreases.

Thus, to maintain plasmid-carrying bacteria in the gut microbiome, it will be necessary to decrease bacterial competition, discourage plasmid loss, or encourage plasmid acquisition via conjugation. This can be done through medication such as antibiotics or bio-engineering techniques to make the plasmid beneficial and more appealing to the cell. In contrast, regardless of the parameter values, the plasmid-free resident bacteria, B_A, will always remain in the gut microbiome. This idea agrees with the biological literature since an established microorganism in the gut will require a lot to remove from the host system.

Lastly, it may interest scientists to maintain a specific ratio of donor, B_P, to resident bacteria, B_A, in the gut. Note

$$\frac{B_P^2}{B_A^2} = \frac{1}{\gamma}\left(\frac{\beta K}{\eta_1} - 1\right).$$

Below are the pertinent parameters and their relationship to the above ratio and the plasmid-carrying donor bacteria population, B_P^2:

- $(\gamma_{\downarrow})$ A decrease $(\downarrow)$ in γ, the relative capacity coefficient, will increase $(\uparrow)$ the ratio and B_P^2. i.e., a decrease in plasmid burden increases the population of plasmid-carrying bacteria.
- $(\beta^{\uparrow})$ An increase $(\uparrow)$ in β, the bacterial conjugation rate, will increase $(\uparrow)$ the ratio and B_P^2. i.e., An increase in plasmid acquisition via conjugation increases the plasmid-carrying bacteria population.
- $(K^{\uparrow})$ An increase $(\uparrow)$ in K, the carrying capacity, will increase $(\uparrow)$ the ratio and B_P^2. i.e., An increase in resources increases the plasmid-carrying bacteria population.
- $(\eta_{1\downarrow})$ A decrease $(\downarrow)$ in η_1, the rate of conversion from donor to resident bacteria, will increase $(\uparrow)$ the ratio and B_P^2. i.e., a decrease in plasmid loss increases the population of plasmid-carrying bacteria.

In summary, System (2.3.1) ($\eta_2 = 0$) is a satisfactory starting point for modeling and understanding plasmids. However, future research should explore other ways to create nuance aside from allowing $\eta_2 = 0$. Biologically, η_2 should be non-zero but much smaller than η_1 as shown by experiments and parameter estimation previously conducted [27]. However, a small η_2 should allow for the eventual elimination of plasmid-carrying donor bacteria, B_P, from the gut. Thus, these models should be expanded to incorporate more complex dynamics to allow for a small η_2 to eliminate B_P eventually. The first natural modification would be to make Model (2.3.1) into a chemostat, then allow nutrient and donor bacteria to be continuously introduced into the homogeneous mixture. Assuming an organism continuously consumes nourishment,

consumes donor bacteria, and homogeneously eliminates contents at a constant rate, this would be a basic gut simulation.

In Chapter 3, notice how dormancy materializes in the models through conversion rates. Out of the three dormancy models presented in Chapter 3, only Model (3.3.1) has an existence and stability condition where conversion rates, δ, and γ, appear to influence the outcome. If conversion were to cease, the elimination term in Table 3.7 would decrease and, thus, increase the possibility that the persistence equilibrium, E^*, in Model (3.3.1) is stable. Therefore, there is a higher chance of population survival when the conversion rates $\delta = \gamma = 0$. Although dormancy impacts the stability conditions, it does not offer much of a survival advantage to microorganisms in this setting. A possible explanation of this observation is the active microorganism's lack of hardship in this model.

The conversion rates, δ, and γ, appear in the non-trivial equilibria values of Models (3.2.2) and (3.3.1) and help determine population sizes. However, dormancy does not seem to play a significant role in Models (3.1.1) and (3.2.2) as the conversion rates do not appear in any existence or stability conditions for these models (Table 3.2, 3.5). Furthermore, conversion rates are absent from Model (3.1.1)'s equilibria values and stability analysis. Thus, dormancy modeled as simple first-order conversion offers no survival advantages in a controlled and closed environment.

Like dormancy and conversion rates, nutrient recycling materializes in the models through the nutrient quotas, q, q_1, and q_2. However, q, q_1, and q_2 do not appear in the stability conditions of the nutrient recycling Models (3.2.2) and (3.3.1). At first glance, nutrient recycling does not seem to play a significant role in the models. On the other hand, nutrient recycling does influence the two outcomes of Model (3.2.2). Nutrient recycling pumps nutrients back into the system as individuals die; this prevents the nutrient supply from depleting. Hence, nutrient recycling allows

motile and non-motile algae to persist and stabilize when introduced to a controlled and closed environment. Contrarily, neither q_1 nor q_2 impact the overall stability of Model (3.3.1) as the in-flowing nutrient concentration rate, R_{in}, can supply nutrients in a chemostat setting.

Lastly, notice how all nutrient quotas, q, q_1, and q_2, appear in both of the non-trivial equilibrium values and affect the population sizes of Models (3.2.2) and (3.3.1). In the batch culture Model (3.2.2), the smaller q is, the higher the population values of E^*, the persistence equilibrium. In other words, the fewer nutrients required per individual algae, the more algae the system can sustain. In the chemostat Model (3.3.1), the smaller q_1 is, the higher the population values of E^*, the persistence equilibrium. In other words, the fewer nutrients required per individual microorganism, the more microorganisms the system can sustain. Furthermore, the greater q_2 is, the higher the population values of E^*, the persistence equilibrium. In other words, the more nutrients are recycled per individual dead microorganism, the more microorganisms the system can sustain.

Overall, the mathematical analysis reveals several findings for the different combinations of topics presented in the models of Chapter 3.

(3.1.1): Dormancy offers no survival advantage to a dormancy-capable plasmid-free resident bacteria with threat-free active resident bacteria in a batch culture.

(3.2.2): Dormancy offers no survival advantage to golden algae with threat-free motile algae in a batch culture; however, nutrient recycling allows the possibility of both motile and non-motile algae co-existence and persistence.

(3.3.1): Neither dormancy nor nutrient recycling provides a survival advantage to a dormancy-capable microorganism with threat-free active microorganisms in a simple chemostat setting.

Thus, the next natural step is to identify and analyze the circumstances under which dormancy and nutrient cycling benefit a microorganism's survival. Future research on dormancy should aim to modify the first-order conversion between the active and dormant populations. Models that allow dormancy to depend on some mechanism, such as nutrient availability, death rate, or toxin presence, have more complex and versatile dynamics [1, 7, 11, 17]. Similarly, there is a multitude of applications and mechanisms that can guide modifications of future nutrient recycling terms [10, 16, 19, 22]. Enhancing these models in such manners should lead to more realistic dynamics. However, acknowledging that these proposed models are one of the first dormancy-plasmid and dormancy-nutrient-recycling models is crucial. As a result, there should be cautious progression with each additional mechanism to ensure a comprehensive understanding of the individual contributions and resulting model complexity.

REFERENCES

[1] Nihan Acar and Nick G Cogan. Enhanced disinfection of bacterial populations by nutrient and antibiotic challenge timing. *Mathematical biosciences*, 313:12–32, 2019.

[2] Fawaz K Alalhareth, Ana Clarisa Mendez, and Hristo V Kojouharov. A simple model of nutrient recycling and dormancy in a chemostat: Mathematical analysis and a second-order nonstandard finite difference method. *Communications in Nonlinear Science and Numerical Simulation*, 132:107940, 2024.

[3] Nathalie Q Balaban, Jack Merrin, Remy Chait, Lukasz Kowalik, and Stanislas Leibler. Bacterial persistence as a phenotypic switch. *Science*, 305(5690):1622–1625, 2004.

[4] Leigh A Baxt and Upinder Singh. New insights into Entamoeba histolytica pathogenesis. *Current opinion in infectious diseases*, 21(5):489, 2008.

[5] E Beretta and Y Takeuchi. Global stability for chemostat equations with delayed nutrient recycling. *Nonlinear World*, 1(3):191–306, 1994.

[6] Edoardo Beretta, GI Bischi, and Fortunata Solimano. Stability in chemostat equations with delayed nutrient recycling. *Journal of Mathematical Biology*, 28:99–111, 1990.

[7] James A Bradley, Jan P Amend, and Douglas E LaRowe. Survival of the fewest: Microbial dormancy and maintenance in marine sediments through deep time. *Geobiology*, 17(1):43–59, 2019.

[8] Linda Bruslind. *General microbiology*. Oregon State University, 2020.

[9] Patrice D Cani. Human gut microbiome: hopes, threats and promises. *Gut*, 67(9):1716–1725, 2018.

[10] Tomás Caraballo, Xiaoying Han, and Peter E Kloeden. Nonautonomous chemostats with variable delays. *SIAM Journal on Mathematical Analysis*, 47(3):2178–2199, 2015.

[11] NG Cogan. Optimal control methods for controlling bacterial populations with persister dynamics. In *AIP Conference Proceedings*, volume 1738. AIP Publishing, 2016.

[12] Jeffrey I Cohen et al. Herpesvirus latency. *The Journal of Clinical Investigation*, 130(7):3361–3369, 2020.

[13] Donald L DeAngelis. *Dynamics of Nutrient Cycling and Food Webs*, volume 9. Springer Science & Business Media, 2012.

[14] Juan C Diaz Ricci and Marría Eugenia Hernández. Plasmid effects on escherichia coli metabolism. *Critical reviews in biotechnology*, 20(2):79–108, 2000.

[15] Xiaoyang Dong, Hristo V. Kojouharov, and James P. Grover. Mathematical models of nutrient recycling and toxin production in a gradostat. *Computers & Mathematics with Applications*, 68(9):972–985, 2014.

[16] Xiaoyang Dong, Hristo V Kojouharov, and James P Grover. Mathematical models of nutrient recycling and toxin production in a gradostat. *Computers & Mathematics with Applications*, 68(9):972–985, 2014.

[17] AC Fowler and HF Winstanley. Microbial dormancy and boom-and-bust population dynamics under starvation stress. *Theoretical Population Biology*, 120:114–120, 2018.

[18] HI Freedman and Xu Yuantong. Models of competition in the chemostat with instantaneous and delayed nutrient recycling. *Journal of Mathematical Biology*, 31(5):513–527, 1993.

[19] Miaomiao Gao, Daqing Jiang, and Jieyu Ding. Dynamical behavior of a nutrient–plankton model with ornstein–uhlenbeck process and nutrient recycling. *Chaos, Solitons & Fractals*, 174:113763, 2023.

[20] Savvas Genitsaris, Konstantinos Ar Kormas, and Maria Moustaka-Gouni. Microscopic eukaryotes living in a dying lake (Lake Koronia, Greece). *FEMS Microbiology Ecology*, 69(1):75–83, 2009.

[21] James P Grover, Kenneth W Crane, Jason W Baker, Bryan W Brooks, and Daniel L Roelke. Spatial variation of harmful algae and their toxins in flowing-water habitats: a theoretical exploration. *Journal of Plankton Research*, 33(2):211–227, 2011.

[22] Brittni Hall, Xiaoying Han, Peter E Kloeden, and Hans-Werner Van Wyk. A nonautonomous chemostat model for the growth of gut microbiome with varying nutrient. *Discrete and Continuous Dynamical Systems-S*, 15(10):2889–2908, 2022.

[23] Huynh A Hong, Reena Khaneja, Nguyen MK Tam, Alessia Cazzato, Sisareuth Tan, Maria Urdaci, Alain Brisson, Antonio Gasbarrini, Ian Barnes, and Simon M Cutting. Bacillus subtilis isolated from the human gastrointestinal tract. *Research in microbiology*, 160(2):134–143, 2009.

[24] Eduardo Ibargüen-Mondragón, Jhoana P Romero-Leiton, Lourdes Esteva, Miller Cerón Gómez, and Sandra P Hidalgo-Bonilla. Stability and periodic solutions for a model of bacterial resistance to antibiotics caused by mutations and plasmids. *Applied mathematical modelling*, 76:238–251, 2019.

[25] Vargas-Maya Naurú Idalia and Franco Bernardo. Escherichia coli as a model organism and its application in biotechnology. *Recent Adv. Physiol. Pathog. Biotechnol. Appl. Tech Open Rij. Croat*, 13:253–274, 2017.

[26] SR-J Jang and J Baglama. Nutrient-plankton models with nutrient recycling. *Computers & Mathematics with Applications*, 49(2-3):375–387, 2005.

[27] LeNaiya Kydd, Priyanka Shiveshwarkar, and Justyn Jaworski. Engineering escherichia coli for conversion of dietary isoflavones in the gut. *ACS Synthetic Biology*, 11(11):3575–3582, 2022.

[28] Patrick Lavelle, R Dugdale, R Scholes, AA Berhe, E Carpenter, L Codispoti, AM Izac, J Lemoalle, F Luizao, P Treguer, et al. Nutrient cycling. *Ecosystems and Human Well-Being: Current State and Trends, Island Press*, 2005.

[29] Katharine Looker, Oakfield House, and Oakfield Grove. Global and regional estimates of herpes simplex virus infection prevalence and incidence in 2016. *Bulletin of the World Health Organization*, 98:315–329, 2020.

[30] Adrián López García de Lomana, Ulrike Kusebauch, Arjun V Raman, Min Pan, Serdar Turkarslan, Alan PR Lorenzetti, Robert L Moritz, and Nitin S Baliga. Selective translation of low abundance and upregulated transcripts in Halobacterium salinarum. *Msystems*, 5(4):e00329–20, 2020.

[31] Schonna R Manning and John W La Claire. Prymnesins: toxic metabolites of the golden alga, Prymnesium parvum Carter (Haptophyta). *Marine Drugs*, 8(3):678–704, 2010.

[32] Ian P Martines, Hristo V Kojouharov, and James P Grover. A chemostat model of resource competition and allelopathy. *Applied Mathematics and Computation*, 215(2):573–582, 2009.

[33] Ian P. Martines, Hristo V. Kojouharov, and James P. Grover. Nutrient recycling and allelopathy in a gradostat. *Computers & Mathematics with Applications*, 66(9):1613–1626, 2013.

[34] Ana Mendez, Fawaz Alalhareth, and Hristo Kojouharov. Population dynamics of golden algae in a batch culture with dormancy and nutrient recycling. *AIP Conference Proceedings*, 2953, (forthcoming) 2023.

[35] Tsuyoshi Mikkaichi, Michael R Yeaman, Alexander Hoffmann, and MRSA Systems Immunobiology Group. Identifying determinants of persistent mrsa bacteremia using mathematical modeling. *PLoS computational biology*, 15(7):e1007087, 2019.

[36] Jacques Monod. La technique de culture continue: theorie et applications. *Selected Papers in Molecular Biology by Jacques Monod*, 79:390–410, 1950.

[37] Daniel S Munther, Michelle Q Carter, Claude V Aldric, Renata Ivanek, and Maria T Brandl. Formation of Escherichia coli O157: H7 persister cells in the lettuce phyllosphere and application of differential equation models to predict their prevalence on lettuce plants in the field. *Applied and environmental microbiology*, 86(2):e01602–19, 2020.

[38] Aaron Novick and Leo Szilard. Description of the chemostat. *Science*, 112(2920):715–716, 1950.

[39] Sarah P Otto and Troy Day. *A Biologist's Guide to Mathematical Modeling in Ecology and Evolution*. Princeton University Press, 2011.

[40] PJ Piggot and JG Coote. Genetic aspects of bacterial endospore formation. *Bacteriological reviews*, 40(4):908–962, 1976.

[41] JI Pitt. The current role of Aspergillus and Penicillium in human and animal health. *Journal of medical and veterinary mycology*, 32(sup1):17–32, 1994.

[42] M Popov, S Petrov, K Kirilov, G Nacheva, and I Ivanov. Segregational instability in e. coli of expression plasmids carrying human interferon gamma gene and its 3'-end truncated variants. *Biotechnology & Biotechnological Equipment*, 23(sup1):840–843, 2009.

[43] Mehbuba Rehim, Lingling Sun, Xamxinur Abdurahman, and Zhidong Teng. Study of chemostat model with impulsive input and nutrient recycling in a polluted environment. *Communications in Nonlinear Science and Numerical Simulation*, 16(6):2563–2574, 2011.

[44] Mehbuba Rehim, Zhenzhen Zhang, and Ahmadjan Muhammadhaji. Mathematical analysis of a nutrient–plankton system with delay. *SpringerPlus*, 5(1):1–22, 2016.

[45] Shigui Ruan. Persistence and coexistence in zooplankton-phytoplankton-nutrient models with instantaneous nutrient recycling. *Journal of Mathematical Biology*, 31(6):633–654, 1993.

[46] Shigui Ruan and Xue-Zhong He. Global stability in chemostat-type competition models with nutrient recycling. *SIAM Journal on Applied Mathematics*, 58(1):170–192, 1998.

[47] Thibaut Sellinger, Johannes Müller, Volker Hösel, and Aurélien Tellier. Are the better cooperators dormant or quiescent? *Mathematical biosciences*, 318:108272, 2019.

[48] Mohammed Shehadul Islam, Aditya Aryasomayajula, and Ponnambalam Ravi Selvaganapathy. A review on macroscale and microscale cell lysis methods. *Micromachines*, 8(3):83, 2017.

[49] M Shilo. The toxic principles of Prymnesium parvum. In *The Water Environment: Algal Toxins and Health*, pages 37–47. Springer, 1981.

[50] Garima Singh, Mehmet A Orman, Jacinta C Conrad, and Michael Nikolaou. Systematic design of pulse dosing to eradicate persister bacteria. *PLoS Computational Biology*, 19(1):e1010243, 2023.

[51] Hal L Smith and Paul Waltman. *The theory of the chemostat: dynamics of microbial competition*, volume 13. Cambridge university press, 1995.

[52] David Summers. *The biology of plasmids*. John Wiley & Sons, 2009.

[53] R Trastoy, T Manso, L Fernández-García, L Blasco, A Ambroa, ML Perez Del Molino, G Bou, R García-Contreras, TK Wood, and M Tomás. Mechanisms of bacterial tolerance and persistence in the gastrointestinal and respiratory environments. *Clinical microbiology reviews*, 31(4):10–1128, 2018.

[54] U.S. Environmental Protection Agency. Nutrient Pollution: Harmful Algal Blooms. https://www.epa.gov/nutrientpollution/harmful-algal-blooms#effect, 08 2022.

[55] U.S. Geological Survey. Water Resources: Nutrients and Eutrophication. https://www.usgs.gov/mission-areas/water-resources/science/nutrients-and-eutrophication, 03 2019.

[56] Wilber Ventura, Tyler Randolph, Jayce Rodriguez, Alicia Prieto Langarica, Betty Scarbrough, Hristo Kojouharov, and James Grover. Resting stages and the population dynamics of harmful algae in batch cultures and chemostats. Mathematics Preprint Series 2011-19, University of Texas at Arlington, 2011.

[57] Stefan S Weber, Roel AL Bovenberg, and Arnold JM Driessen. Biosynthetic concepts for the production of β-lactam antibiotics in Penicillium chrysogenum. *Biotechnology Journal*, 7(2):225–236, 2012.

[58] Philip C Withers and Christine Cooper. Dormancy. In *Encyclopedia of ecology*, pages 952–957. Elsevier, 2008.

[59] Sanling Yuan, Weiguo Zhang, and Maoan Han. Global asymptotic behavior in chemostat-type competition models with delay. *Nonlinear Analysis: Real World Applications*, 10(3):1305–1320, 2009.

BIOGRAPHICAL STATEMENT

Ana Clarisa Mendez was born in Dallas, Texas in 1998. She earned her B.A. and M.S. degrees in Mathematics at the University of North Texas at Dallas and at the University of Texas at Arlington in 2019 and 2021, respectively.